
Defense Special Weapons Agency
Alexandria, VA 22310-3398


DNA-TR-95-68

# Space Power Experiments Aboard Rockets
## SPEAR-3

**W. John Raitt**
**Utah State University**
**Center for Atmospheric & Space Sciences**
**Logan, UT 84322-4405**

**July 1997**

**Technical Report**

**CONTRACT No. DNA 001-90-C-0166**

**Approved for public release;
distribution is unlimited.**

DESTRUCTION NOTICE:

Destroy this report when it is no longer needed.
Do not return to sender.

PLEASE NOTIFY THE DEFENSE SPECIAL WEAPONS AGENCY, ATTN: CSTI, 6801TELEGRAPH ROAD, ALEXANDRIA, VA 22310-3398, IF YOUR ADDRESS IS INCORRECT, IF YOU WISH IT DELETED FROM THE DISTRIBUTION LIST, OR IF THE ADDRESSEE IS NO LONGER EMPLOYED BY YOUR ORGANIZATION.

# DISTRIBUTION LIST UPDATE

This mailer is provided to enable DSWA to maintain current distribution lists for reports. (We would appreciate your providing the requested information.)

☐ Add the individual listed to your distribution list.

☐ Delete the cited organization/individual.

☐ Change of address.

**NOTE:**
**Please return the mailing label from the document so that any additions, changes, corrections or deletions can be made easily. For distribution cancellation or more information call DSWA/IMAS (703) 325-1036.**

NAME: _____

ORGANIZATION: _____

| OLD ADDRESS | CURRENT ADDRESS |
|---|---|
| _____ | _____ |
| _____ | _____ |
| _____ | _____ |

TELEPHONE NUMBER: ( ) _____

| DSWA PUBLICATION NUMBER/TITLE | CHANGES/DELETIONS/ADDITIONS, etc.) *(Attach Sheet if more Space is Required)* |
|---|---|
| _____ | _____ |
| _____ | _____ |
| _____ | _____ |

DSWA OR OTHER GOVERNMENT CONTRACT NUMBER: _____

CERTIFICATION OF NEED-TO-KNOW BY GOVERNMENT SPONSOR (if other than DSWA):

SPONSORING ORGANIZATION: _____

CONTRACTING OFFICER OR REPRESENTATIVE: _____

SIGNATURE: _____

CUT HERE AND RETURN

DEFENSE SPECIAL WEAPONS AGENCY
ATTN: IMAS
6801 TELEGRAPH ROAD
ALEXANDRIA, VA 22310-3398

DEFENSE SPECIAL WEAPONS AGENCY
ATTN: IMAS
6801 TELEGRAPH ROAD
ALEXANDRIA, VA 22310-3398

# REPORT DOCUMENTATION PAGE

*Form Approved*
*OMB No. 0704-0188*



| 1. AGENCY USE ONLY (Leave blank) | 2. REPORT DATE | 3. REPORT TYPE AND DATES COVERED |
|---|---|---|
| | 970701 | Technical 910411 - 941115 |

**4. TITLE AND SUBTITLE**
Space Power Requirements Aboard Rockets
SPEAR-3

**5. FUNDING NUMBERS**
C - DNA 001-90-C-0166
PE - 62715H
PR - SF
TA - SD
WU - DH307820

**6. AUTHOR(S)**
W. John Raitt

**7. PERFORMING ORGANIZATION NAME(S) AND ADDRESS(ES)**
Utah State University
Center for Atmospheric & Space Sciences
Logan, UT 84322-4405

**8. PERFORMING ORGANIZATION REPORT NUMBER**

**9. SPONSORING/MONITORING AGENCY NAME(S) AND ADDRESS(ES)**
Defense Special Weapons Agency
6801 Telegraph Road
Alexandria, VA 22310-3398
RAST/Filios

**10. SPONSORING/MONITORING AGENCY REPORT NUMBER**
DNA-TR-95-68

**11. SUPPLEMENTARY NOTES**
This work was sponsored by the Defense Special Weapons Agency under RDT&E RMC Code B7664D SF SD 00312 1950A 25904D. Additional support and funding provided by the Ballistic Missile Defense Organization.

**12a. DISTRIBUTION/AVAILABILITY STATEMENT**
Approved for public release; distribution is unlimited.

**12b. DISTRIBUTION CODE**

**13. ABSTRACT** (*Maximum 200 words*)

The SPEAR-3 program was a sounding rocket payload designed to study the interaction of a charged body with the Earth's upper atmosphere with particular reference to the discharging ability of selected active devices carried on the payload. Since some of the devices and natural outgassing provide a source of gaseous effluent release, instrumentation was included to study effluent dispersion around the payload. It was found that neutral gas release was most effective at discharging the payload when it was more negative than ~500 V. Electron emission was effective only when the currents driving the body negative were lower than the limited current available from the low perveance devices used. The hollow cathode was an ineffective grounding system on this flight due to cathode poisoning believed to have occurred during the vehicle ascent. The grounding data and HV interactions were diagnosed by a variety of instruments measuring both steady state and transient currents and voltages.

**14. SUBJECT TERMS**
SPEAR-3
Space Power
Rocket Payload
Vehicle Charging
Diagnostic Testing
High Voltage Interaction

**15. NUMBER OF PAGES**
70

**16. PRICE CODE**

| 17. SECURITY CLASSIFICATION OF REPORT | 18. SECURITY CLASSIFICATION OF THIS PAGE | 19. SECURITY CLASSIFICATION OF ABSTRACT | 20. LIMITATION OF ABSTRACT |
|---|---|---|---|
| UNCLASSIFIED | UNCLASSIFIED | UNCLASSIFIED | SAR |

NSN 7540-280-5500

Standard Form 298 (rev. 2-89)
Prescribed by ANSI Sta. 239-18
298-102

CLASSIFIED BY:

N/A since Unclassified.

DECLASSIFY ON:

N/A since Unclassified.

## SUMMARY

The SPEAR-3 science-oriented sounding rocket payload was initiated as a follow-on to the previous two payloads in the SPEAR program. It was designed to answer questions raised by the SPEAR-1 project with respect to HV space-environment interactions in general and the effectiveness of active systems in reducing the vehicle charge and hence its potential with respect to its environment. Associated with the relief of electrical charging, the dispersion of released effluents in some of the active sub-systems was another objective of the mission. The focus of the experiments on SPEAR-3 was on different methods of discharging, or grounding, the payload to study means of controlling the potential of low-earth-orbit satellites which have been observed to charge to high negative potentials when traversing the Earth's auroral zones.

The SPEAR-1 biasing arrangement of applying a potential between a deployed sphere and the payload structure was used to design a payload which would reach maximum potentials up to 2 kV negative relative to its surroundings, thereby simulating the maximum potentials observed in low-earth-orbit vehicles resulting from natural charging mechanisms. Two general categories of grounding devices were included in the payload: Electron emission systems to physically eject the surplus electrical charge; and effluent emitting systems to enhance the plasma density in the vicinity of the charged body.

One of the electron emitting devices was a conventional thermionic emitter, but using a tungsten filament rather than an activated cathode to avoid the poisoning effect of contaminants at the payload surface. The other device used a developing technology of field emission from arrays of very sharp points induced to emit electrons by very high electric fields at the small radius tips.

The effluent emission devices were a hollow cathode plasma contactor designed to emit plasma by internal ionization of a flowing stream of argon gas and a neutral gas release system which could emit nitrogen gas from four nozzles arranged to produce no disturbing torques or forces on the payload.

In addition to the means of charging the vehicle and the systems to attempt to discharge it to the Earth's ionosphere, the payload carried an array of diagnostic devices to help interpret the physical mechanisms involved in the discharging effect. Two vehicle potential measuring devices were included, one using a floating probe which was located on a boom to be outside the vehicle charge sheath at voltages below about 300 V, and another to measure the spectra of ions accelerated into the vehicle by negative potentials from ~50 V up to ~5000 V induced by the charging system. Additional experiments were included to study the dispersion of released effluents by optical imagery of light from excited states of the effluent, to study the effect of the high negative potentials on different types of solar cells and to monitor both steady and transient currents and voltages. The ambient environment was monitored by a Langmuir probe for electron density, and a cold cathode ionization gauge to measure the neutral pressure close to the payload skin.

The conclusions obtained for the experiments on grounding the payload were that the gas emission was always effective at discharging the payload for potentials more negative than ~500 V. The electron emission devices worked when the ionospheric plasma density was low enough that their emitted currents exceeded the electrons being collected by the deployed sphere being used to drive the payload negative. The hollow cathode plasma contactor was ineffective at discharging the payload because of a suspected failure of the cathode resulting from poisoning of its surface when the ground gas purge system was removed just before launch. The effect of early dispersion of effluents was deduced from external breakdown in the gas cloud surrounding the payload on the upleg which was not apparent on the downleg. No imagery of this effect or the ionization associated with the gas release system was obtained due to the failure of one of the telemetry transmitters carrying two camera signals.

In summary, the SPEAR-3 mission was successful considering the complexity of the payload which represented the limit obtainable in a Black Brant sized payload. The most significant failures were the loss of the LLLTV telemetry transmitter and the failure of the hollow cathode system to generate plasma. Despite these setbacks, the payload demonstrated the capabilities of grounding negatively charged space platforms, and contributed to our knowledge in general of the interaction of charged bodies with the upper atmosphere.

## CONVERSION TABLE

Conversion factors for U.S. Customary to metric (SI) units of measurement

| MULTIPLY → / TO GET ← | BY → / BY ← | | TO GET → / DIVIDE ← |
|---|---|---|---|
| angstrom | 1.000 000 | XE -10 | meters (m) |
| degree (angle) | 1.745 329 | XE -2 | radian (rad) |
| degree Fahrenheit | $T_K = (T\ °F + 459.67)/1.8$ | | degree kelvin (K) |
| electron volt | 1.602 19 | XE -19 | joule (J) |
| inch | 2.540 000 | XE -2 | meter (m) |
| mile (international) | 1.609 344 | XE +3 | meter (m) |
| ounce | 2.834 952 | XE -2 | kilogram (kg) |
| pound-force/inch$^2$(psi) | 6.894 757 | | kilo pascal (kPa) |
| torr (mm Hg, 0° C) | 1.333 22 | X E -1 | kilo pascal (kPa) |

## TABLE OF CONTENTS

## FIGURES

# SECTION 1

# INTRODUCTION

The Space Power Experiments Aboard Rockets (SPEAR) program was initiated in 1985 by the Strategic Defense Initiative Office, Innovative Science and Technology division (SDIO/IST) and has been managed by the Defense Nuclear Agency (DNA) to study the interaction of electrically charged space platforms and space flight components with the low-earth-orbit (LEO) environment. The principal objective of the SPEAR-3, the third mission in the series, was to study the interaction of a differentially charged space platform with the upper atmospheric environment with and without active devices to reduce the impedance of the negative element to the ionosphere. An additional objective was to study the dispersion of effluents used in that category of impedance reducing systems (*Raitt et al.*, 1995a).

A Black Brant 9A sounding rocket successfully launched SPEAR-3 on March 15, 1993, from NASA's Wallops Flight Facility, VA. The payload was launched at 21:12:41 EST, the payload reached an apogee of 289 km. All mechanical systems functioned as planned, and the attitude maneuvering system completed its program of orienting the payload in different directions relative to the geomagnetic field.

The interaction between electrically biased parts of the payload results from the presence of the ionosphere at LEO altitudes. This region is a weakly ionized plasma, and as such it will allow currents to flow from/to those parts of the system biased relative to the plasma. The current flow from the positive parts is determined by electron collection, while that to the negative parts is determined by ion collection and secondary electron emission. The collecting characteristics for the two polarities are quite different because of the large mass difference between the ions and the electrons and the high yield of secondary electrons from energetic ion impact on metal surfaces.

To explore the HV interaction, SPEAR-3 was similar in configuration to SPEAR-1 in that the electrical biasing potentials of the system were determined by connecting a charged capacitor between a boom-deployed sphere and the rocket body with polarity such that the sphere was driven positive and the body negative relative to the ambient ionosphere. The principal objective of the flight was to use the negative bias on the body to simulate the highest degree of electrical charging seen on polar orbiting satellites at ~800 km altitude, and then test different means of reducing the potential of the vehicle, that is, grounding it to the ionosphere. The grounding devices were categorized into two basic types, one emitting electrons to reduce the charge on a negative object, the other emitting neutral or ionized effluent from the charged body and relying on local ionization of the enhanced effluent density around the vehicle to provide increased plasma currents to discharge the vehicle. The use of effluent release allowed experiments to be performed to study the effectiveness of the enhanced effluent density around the vehicle to diminish localized differential charging of surfaces.

This report describes the SPEAR-3 science objectives, the payload instrumentation and mission plan designed to achieve the science objectives, the results of the flight performance, and the implications regarding the effectiveness of the grounding devices.

## SECTION 2

## SCIENCE OBJECTIVES

The overall science objectives of the mission were as follows:

1. To test a variety of space platform grounding schemes for bias levels up to ~2 kV negative potential as a function of:
   (i) Altitude in LEO region
   (ii) Attitude relative to geomagnetic field
   (iii) Different bias levels
2. To diagnose the physics of the operation of the grounding devices
3. To study the dispersion of gaseous effluent emitted from a space platform
4. To study the effects of high bias voltages on the performance of a solar cell module in the presence of emitted gaseous effluents
5. To test the effectiveness of the grounding techniques in reducing local differential charging on a diagnostic probe and on solar cells
6. To monitor the undisturbed and disturbed plasma and neutral gas environments of the payload

# SECTION 3

# INSTRUMENTATION DESCRIPTION

## 3.1 HIGH VOLTAGE SYSTEM.

The high voltage to bias the vehicle, and to provide sufficient current to ground it to the ionosphere was derived from a capacitor charged to 10 kV from a high voltage power supply. Since the current capacity of the power supply resulted in a charging time of ~4 secs for the 2 μF capacitor used, two capacitors were employed so that while one was being used to charge the vehicle, the other was being charged from the power supply. The time periods of the charge and discharge periods were such that a fully charged capacitor was available as soon as a discharge cycle was completed. In addition to the switching to accomplish the charge and discharge phases, additional switching was included to either apply the voltage "instantaneously", i.e., over the time period represented by relay closure, or to ramp up the voltage over a time period of 10s of mS by an RC network. The two methods of applying the differential bias were alternated throughout the flight.

The high voltage system included monitors of the biasing voltage as well as the currents flowing through the branches of the system, from which the current flowing from the ionosphere to the vehicle could be deduced.

## 3.2 GROUNDING DEVICES.

The four grounding devices referred to earlier were tested on the payload in synchronism with the application of the vehicle bias voltage. The independently operating Attitude Control System (ACS) provided additional short periods of effluent release when the control jets operated, releasing nitrogen.

### 3.2.1 Neutral Gas Release System.

The Neutral Gas Release System (NGRS) consisted of two pairs of horizontally opposed jets with axes of symmetry tangent to a cross section of the payload skin. The gas flows in the four jets were closely matched, so that no significant torques or thrusts resulted from the programmed gas releases. A regulator reduced the tank pressure to a line pressure with gas flowing of ~200 psi, and a single valve for each pair of nozzles mounted close to the nozzles controlled the gas releases. This reduced the residual outgassing of the system once the gas was cut off. An additional regulator gave a lower flow rate for half of the gas releases. The flow rates were 2 g/sec per nozzle at the high level and 0.2 g/sec at the low level. Most gas pulses were 100 msec, but each discharge sequence was initiated with a 200 msec pulse. The gas used was argon. Figure 3-1 illustrates the mechanical design of the region near one pair of jets as well as an enlarged view of one of the screw-in nozzles. Each nozzle had a throat diameter of .74 mm and an exit diameter of 1.75 mm to give an exit velocity of Mach 4.

### 3.2.2 Hollow Cathode Plasma Contactor (HCPC).

The plasma contactor grounding device (HCPC) was designed to produce a plume of plasma at its orifice by ionizing xenon gas flowing through the electron flux produced in the hollow cathode. The orifice was deployed to be outside the plane of the vehicle skin, and the axis of symmetry was in a radial direction. Provision was made to pre-heat the cathode on the ascent part of the trajectory, thereby allowing a fast start-up once operating altitude was reached. In addition to the plasma generated, the hollow cathode emitted neutral xenon, but at a much lower flow rate than the gas release system. The current capacity of the hollow cathode was designed to be at least 10 amperes for either ion or electron collection. Figure 3-2 is a drawing of the cathode assembly.

### 3.2.3 Thermionic Emitter (TE).

A heated tungsten filament with a saturation emission current capacity of 1.2 amperes (TE) was mounted to be exposed just below the plane of the vehicle skin after door deployment. The normal to the disc shaped cathode was oriented to be in a radial direction. The cathode was constructed using a Tungsten/Rhenium alloy (97/3 %) wire. The cathode was heated by an alternating current at a frequency of 2.0 kHz. The electrons were accelerated into the charge sheath around the vehicle by a 15 volt negative bias applied to the cathode. Although the cathode was just below the plane of the skin, it was located in a

well that was nine times the diameter of the filament disc. Figure 3-3 shows the mechanical assembly of the thermionic emitter filament, which is in the shape of a "potato masher."

### 3.2.4 Field Emission Device.

The Field Emission Device (FED) was designed to emit electrons on the application of an electric field to very-small-radius points fabricated on a substrate. Each individual device was housed in a TO-5 transistor can, and the driving electronics were designed to set the maximum emitted current at 10 mA per device. A total of nine devices were used to provide a maximum capacity of 90 mA from the unit. Control of the device was achieved by the application or removal of the voltage to an integrated electrode over the points used to produce the extraction electric field necessary for field emission ($80V < V < 200V$). Figure 3-4 gives (a) a schematic and (b and c) micrographs of a prototype FED device.

## 3.3 DIFFERENTIAL SURFACE CHARGING.

One of the objectives was to study the influence of the effluent releases on the reduction of differential charging on surfaces mounted on the vehicle. This was achieved by two devices. In one the differential charge was deliberately applied, and in the other the observed tendency for solar cells to develop regions of localized charge build-up when negatively biased relative to a plasma was exploited.

### 3.3.1 Differential Charge Device (DCD).

This device (DCD) consisted of an isolated metal plate capable of being charged 2000 volts more negative than the skin of the vehicle. The size of the plate was 90 x170 mm, and it was made of the same material as the vehicle skin and underwent the same surface finishing process (alochrom). The potential of the plate was monitored as it was allowed to discharge back to vehicle skin potential through the external plasma environment. The impedance of the voltage monitor and a fixed shunt capacitor set the decay time constant of the device to be ~500 msec in the absence of external plasma. Figure 3-5 is a block diagram of the DCD electrical system, and Figure 3-6 shows the mechanical layout of the DCD.

### 3.3.2 Solar Cell System.

An assembly of four different types of solar cell arrays were mounted to a metal baseplate which was deployed into the vehicle sheath at operating altitude. Two of the cell arrays were the type planned for the Space Station, the other two were advanced design gallium arsenide cells. Provision was made to count pulses of current associated with discharges from the individual cell arrays and also to test the operation of the cells by periodically illuminating them with a light source. The steady current generated by the illumination and the plasma current to the biased cells was also measured. The biasing range for the solar cells was extended by adding a positive bias source at 500 volts, which overcame the vehicle bias part way through its sweep and resulted in the solar cells being positively biased relative to the plasma. The location of the arcs on the solar cells was planned to be observed by a Low Light Level Television (LLLTV) directed at the deployed array and sensitized only when the cell illumination was off. Figure 3-7 shows the deployed position of the solar cell system as viewed from above. Each of the shapes on the rectangular area represents a solar cell.

## 3.4 VEHICLE POTENTIAL.

### 3.4.1 Electrostatic Analyzer.

The Electrostatic Analyzer (ESA) measured the energy of positive ions arriving at its aperture in the energy range 10 eV to 25 keV using a pair of sensors to split the total energy range into 10 - 750 eV and 0.33 - 25 keV. The shape of the spectrum of ion energy should peak at the energy given to those ions accelerated through the vehicle sheath and therefore provide a measure of the electrostatic potential of the vehicle relative to the undisturbed plasma. The energy resolution of the instrument was 7%, and the sweep time was 32 msec using 64 energy steps of 500 μsec duration. Two sensor pairs with different entrance aperture sizes provided a total dynamic range of ion flux from 0.2 - 2000 $\mu A/m^2$. The field of view of each sensor was 20° x 5° about a radial direction, with the direction of the wider field of view parallel to the longitudinal axis of the vehicle. Figure 3-8 is a block diagram of the ESA, and Figure 3-9 is drawing of an assembled sensor.

### 3.4.2 Floating Probe

The floating probe system was designed to provide vehicle potential measurements at the lower end of the expected range with higher time resolution than the ESA. The probe was a 64 mm diameter aluminum sphere mounted on a 2.5 m Weitzmann boom extended when the payload reached operational altitude. The surface of the boom had a conducting bare beryllium-copper surface. Figure 3-10 shows a circuit diagram of the important components of the floating probe sensor. *Siefring et al.* (1995) present a detailed description of each of these components and theory behind the measurement.

## 3.5 VEHICLE ENVIRONMENT.

Two of the most important parameters of the vehicle environment concerned with the HV vehicle - space interaction are the neutral gas density and the plasma density. Instruments to measure the ambient gas pressure close to the vehicle skin and also the ambient plasma density during the quiescent periods in the capacitor discharge program were included in the payload.

### 3.5.1 Neutral Pressure Gauge.

The pressure gauge used was a cold cathode ionization gauge similar to instruments flown on SPEAR-1 and SPEAR-2. The gauge was launched with a backfill of nitrogen and opened at altitude, thereby guaranteeing a fast start as the internal gauge pressure swept through the Paschen minimum. The access of gas to the ionization chamber was designed such that the time constant of the instrument to pressure changes was a few msec. Figure 3-11 is a schematic illustration of the magnetron sensor used within the neutral pressure gauge.

### 3.5.2 Langmuir Probe.

The Langmuir probe had cylindrical geometry, and the collecting area and a guard electrode were deployed a short distance from the vehicle skin. The probe was a gold plated cylinder with a length of 140 mm and a diameter of 2.4 mm. The bias to the probe consisted of a 0.9 sec fixed positive bias followed by a down/up sweep with a total duration of 0.1 sec. This ensured that the probe swept through the probe i-V characteristic at least once during the 1 sec quiescent periods enabling both $T_e$ and the ion current to be measured during the undisturbed times during the flight. Figure 3-12 shows the mechanical configuration of the Langmuir probe.

## 3.6 VEHICLE RETURN CURRENT.

### 3.6.1 Skin Current Probes (SCP).

Two current collecting probes were set in the skin of the vehicle. Each probe was 74 x 165 mm in area and was fabricated and finished using the same material and surface treatment as the vehicle skin. One probe (SCP1) was mounted in the upper section of the payload and the other (SCP2) in the lower section, closer to the effluent releasing systems. Figure 3-13 presents a block diagram of the SCP1 electronics, and Figure 3-14 shows the mechanical assembly of SCP1.

## 3.7 EFFLUENT IONIZATION.

### 3.7.1 Optical Imaging Spectrometer.

A compact grating spectrograph with a total wavelength range of 1000Å and a spectral resolution of 5Å was coupled to a LLLTV camera which allowed both spectral and spatial resolution in two orthogonal directions in the camera image plane. The sensitivity of the camera's CCD (Charged Coupled Device) detector determined that the 1000Å range selected should fall within the overall range of 3500 - 8000Å. A 45° mirror deployed beyond the skin of the vehicle allowed the spectrometer to study optical emissions from the effluent gases from close to the skin out to about 3 m from the skin.

### 3.7.2 Low Light Level Televisions.

Two conventional white light imaging intensified LLLTV systems were also included in the payload. The cameras were each housed in a container pressurized to one atmosphere to protect the image intensifier from arcing. One of the units was pointed towards the graded boom to look for the presence of glow discharges around the grading rings and the biased sphere. The other camera was deployed far

enough away from the vehicle skin that an integral 45° mirror allowed a view parallel to the vehicle skin with a field-of-view including the complete solar cell system mounting plate after it had been deployed. The prime purpose of this camera was to record arcs on the biased solar cell arrays. However, the field of view was not completely filled by the arrays, and part of the region of effluent release was visible around the edges of the solar cell panel. The video signals from each camera were fed into a frame splitter, and the composite image was telemetered on a single TV downlink.

## 3.8 ARC MONITORS.

### 3.8.1 Transient Pulse Monitor.

The transient pulse monitor allowed the properties of impulsive signals to be characterized by peak positive and negative amplitudes, maximum rise and fall rates and the total time integral of the pulse signal. Three sensors were used to detect transient signals. A broadband current transformer monitored transient currents in any of the solar array samples. Transient longitudinal skin currents were measured at a slot machined into the payload skin. The third sensor used an active dipole/preamplifier to detect transient electric fields on the vehicle's surface.

## 3.9 HIGH SPEED DATA SYSTEM.

In order to measure the complete waveform of selected transient signals, a high-speed data system was included in the payload. The unit allowed the collection of data from a snapshot of 16 msec duration during which each of three channels were sampled at 1 MHz sampling rate. The initiation of the snapshot was controlled by a trigger signal, and provision was made to adjust the delay between receiving the trigger and starting the digitizing. This enabled the unit to be "tuned" to compensate for propagation delays in the systems being triggered. The three channels selected for high-speed sampling were the sphere to body potential, the sphere current through a Rogowski coil, and one of the skin current probes (SCP1). The synchronization was made to the initial application of the capacitor voltage to the sphere. Provision was made to read out the memories at a rate commensurate with the telemetry system capacity and the recharging time of the HV capacitors. Examples of the transient development of the current to the payload skin have been presented by *Thompson et al.* (1995).

## 3.10 PAYLOAD LAYOUT.

The instruments and support systems were packaged to fit into the 0.43 m diameter envelope of a Black Brant sounding rocket. The large number of instruments resulted in a very long payload which required extensive stress analysis to demonstrate that it would remain stable during the powered ascent to operational altitudes.

### 3.10.1 Longitudinal.

Figure 3-15 shows the arrangement of the different sections of the payload, and the instruments and support systems contained in the sections. The total length of the payload skin to the top of the HV section was 5.2 m, the telescopic boom supporting the sphere and graded boom was 2.0 m long, and the graded boom was 1.2 m long.

The sphere, graded boom and support boom were housed under the nosecone and deployed to the configuration shown in Figure 3-15 at nosecone release. The baseplate of the support boom housed the forward viewing LLLTV and the optical spectrometer and its deployment mechanism.

The high voltage originated in the high voltage section immediately below the nosecone and was conveyed to the sphere by a cable running up the support boom and inside the graded boom. The HV section was sealed and remained at a pressure of one atmosphere of dry air throughout the flight. It housed the HV power supply and capacitors, the HV switching relays and the HV monitoring sensors and signal conditioners.

Aft of the HV section was the first of the sections containing science instruments. The figure lists the instruments in that section which were, in general, either those needing to be further away from the effluent releasing devices or active devices which did not contribute to the effluent environment of the payload. The two electron emitting grounding devices were housed in this section.

The first science section was separated from the second by the vehicle service module. This section housed the support systems of power, telemetry and sequencing.

The second science section, aft of the vehicle service module, primarily housed the effluent releasing grounding devices and some instruments measuring the effect of the releases.

The final section of the payload, just ahead of the adapter ring to mate the payload to the rocket motor, was the attitude control system which provided control of the payload orientation in all three axes by releasing jets of cold nitrogen gas.

3.10.2 Azimuthal.

The azimuthal view, showing emission or deployment directions of the different instruments, is displayed in Figure 3-16. The figure is a view from the nosecone to the aft of the payload. Those instruments which view parallel to that direction have their look direction indicated by the dot and cross symbols indicating forward and aft directions respectively. The figure also indicates the direction of the geomagnetic field for the three orientations of the vehicle.

## SECTION 4

## INSTRUMENT CALIBRATIONS

Table 4-1. The SPEAR-3 instrument channels calibrations.

| Signal | Description | Units | Min Value | Max Value | Resolution |
|---|---|---|---|---|---|
| SCSCUR1 | Solar Cell #1 Current | μA | -11.03 | 9.01 | 0.07859 |
| SCSCUR2 | Solar Cell #2 Current | μA | -11.22 | 8.97 | 0.07919 |
| SCSCUR3 | Solar Cell #3 Current | μA | -10.88 | 8.96 | 0.07780 |
| SCSCUR4 | Solar Cell #4 Current | μA | -10.83 | 8.86 | 0.07722 |
| ESAAH | ESA Low Gain/High Energy | eV | 390 | 29000 | 7% |
| | | /E-cm$^2$-ster-s | 0 | $6.1 \times 10^{13}$ | $1.5 \times 10^{10}$ |
| ESAAL | ESA Low Gain/Low Energy | eV | 12 | 897 | 7% |
| | | /E-cm$^2$-ster-s | 0 | $6.1 \times 10^{13}$ | $1.5 \times 10^{10}$ |
| ESABH | ESA High Gain/High Energy | eV | 390 | 29000 | 7% |
| | | /E-cm$^2$-ster-s | 0 | $2.4 \times 10^{11}$ | $5.9 \times 10^{7}$ |
| ESABL | ESA High Gain/Low Energy | eV | 12 | 897 | 7% |
| | | /E-cm$^2$-ster-s | 0 | $2.4 \times 10^{11}$ | $5.9 \times 10^{7}$ |
| DCDLIN | DCD Linear Voltage | V | -2510 | 2499 | 19.61 |
| DCDLOG | DCD Log Voltage | V | -4385 | 11670 | 8.0% |
| TEACHTHIM | TE Cathode Current | mA | -22.22 | 227.8 | 0.9804 |
| FEDGATEI | FED Gate Current | mA | -1.816 | 2.216 | 0.01581 |
| FEDCATHI | FED Cathode Current | mA | -112.5 | 137.5 | 0.9804 |
| RNGIM | Ring (Boom) Current | mA | -7.002 | 99.97 | 0.4195 |
| DISIM | Capacitor Discharge Current | mA | -42.26 | 203.5 | 1.606 |
| | | | 203.5 | 1109 | 8.864 |
| LOGSPHER | Sphere Voltage | kV | ~ -200 | ~ 200 | 8.6% |
| LOGROG | Rowgowski Coil Current | A | ~ -2000 | ~ 2000 | 15.3% |
| LPELEC | LP Electron Current | A | $-3.0 \times 10^{-9}$ | $1.8 \times 10^{-5}$ | 6.2% |
| LPION | LP Ion Current | A | $3.2 \times 10^{-10}$ | $1 \times 10^{-3}$ | 6.5% |
| NPNPM | Neutral Pressure | Torr | $1.3 \times 10^{-7}$ | $8.3 \times 10^{-4}$ | 3.5% |
| PCRETNI | HCPC Neutralize Current | mA | 0 | 560 | 2.196 |
| SCP1CUR | SCP1 Linear Current | μA | -934.0 | 956.2 | 7.412 |
| LOGSCP1 | SCP1 Log Current | μA | -5025 | 8318 | 8.6% |
| SCP2CUR | SCP2 Linear Current | μA | -9693 | 10857 | 80 |
| LOGSCP2 | SCP2 Log Current | μA | -12740 | 10670 | 7.2% |
| FPHF21 | FP High Frequency | V | -97 | 97 | 0.7608 |
| FPV12M | FP Medium Gain 1 | V | -193 | 194 | 1.520 |
| FPV21H | FP High Gain | V | -24.2 | 24.2 | 0.1900 |
| FPV12L | FP Low Gain | V | -1550 | 1550 | 12.16 |
| FPV1S | FP Medium Gain 2 | V | -710 | 115 | 3.235 |
| TPMPAMP1 | Electric Field Pos Amplitude | V/m | 0 | $1.6 \times 10^{4}$ | 6.9% |
| TPMNAMP1 | Electric Field Neg Amplitude | V/m | 0 | $1.8 \times 10^{4}$ | 5.6% |
| TPMPDER1 | Electric Field Pos Derivative | V/m-s | 0 | $9.5 \times 10^{12}$ | 6.5% |
| TPMNDER1 | Electric Field Neg Derivative | V/m-s | 0 | $8.8 \times 10^{12}$ | 9.2% |
| TPMINT1 | Electric Field Integral | V-s/m | 0 | $3.3 \times 10^{-2}$ | 3.3% |
| TPMPAMP2 | Bdot Pos Amplitude | A/m | 0 | $7.5 \times 10^{1}$ | 4.4% |
| TPMNAMP2 | Bdot Neg Amplitude | A/m | 0 | $6.9 \times 10^{1}$ | 3.0% |
| TPMPDER2 | Bdot Pos Derivative | A/m-s | 0 | $7.5 \times 10^{9}$ | 6.9% |
| TPMNDER2 | Bdot Neg Derivative | A/m-s | 0 | $7.8 \times 10^{9}$ | 7.1% |
| TPMINT2 | Bdot Integral | A-s/m | 0 | $5.4 \times 10^{-5}$ | 3.7% |
| TPMPAMP3 | SCS Pos Current Amplitude | A | 0 | $7.4 \times 10^{0}$ | 3.8% |
| TPMNAMP3 | SCS Neg Current Amplitude | A | 0 | $7.0 \times 10^{0}$ | 3.8% |
| TPMPDER3 | SCS Pos Current Derivative | A/s | 0 | $9.3 \times 10^{8}$ | |
| TPMNDER3 | SCS Neg Current Derivative | A/s | 0 | $9.4 \times 10^{8}$ | 9.4% |
| TPMINT3 | SCS Current Integral | A-s | 0 | $6.1 \times 10^{-6}$ | 4.3% |

## SECTION 5
## BIASING TECHNIQUE

The biasing technique used was to connect a charged capacitor between a deployed sphere and the payload structure. To avoid electric field concentrations near the biased sphere support, the sphere was mounted on a boom containing grading rings which were interconnected by resistors, allowing a controlled fall off in the electric potential away from the sphere mount. Pre-flight calculations showed that the system geometry, combined with expected ionospheric plasma densities, required a capacitor bias of 10 kV to bias the payload to at least -2 kV relative to the ionosphere at operational altitudes. A capacitor was chosen as the prime source of bias potential because it would be able to sustain high currents if external discharges occurred, moreover as the capacitor discharged through fixed resistors and the ionospheric plasma, the bias voltage would sweep through a range of values. A 2 μF capacitor was chosen to allow a time constant commensurate with the telemetry sampling intervals, maximizing the number of capacitor discharges for the flight time. The latter requirement was aided by using two capacitors such that one was being charged while the other was in its discharge cycle. The current from the capacitors was limited to 5 amps by a 2 kΩ resistor in series with the capacitor. Figure 5-1 shows a simplified schematic diagram of the biasing technique and the relative locations of the sphere to the payload and to the payload voltage monitoring instruments.

It was decided that two modes of HV connection to the sphere would be used. One allowed the voltage to rise as rapidly as it could following the closure of a HV relay between the sphere and the charged capacitor - this was called the switched mode. The other mode interposed a resistor/capacitor network between the relay and the sphere to slow down the rise in potential such that it took about 30 msec to reach its peak value - this was called the ramped mode. Simplified schematics of the two biasing schemes are shown in Figure 5-2. The parallel combination of the fixed 700 kΩ resistors and the 1 MΩ resistance built into the graded boom set the decay time constant of the 2 μF capacitor to be 0.82 sec in the absence of external plasma. In the ramped mode, the 30 kΩ resistor in the delay circuit and the charge shared with the 0.5 μF capacitor reduced the peak voltage between the sphere and the payload from the initial voltage across the 2 μF capacitor of 10 kV to ~8 kV. Figure 5-2 also shows the electrical configuration of the sphere and the payload during the one second passive period which followed each four second discharge period.

# SECTION 6
# MISSION OPERATIONS

## 6.1 LAUNCH.

The payload was launched from the NASA range at Wallops Island, Virginia, at 21:12:41 EST on March 15, 1993 in an easterly direction. A digisonde ionospheric sounder located near the range determined the peak ionospheric plasma density to be ~$3 \cdot 10^{11}$ $m^{-3}$ with the altitude of the F-region peak at 340 km, considerably above the apogee altitude. The launch time was within the window required for darkness at apogee.

## 6.2 TRAJECTORY.

The trajectory of the payload reached an apogee of 289 km 278 sec after launch. This was under the goal of 300 km but was close enough to provide time to exercise all of the planned modes before the payload ceased functioning upon re-entry. The azimuth of the trajectory was ~100°.

## 6.3 ATTITUDE MANEUVERS.

Three science-related attitude maneuvers were made during the flight. Figure 6-1 shows the times of the maneuvers and a diagrammatic sketch of the payload orientations after each maneuver. The first position resulted in the payload longitudinal axis and the axes of symmetry of the four gas release system plumes being perpendicular to the geomagnetic field. The second maneuver rolled the payload 90° about its longitudinal axis to orient the gas release system plumes to be parallel to the geomagnetic field, but still keeping the geomagnetic field perpendicular to the payload axis. In both of these attitudes the maximum magnetic insulation was achieved between the biased sphere and the payload skin and effluent release devices.

The final attitude placed the geomagnetic field parallel to the payload axis. This provided a situation where there was the greatest possibility for reduced impedance between the sphere and the payload because of the low impedance to plasma currents parallel to magnetic fields.

## SECTION 7

## FLIGHT OBSERVATION PROGRAM

The flight observation program consisted of cycling through the four grounding devices interspersed with periods when no planned grounding was initiated. The high voltage biasing was initiated at an altitude of 150 km about 100 sec after lift-off.

In each sequence, the grounding device to be tested was active for a total of four discharges of the biasing capacitors. The first pair tested the effectiveness of the grounding device for a ramped and a switched application of the bias. Also, when feasible, the grounding device was activated about 100 msec prior to the capacitor discharge for each of the two switching modes. The second pair of biasing capacitor discharges with the selected grounding device again tested the ramped and switched modes, but in this case the grounding device was activated about 100 msec after the capacitor discharge. Thus the exercise of a given grounding device occupied four capacitor discharge cycles, a total of 20 sec.

The order of using the grounding devices and their distribution in altitude and attitude is shown in Figure 7-1 where letters signifying the device used are plotted on an altitude trajectory. The periods of time when the ACS was used to re-orient the payload are shown by the gray bars.

High-speed data snapshots of the three channels described earlier were taken for the first 16 msec of each of the capacitor discharges.

# SECTION 8
# RESULTS

## 8.1 INSTRUMENT FLIGHT PERFORMANCE.

The majority of the instruments and support sub-systems worked well during the flight. All of the mechanical functions performed as expected and at the planned times. All prime power systems worked correctly and maintained adequate bus voltages throughout the flight.

The support system which failed was one of the TV telemetry transmitters. The transmitter performed well through all of the powered flight, and video images from the two cameras it was supporting were as expected. At about 70 sec into the flight the telemetry signal was lost and never re-appeared.

Two of the instruments appeared to suffer some malfunction. The hollow cathode plasma contactor did not produce the expected emission current and was unable to provide the grounding function expected. It is suspected that the cathode was poisoned prior to lift-off during the short period it was exposed to the payload purge gas. The field emission device was believed to have lost some of its nine modules when it was initially activated. This was thought to be a consequence of contamination around the payload which had not reduced sufficiently at the first activation time. However, although this reduced its current capacity, there was enough current to discharge the vehicle at lower ionospheric plasma densities.

The attitude control system worked well and re-oriented the payload to the required positions at the planned times. Since these attitude changes were planned to occur during times when the payload was biased, the ACS provided an alternate gas release grounding system.

## 8.2 BIASING ACHIEVED.

The biasing program consisted of alternating the ramped and switched modes of sphere bias throughout the flight. After 4 secs of connection time for the capacitor to the sphere, the sphere was grounded by another HV relay for a period of one second. This operation provided one second of quiescent data each capacitor discharge, and also drained any residual charge from the biasing capacitor before it started its next charging cycle.

Figure 8-1 shows the simplified schematic including the external plasma impedances between the sphere and payload to the undisturbed ionosphere. Under normal circumstances these two impedances are large compared with other circuit impedances. However, in the event of and external discharge at either the sphere, the payload or both, these impedances become small and influence the attainment of the desired potentials because of the current limiting provided by the 2 kΩ resistor in series with the biasing capacitor. Reduced plasma impedance also increased the rate of decay of the potential between the sphere and the payload.

The effect of external discharge was seen early in the SPEAR-3 flight. Figure 8-2 shows the measured sphere to payload potential for the ramped mode followed by the switched mode at two times during the flight. At the earlier time neither capacitor discharge reaches its expected potential, and the switched mode achieves a lower potential than the ramped mode. This is interpreted as an external discharge triggered at sphere bias initiation, and occurring at a lower threshold for the switched case than for the ramped case. At the later flight time the sphere potentials are seen to behave as expected. This effect has been studied in more detail and related to payload outgassing (*Raitt et al.,* 1995b).

## 8.3 GROUNDING EFFECTIVENESS.

### 8.3.1 Neutral Gas Release System (NGRS).

An example of payload grounding achieved by the neutral gas release system is shown in Figure 8–3. The figure shows a plot of several parameters against mission elapsed time (time from launch) for the duration of one biasing capacitor cycle when the neutral gas release system was operated in the mode of being activated after the HV bias was applied. The top bars show the capacitor discharge on when the line is thick, followed by the times when the high gas flow valves are open, then the times when the low gas flow rate valves are open. The first high flow period lasts for 200 msec while the subsequent ones

have a duration of 100 msec. The upper plot panel shows the regulator pressure responding to the valve openings, and the lower panel shows the payload potential measured by the floating probe.

The plot shows that the payload potential falls to a negative voltage beyond the range of the floating probe channel used as soon as the biasing capacitor is connected. When the high flow rate gas emission is initiated, the payload potential immediately drops to ~ -230V. The return to a high negative potential is slow and is stopped by the low flow rate gas emission. After remaining low for a period exceeding the gas flow period, the potential eventually jumps back to a high negative potential but is brought down again by the next high flow rate period. Finally, after 306.5 sec the biasing capacitor has discharged to a level that the payload is no longer at a high enough bias to allow the gas released to be ionized, and there is no more grounding by the system. This effect has been compared with other sound rocket payloads by *Berg et al.* (1995).

This behavior is typical of that seen throughout the flight. The most apparent anomalous result seen is the delay in the return of the payload to high negative potential after the gas flow is shown as having stopped.

### 8.3.2 Hollow Cathode Plasma Contactor.

We believe that the hollow cathode plasma contactor suffered a cathode failure as discussed earlier, so it was unable to perform its grounding function as planned. Figure 8-4 shows a capacitor discharge period when the hollow cathode plasma contactor was activated. The top bars show the capacitor discharge period, and below it the enable command for the hollow cathode plasma contactor. The upper plot panel shows evidence of the electrical functioning of the system where the keeper voltage is plotted. The lower panel shows the payload potential measured by the floating probe. It can be seen that the payload potential is just changing in a way which tracks the exponential decay of potential on the biasing capacitor. There is some evidence that the time constant is reduced, which may be due to ionization of the gas emitted by the device at a low flow rate.

### 8.3.3 Thermionic Emitter.

The thermionic emitter was activated by applying power to heat the filament to emission temperatures. An example of the grounding achieved with this device is shown in Figure 8-5. The top two bars showing the biasing cycle and the filament activation indicate that this was a case where the grounding was initiated after the bias had been established. In the case of this device, the grounding was not immediate since the filament took about 200 msec to reach emission temperature as is shown by the rise in the cathode current. The lower plot panel shows the floating probe measure of payload potential which is reduced from a high negative value to ~ -100V when the electron emission occurs. The payload potential then decays at an accelerated rate until reaching plasma potential. During an earlier grounding sequence, the TE charged the vehicle a few volts positive

During the course of the flight we found that effective grounding of the payload only happened at positions in the trajectory where the ambient plasma density was low. We believe that this is due to the low perveance of the electron emitter which cannot supply enough current to balance that collected by the biased sphere at higher plasma densities.

### 8.3.4 Field Emission Device.

The behavior of the field emission device was similar to the thermionic emitter. Figure 8-6 shows a plot of parameters associated with the field emission device and the response of the payload potential measured by the floating probe.

The upper bars show the biasing cycle and the field emission device activation. The device was activated after biasing was established, but like the thermionic emitter there is a further delay before it is capable of emitting electrons. In this case the delay is a controlled ramp up of the gate potential over a period of one second to reduce the risk of tip arcs. The upper panel shows the total current emitted by the devices reflecting the ramp up of the extraction potential. The lower panel shows that the payload potential initially falls to a high negative value on the application of the bias. This is followed by an attempt to return to low values when the field emission device ramp-up starts, but this is a transient event, and the grounding does not occur until the full emission current is established. The payload potential is then brought to ~ -200V and remains low for the rest of the capacitor discharge cycle.

The flight history of the effectiveness of the field emission device to ground the payload was similar to the thermionic emitter. The perveance of this device is also low and the current delivered does not appear to be sufficient to cope with the collected current at high ionospheric plasma densities.

## 8.4 VEHICLE ENVIRONMENT.

### 8.4.1 Neutral Pressure Gauge (NPG).

The NPG functioned well throughout flight. Figure 8-7 compares the pressure measurements made by the NPG with two models: the model represented by the solid line is the MSIS-86 model atmosphere for the time of flight (*Hedin*, 1987), and the model represented by the dashed line is what the NPG would measure in the MSIS-86 model atmosphere based on the vehicle velocity. The NPG measurement exceeded the model throughout flight, merging on reentry. The elevation in pressure is presumed to result from outgassing of the payload. The SPEAR-1 pressure measurement exhibited a similar profile.

Also evident in the NPG measurement are pressure enhancements associated with gas releases. The larger enhancements correspond to releases by the NGRS, and the smaller enhancements correspond to ACS jet firings. On closer inspection it is observed that the roll jets caused much larger enhancements than the pitch/yaw jets and that, of the pitch/yaw jets, only the one directly below the NPG caused any perceptible enhancements. These observations suggest that collisions with the vehicle play an important role in scattering the neutral gas into the NPG.

### 8.4.2 Langmuir Probe.

During most periods when no grounding devices were operating and the high-voltage sphere was shorted to the rocket body, the current characteristics of the Langmuir probe were close enough to classical curves to compute estimates of the electron density and temperature. Figure 8-8 plots estimates of the electron density, and Figure 8-9 plots estimates of the electron temperature. The electron density estimate appears to be quite reliable, and, at apogee, it agrees well with the density measured by the Wallops ionosonde. The electron temperature estimate in Figure 8-9 does not appear to be as reliable, being widely scattered between 500 and 1000 K, showing a tendency to peak near 200 km. A realistic temperature profile would be expected to increase monotonically at these altitudes.

A piecewise polynomial curve fit of the electron density deduced from the Langmuir probe data has been incorporated into the on-line SPEAR-3 database at Utah State University.

## SECTION 9
## CONCLUSIONS

The SPEAR-3 experiment performed well during its flight with the following exceptions:

(i) One TV telemetry link failed ~70 sec after lift-off

(ii) The hollow cathode plasma contactor current was low

(iii) There appeared to be a failure of some FED modules at initial switch-on

The grounding devices worked with varying degrees of effectiveness at different altitudes, which appears to be related to their current carrying capability to match the electron current collected by the positively biased sphere. In summary:

(i) The neutral gas release provided consistent grounding at all operational altitudes to a payload potential of ~ -230V using an 8g/sec flow rate.

(ii) The hollow cathode plasma contactor was unable to achieve grounding of the payload due to low emission current believed to have been caused by a poisoned hollow cathode.

(iii) The thermionic emitter was most effective at lower altitudes when the ionospheric plasma density was low and the emission current could match the sphere current.

(iv) The field emission device was found to be more effective later in the flight, again when the ionospheric plasma density was low. The low plasma density ascent data was affected by suspected module arcing when the payload was still outgassing heavily.

Early application of HV bias to the system showed evidence of local breakdown during the heavy outgassing period which prevented the full bias voltages from being achieved. This differed from the SPEAR-1 experience but is consistent with the much later, higher altitude of the initiation of biasing on the SPEAR-1 flight. SPEAR-1 did show a similar breakdown late in the flight upon re-entry.

SPEAR-3 provided much valuable data on grounding devices and the associated HV-space environment interaction. Together with the SPEAR-1 data this provides a good indicator of these effects from a slow moving space platform. The next major advance in this area of study will come from the measurement of HV-environment interactions from orbital platforms. The transition from subsonic to supersonic (for ions) has a significant effect on ion collection, and new experimental data needs to be taken. Also the initial outgassing of sounding rockets due to their short exposure to the upper atmosphere clearly has a significant influence on the HV interaction.

The generation of the HV for biasing can conveniently be developed on orbital platforms by the use of electrodynamic tethers. We hope to see more experiments beyond those currently planned in this area in the next few years. Finally, the practical applications of the results of HV interaction studies are primarily going to be applied to orbiting systems, so it is time to move into this domain with our experiments.

## SECTION 10
## REFERENCES


Berg, G. A., W. J. Raitt, D. C. Thompson, B. E. Gilchrist, N. B. Myers, P. Rodriquez, C. L. Siefring, H. R. Anderson, D. W. Potter, Overview of the effects of neutral gas releases on high-voltage sounding rocket platforms, *Advances in Space Research, 15*, 12, (12)83-(12)86, 1995.(U)

Hedin, A. E., MSIS-86 Thermospheric model, *J. Geophys. Res., 92*, 4649, 1987.(U)

Raitt, W. J., G. Berg, D. Thompson, A. B. White, B. Peterson, M. Roosta, M. Jensen, L. Allen, J. Antoniades, P. Rodriguez, C. Siefring, H. Anderson, D. Potter, J. Jost, R. Adamo, D. Dana, C. Holland, J. Pickett, R. Merlino, M. Adrian, N. Grier, N. Poirier and R. Morin, SPEAR-3: A sounding rocket experiment to study methods of electrically discharging a negatively charged space platform at LEO altitudes, J. Spacecrafts and Rockets, 1995a.(U)

W. J. Raitt, G. A. Berg, D. C. Thompson and S. Sazykin, Measurements of electrical breakdown in the vicinity of a sounding rocket differentially charged to 10 kV, *Advances in Space Research, 15,* 12, (12)79-(12)82, 1995b.(U)

Siefring, C. L., P. Rodriguez, M. M. Baumback, J. A. Antoniades, and D. N. Walker, A method for measuring large changes in the payload voltage of rockets and satellites, submitted to *Reviews of Scientific Instruments*, 1995.(U)

Thompson, D. C., W. J. Raitt, G. A. Berg, Transient measurements of HV interaction with the ambient and perturbed space environment, *Advances in Space Research, 15,* 12, (12)91-(12(94), 1995.(U)

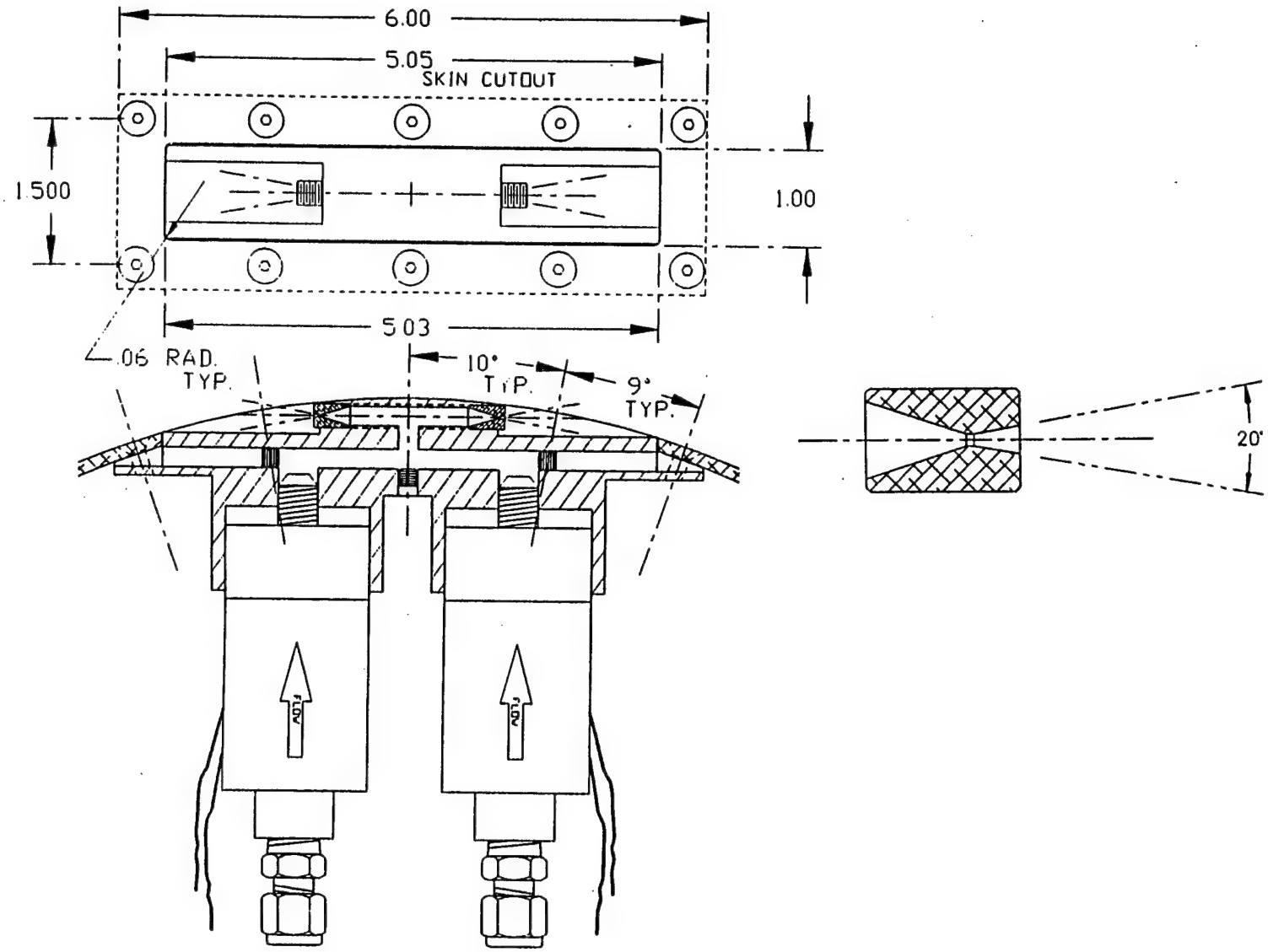


Figure 3-1. Assembly drawing of a nozzle block from the neutral gas release system and an enlarged view of a single screw-in nozzle.

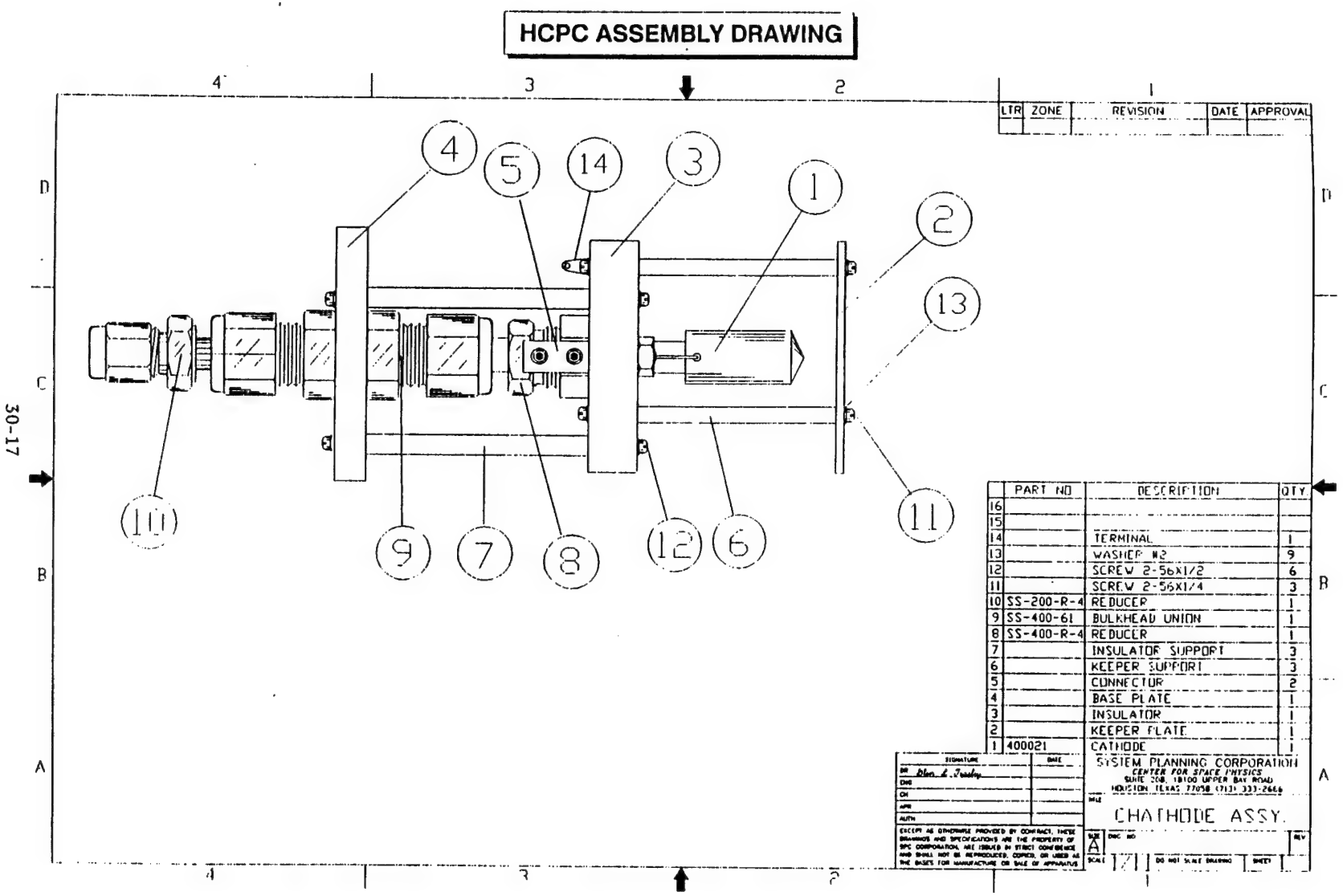


Figure 3-2. Assembly drawing of the cathode for the hollow cathode plasma contactor.

# THERMIONIC EMITTER FILAMENT ASSEMBLY
## (Semicon Part #LRF003)

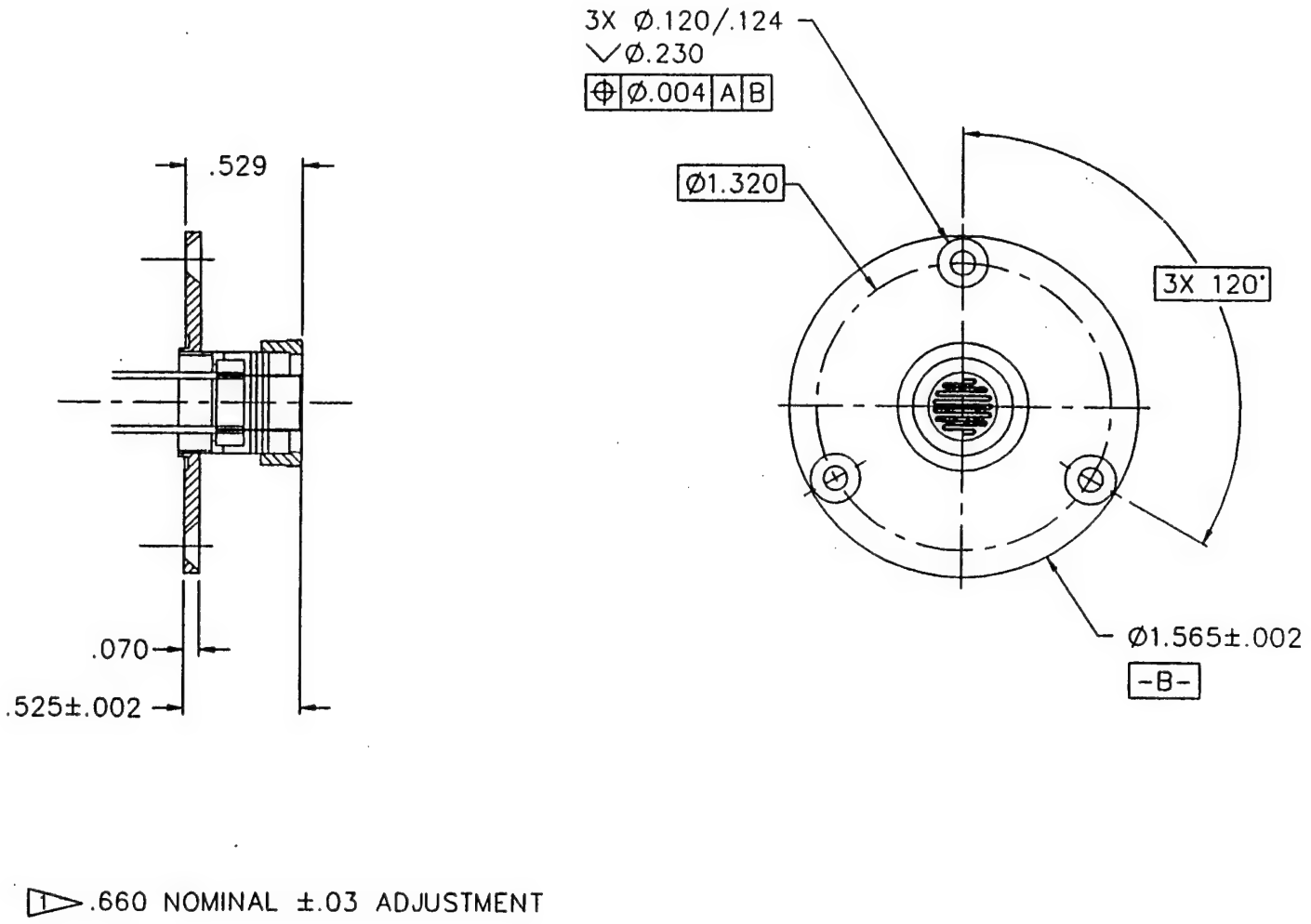


Figure 3-3. Assembly drawing of the thermionic emitter filament.

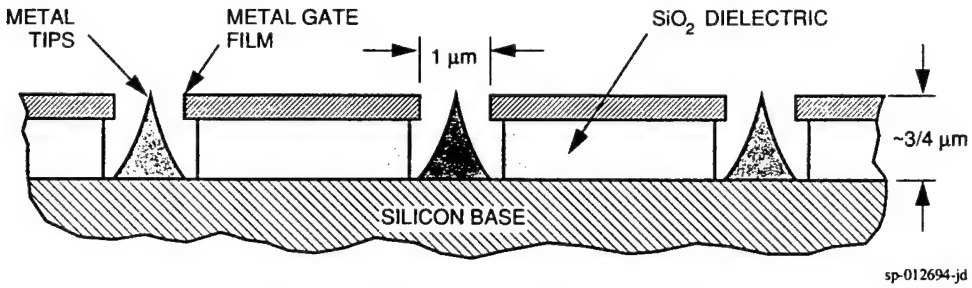


(a) SCHEMATIC OF A SPINDT CATHODE ARRAY

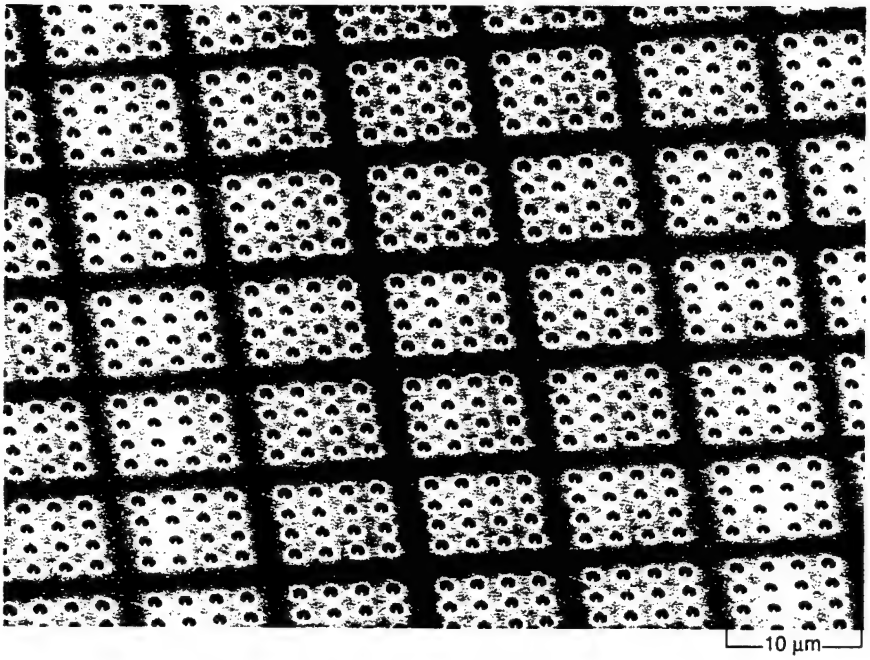


(b) SEM MICROGRAPH OF SPINDT CATHODE ARRAY

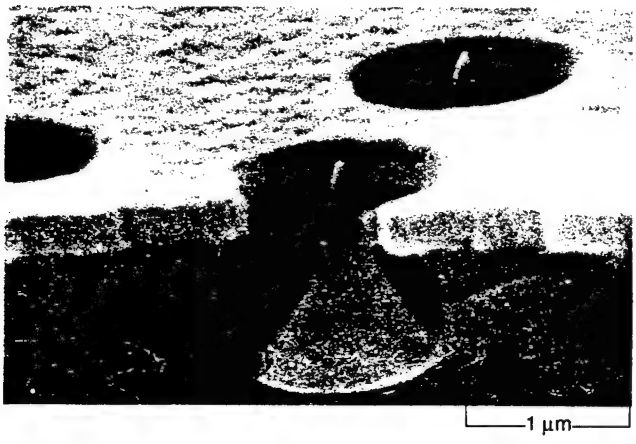


(c) SEM MICROGRAPH OF SPINDT CATHODE

Figure 3-4. (a) Schematic illustration of enlarged view of an FED array. (b) Micrograph of a region from an FED array. (c) Micrograph of a single FED cathode.

# DIFFERENTIAL CHARGE DEVICE BLOCK DIAGRAM

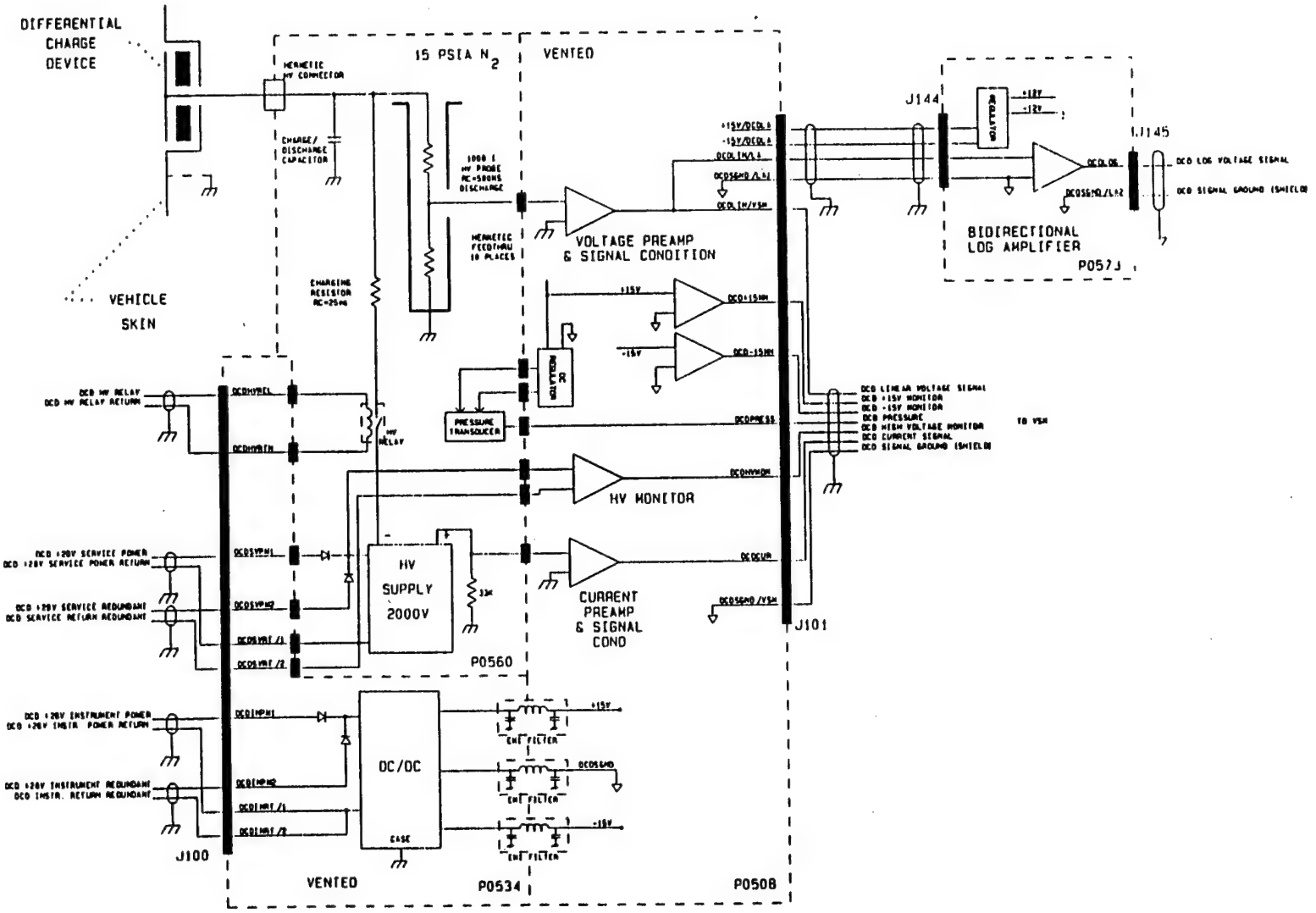


Figure 3-5. Electrical block diagram of the differential charge device.

# DIFFERENTIAL CHARGING DEVICE

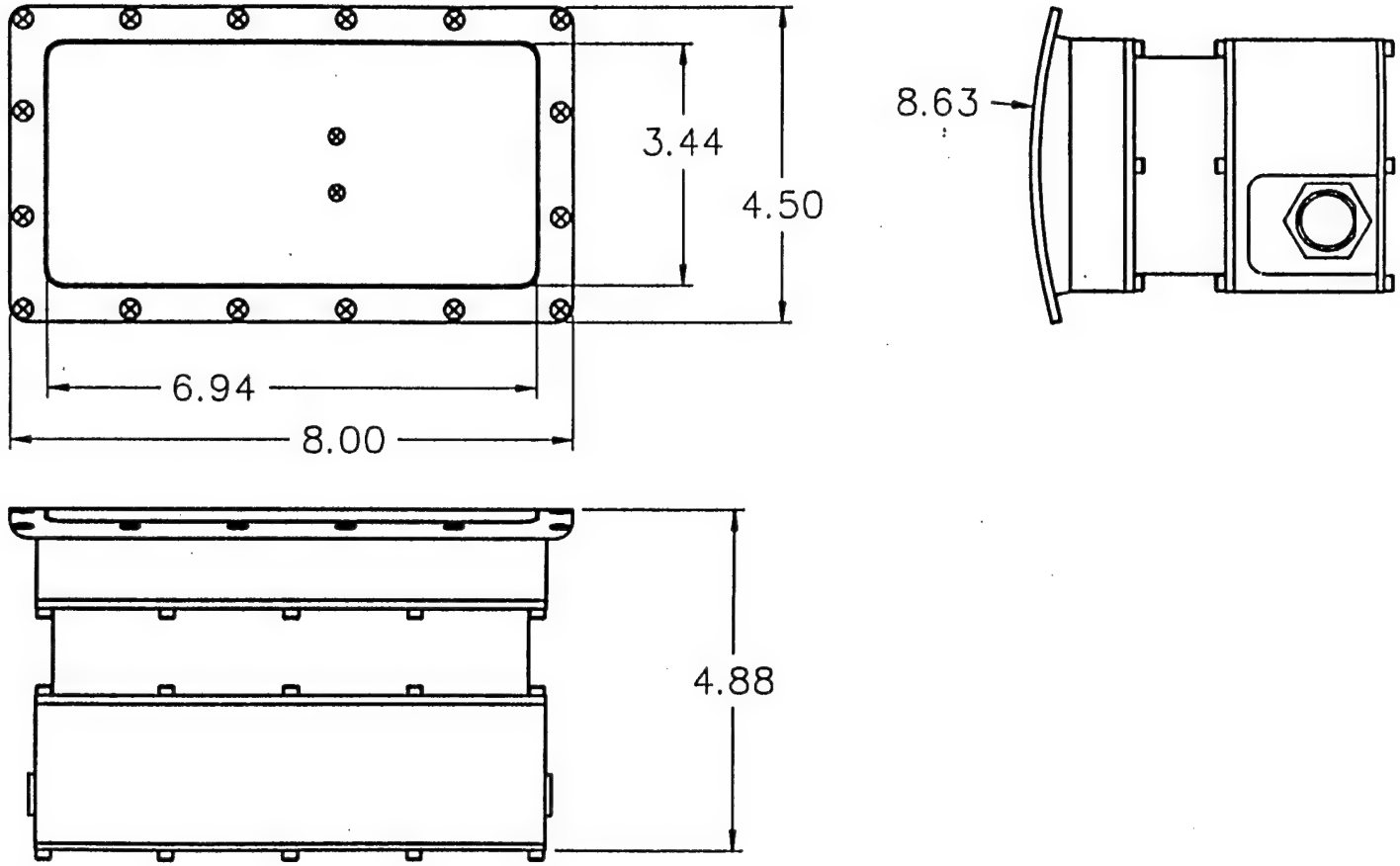


Figure 3-6. Assembly drawing of the differential charge device.

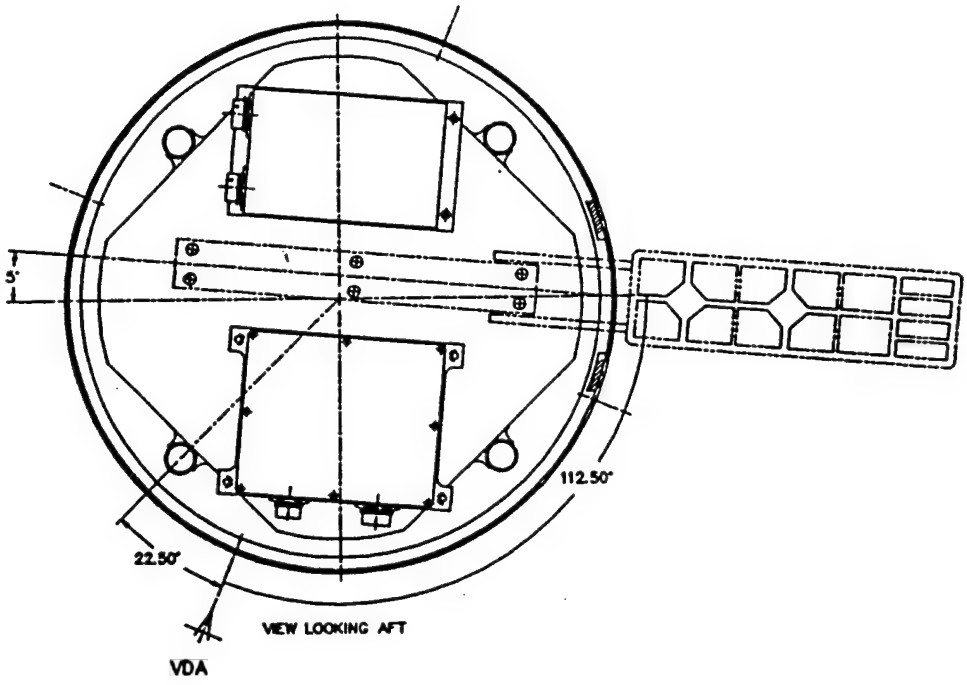


Figure 3-7. Deployed position of the solar cell system.

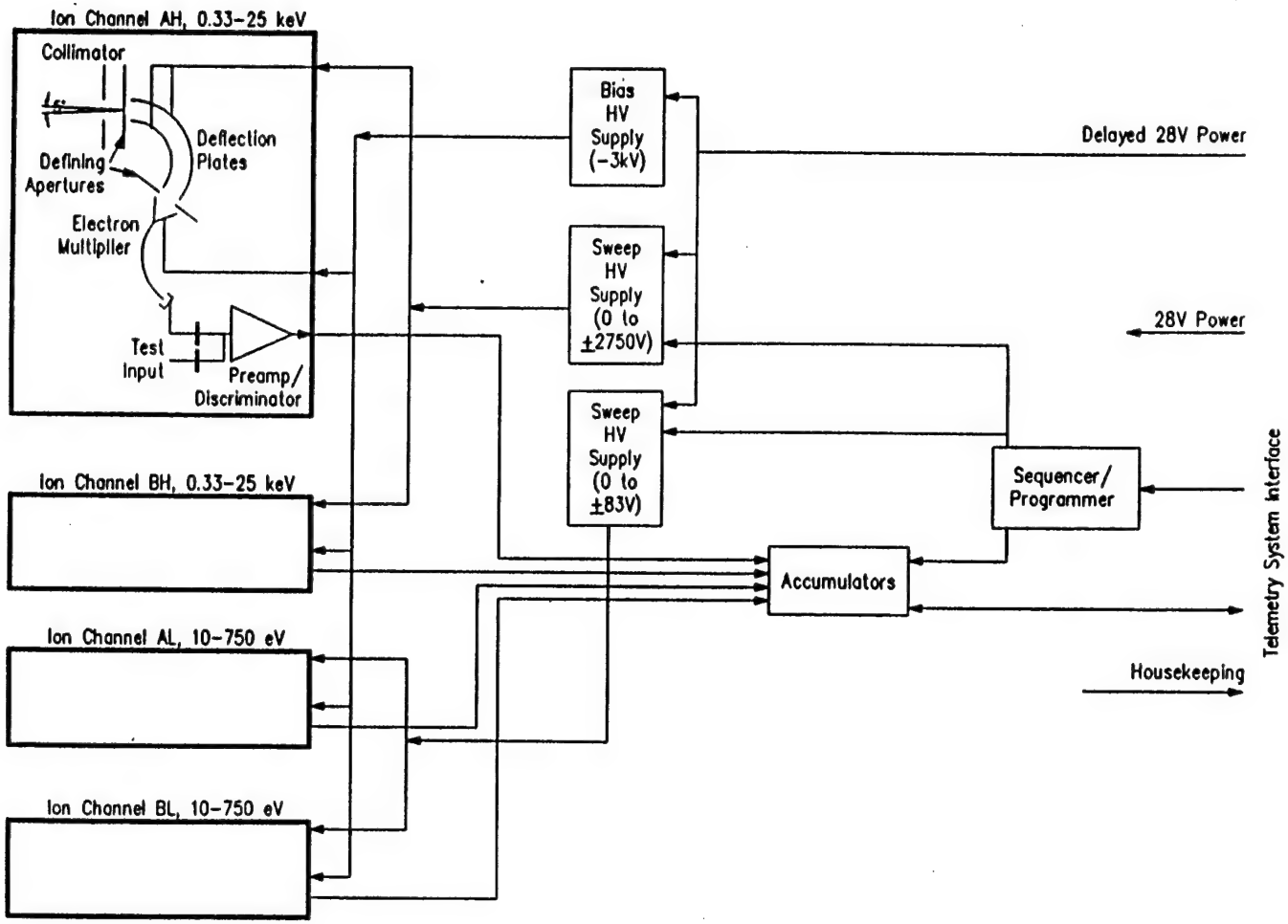


Figure 3-8. Block diagram of the electrostatic analyzer.

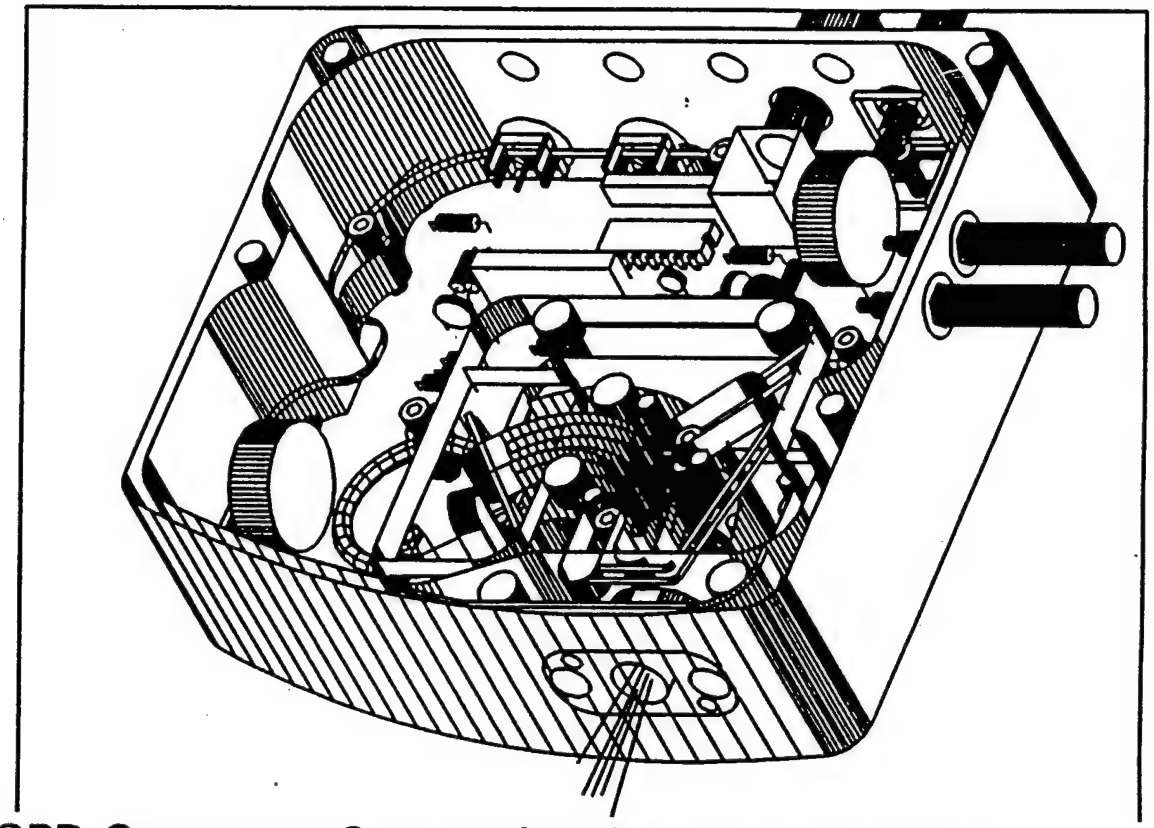


Figure 3-9. Drawing of an assembled ESA sensor.

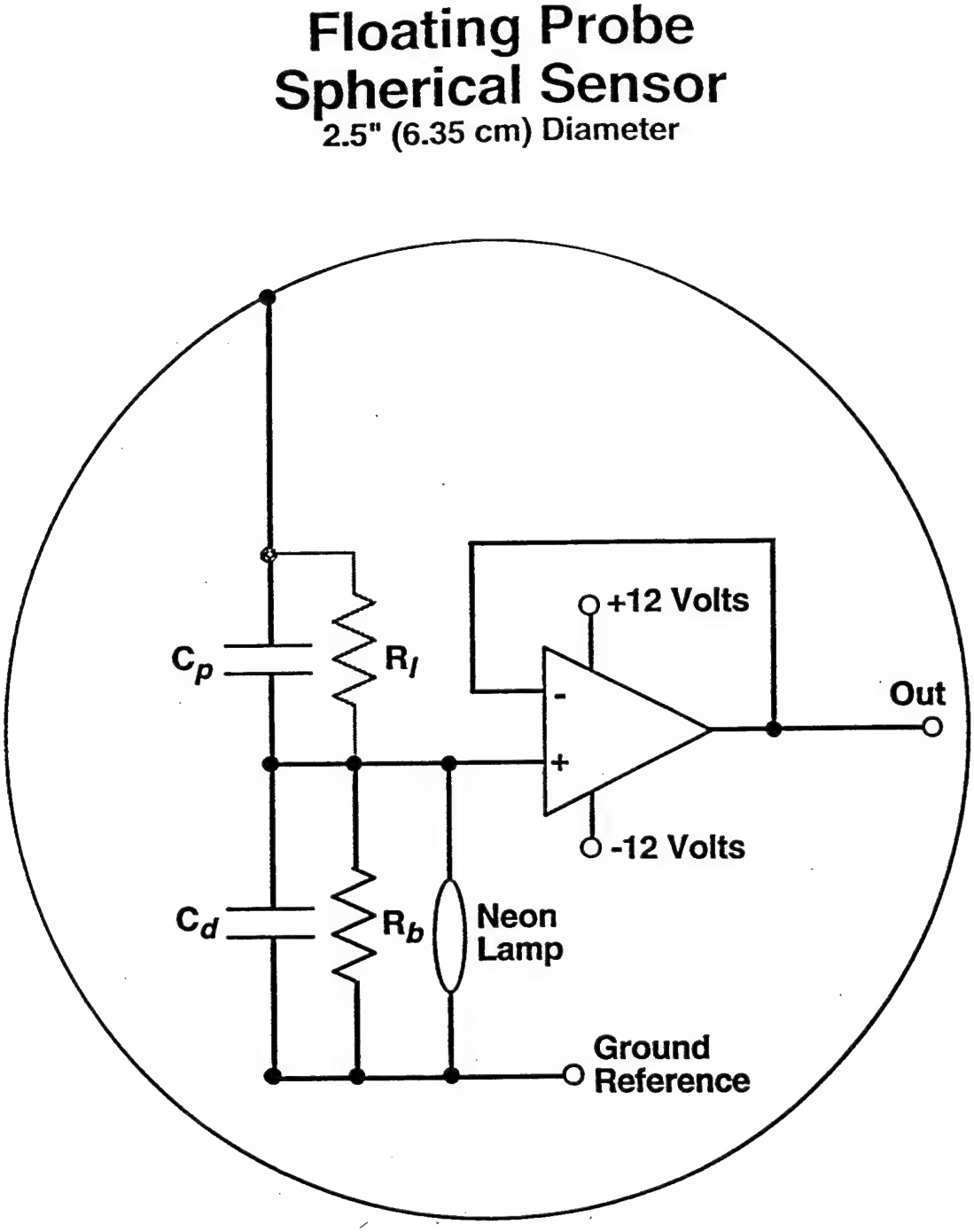


Figure 3-10. Circuit diagram of the floating probe sensor.

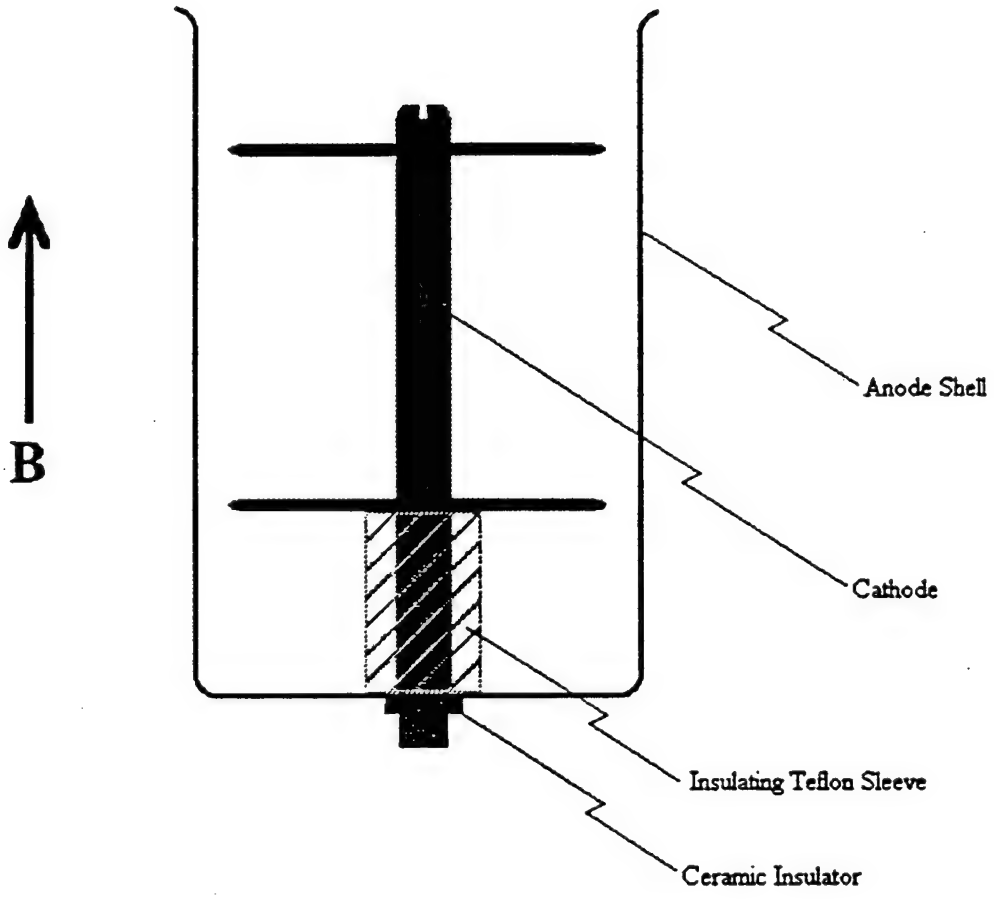


Figure 3-11. Schematic drawing of the magnetron sensor used in the neutral pressure gauge.

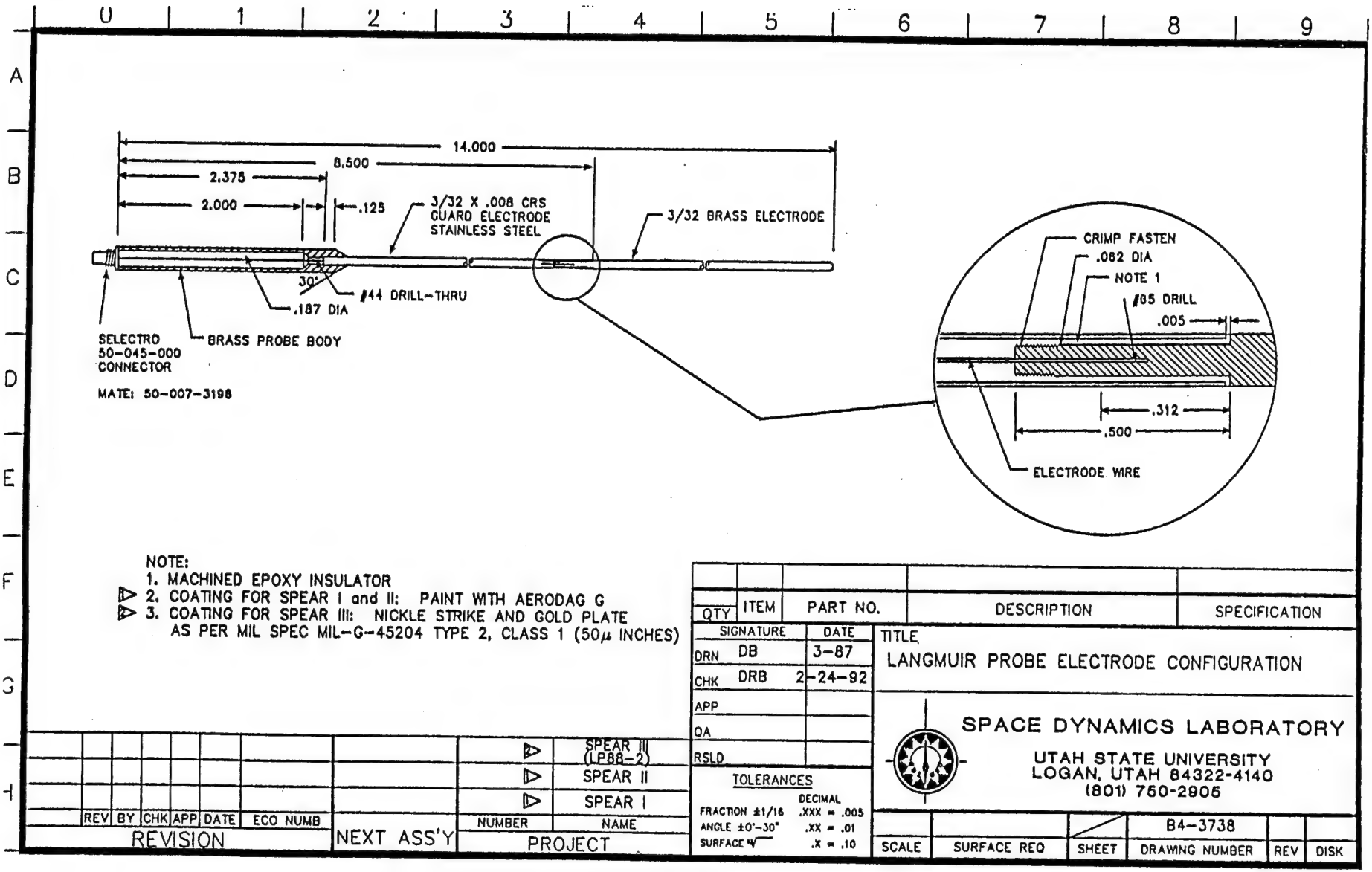


Figure 3-12. Assembly drawing of the Langmuir probe electrode configuration.

# SKIN CURRENT PROBE #1 BLOCK DIAGRAM

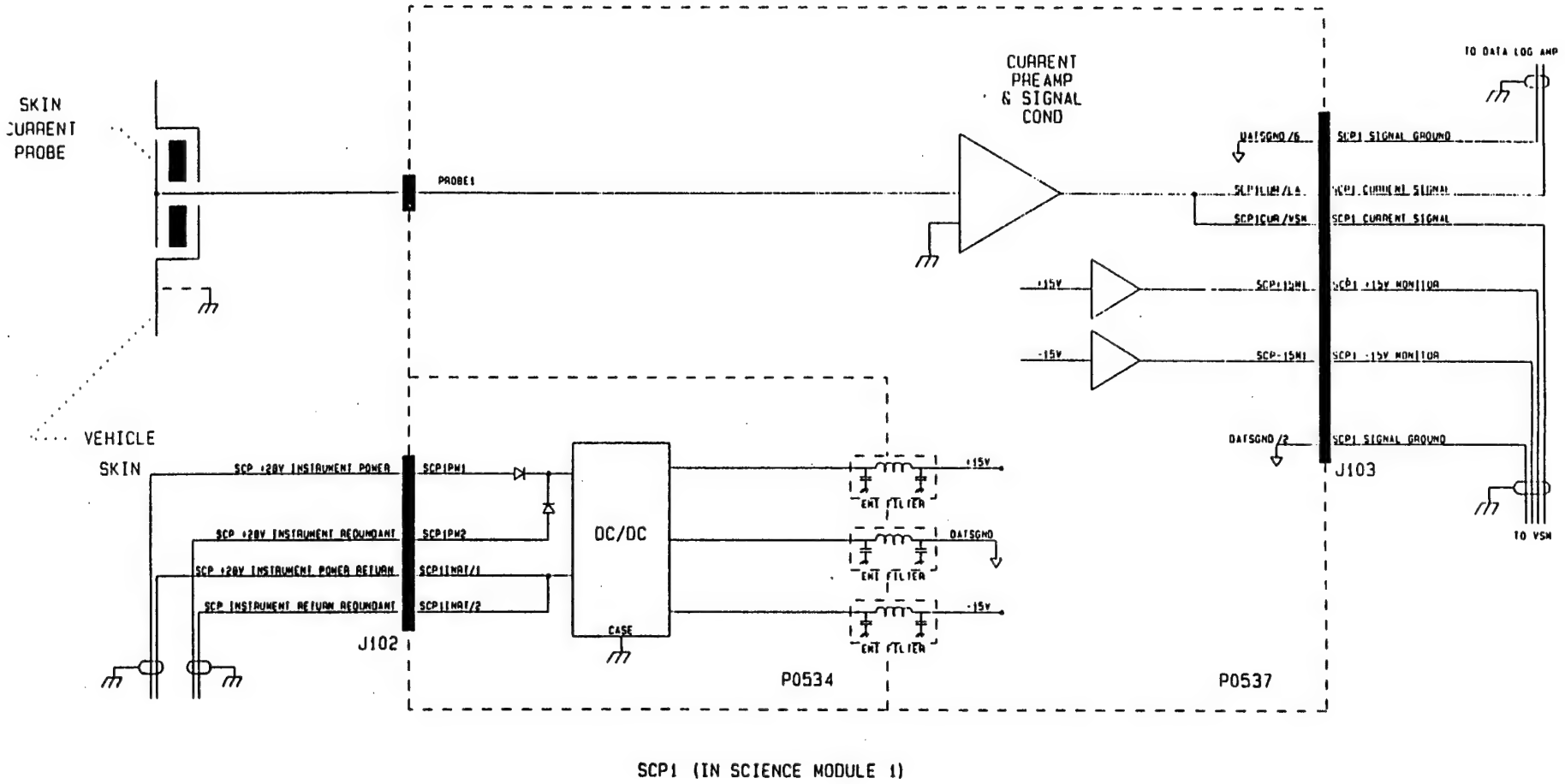


Figure 3-13. Electrical block diagram of skin current probe #1.

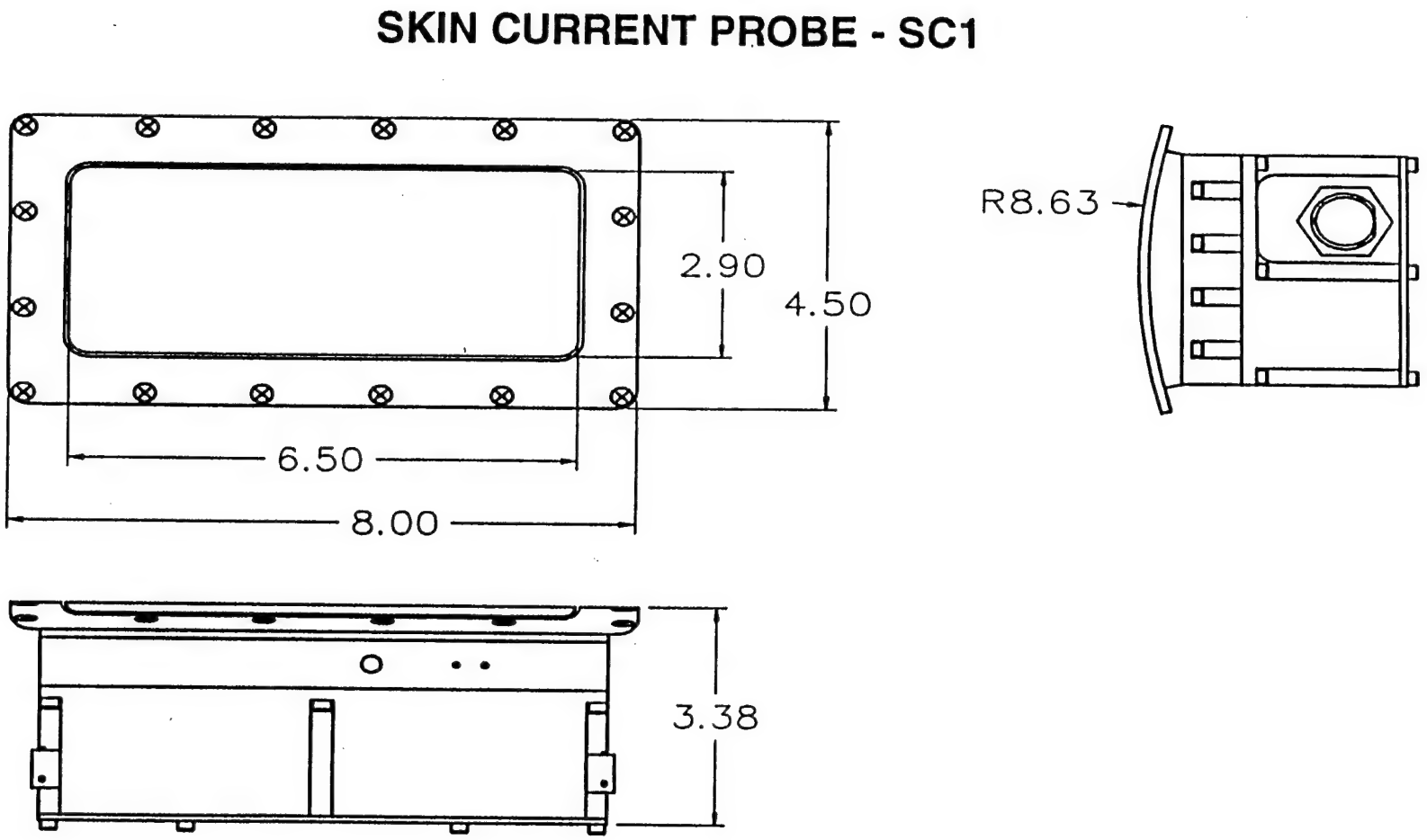


Figure 3-14. Assembly drawing of skin current probe #1.

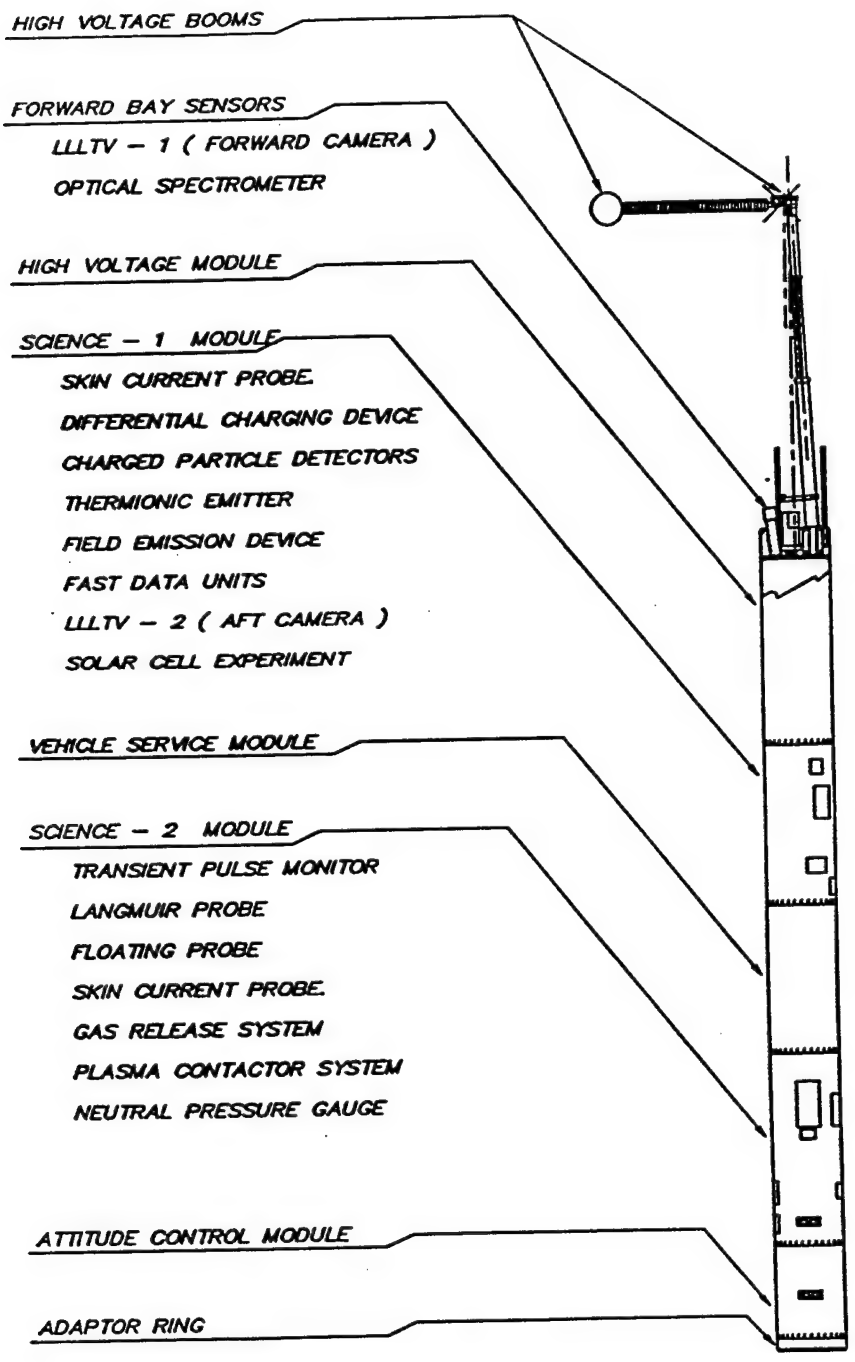


Figure 3-15. Instrument arrangement for SPEAR-3 payload.

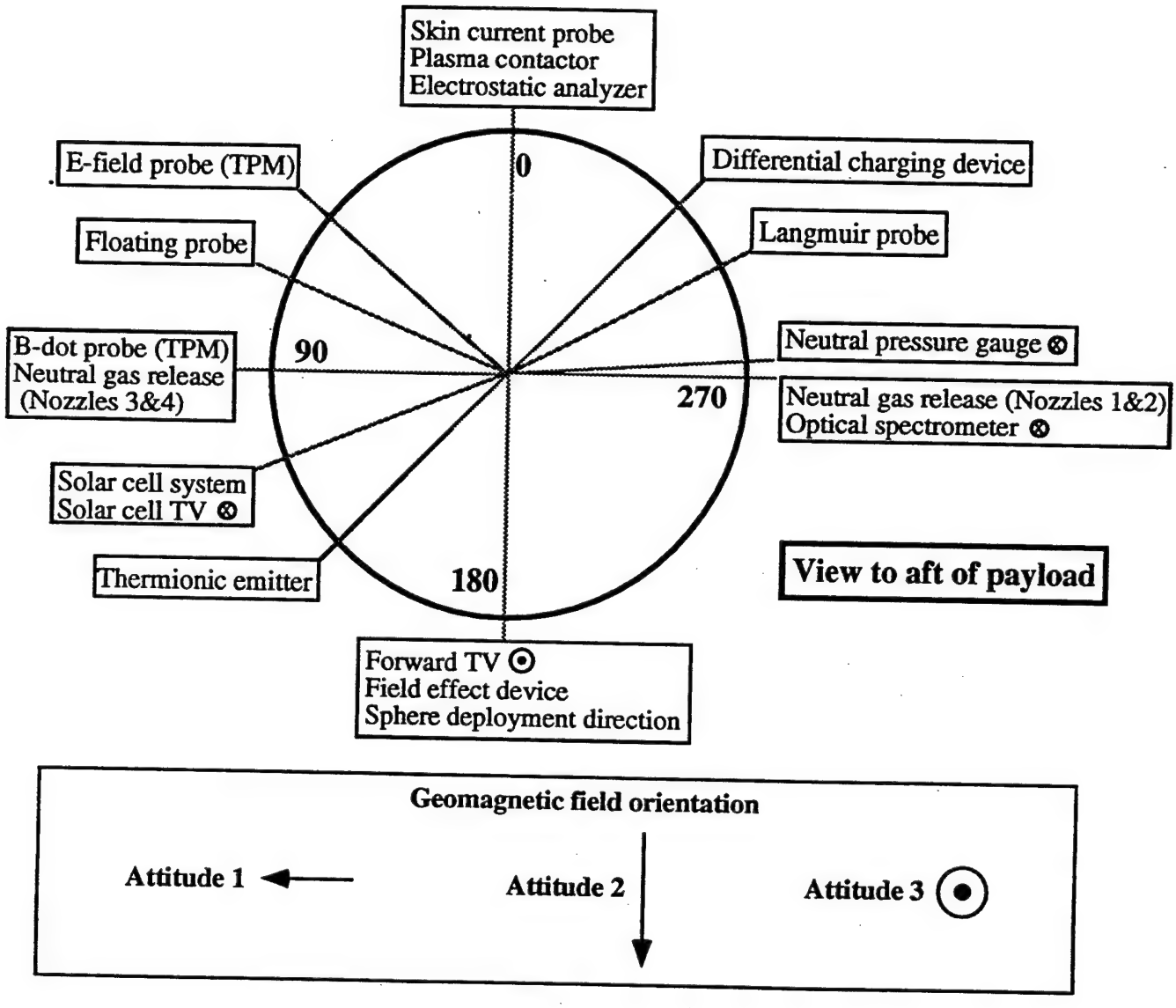


Figure 3-16. Azimuthal orientation of SPEAR-3 instruments with external access/viewing.

# SPEAR-3
# Electro-mechanical arrangement

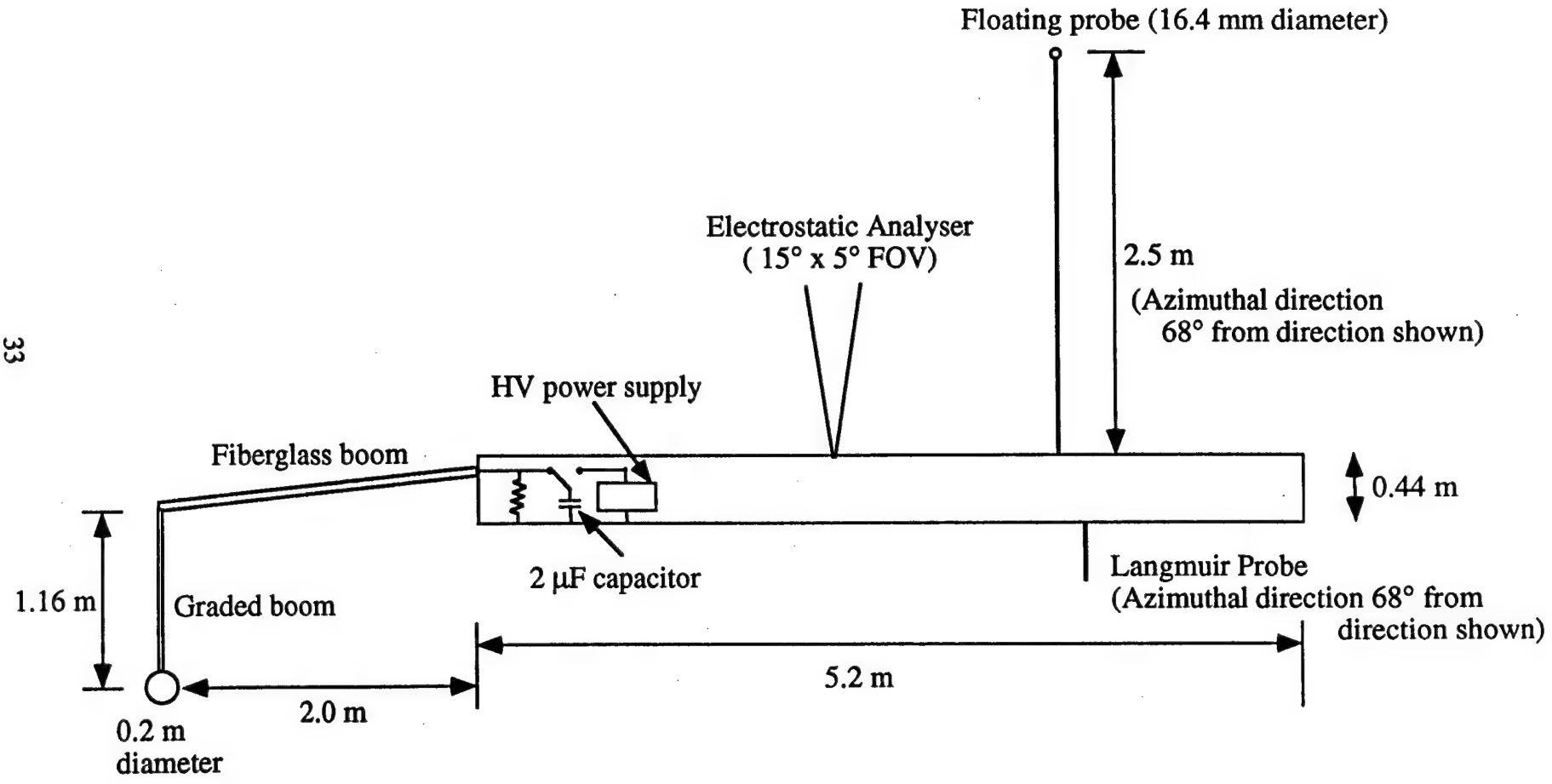


Figure 5-1. Electro-mechanical arranagement for SPEAR-3 biasing.

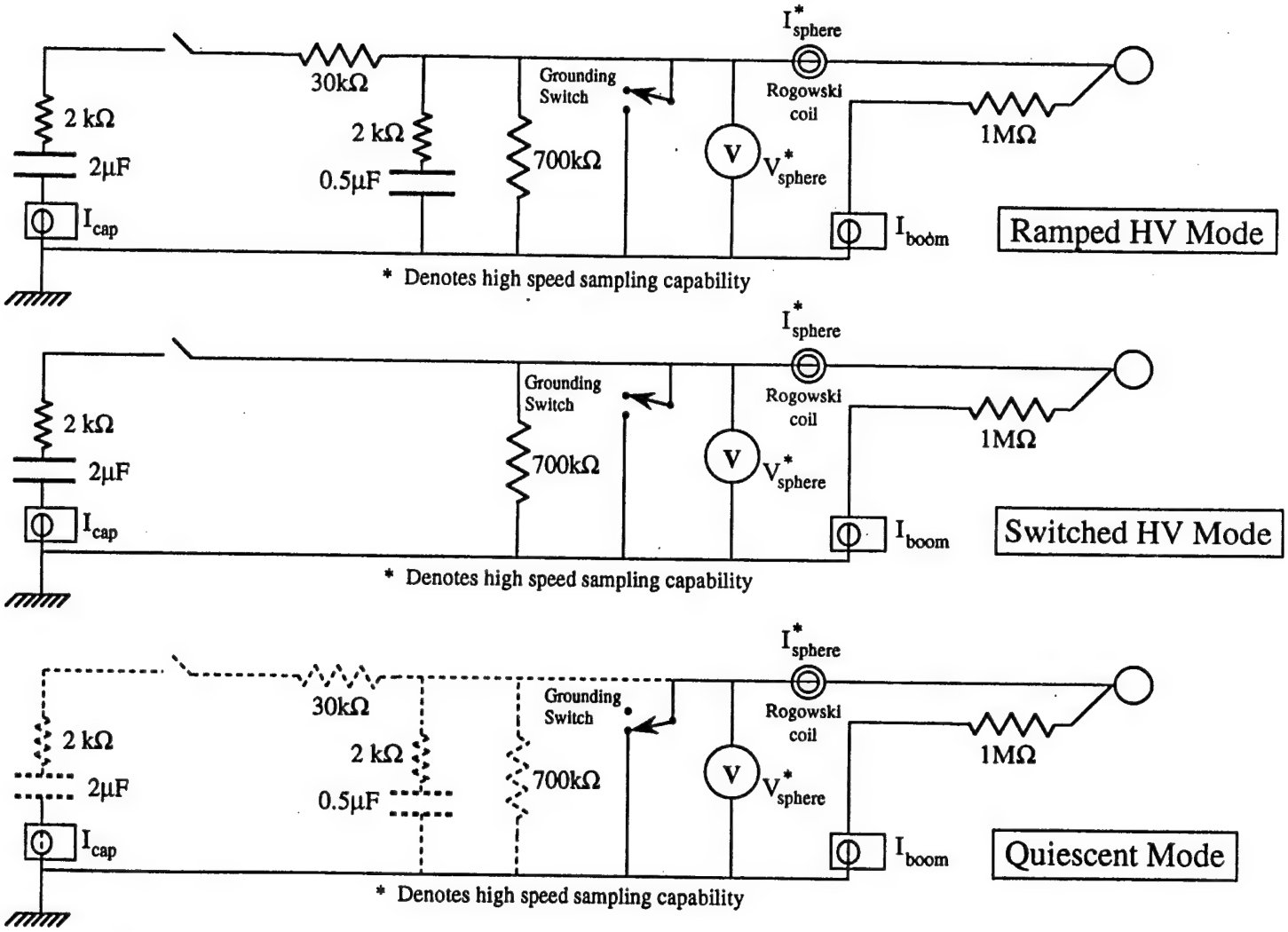


**Simplified Schematic Diagrams of HV Capacitor Discharge Modes and Quiescent Mode**

Figure 5-2. Simplified electrical schematic of ramped and switched HV modes.

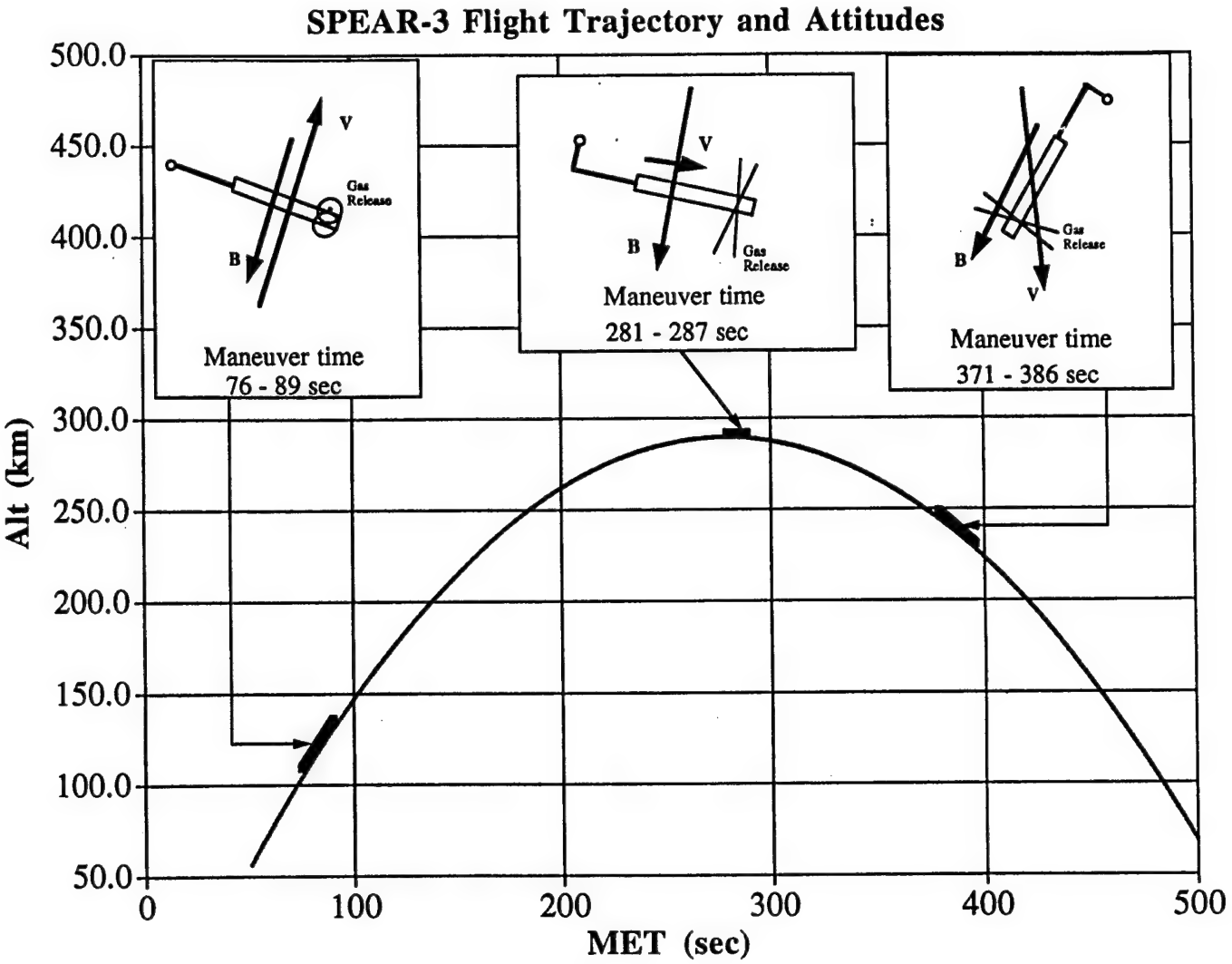


Figure 6-1. SPEAR-3 flight altitude trajectory and payload orientations.

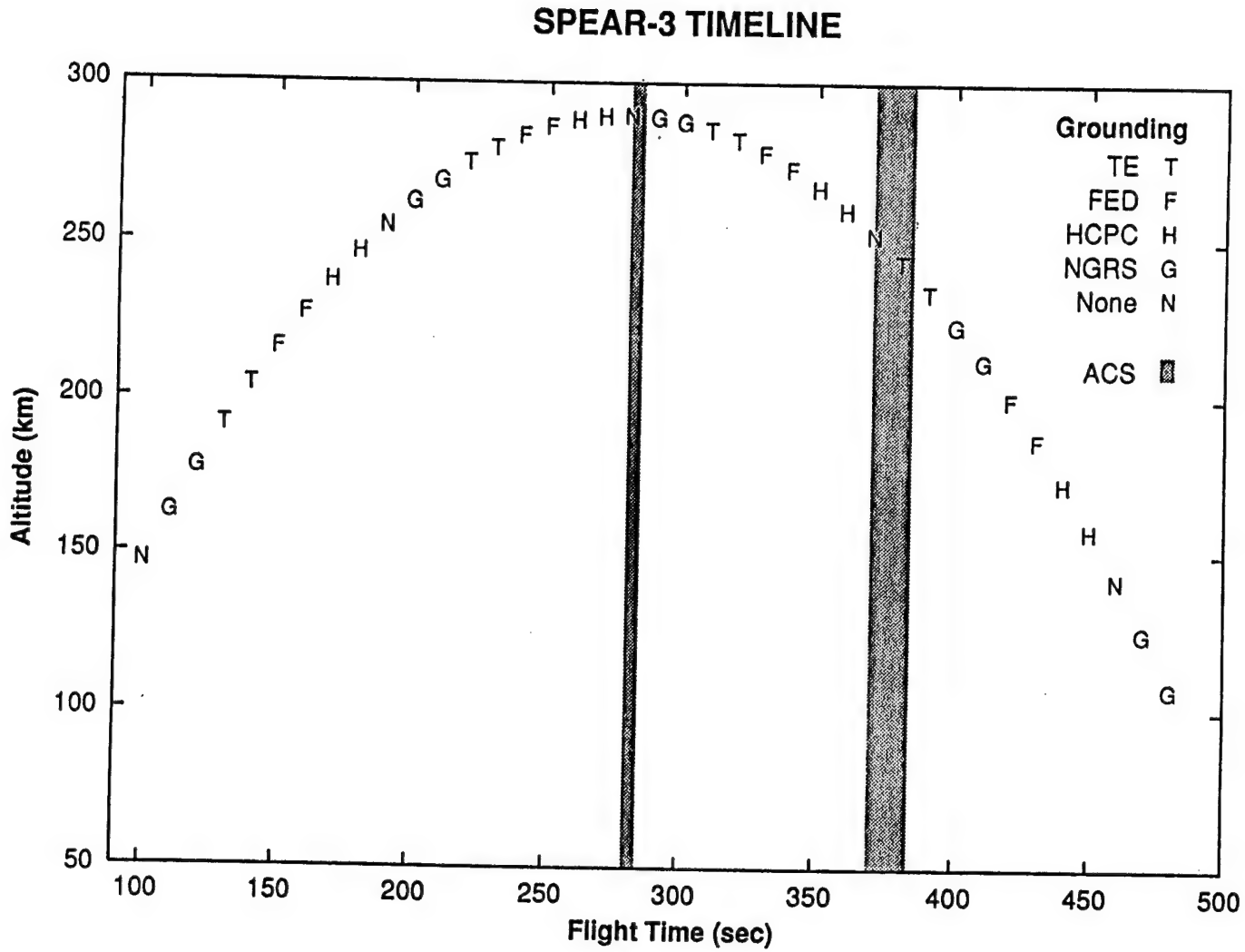


Figure 7-1. Timeline of grounding device operations.

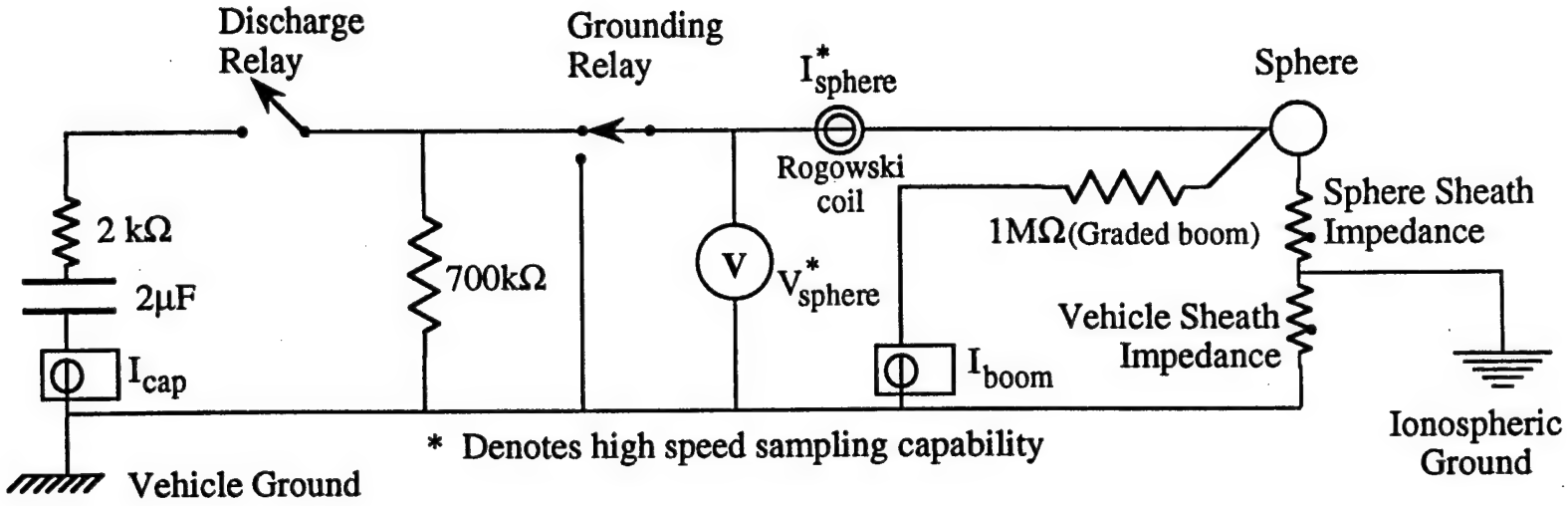


**Simplified Schematic Diagram of HV System Showing Plasma Sheath Impedances**

Figure 8-1. Simplified electrical schematic of HV system showing sheath impedances.

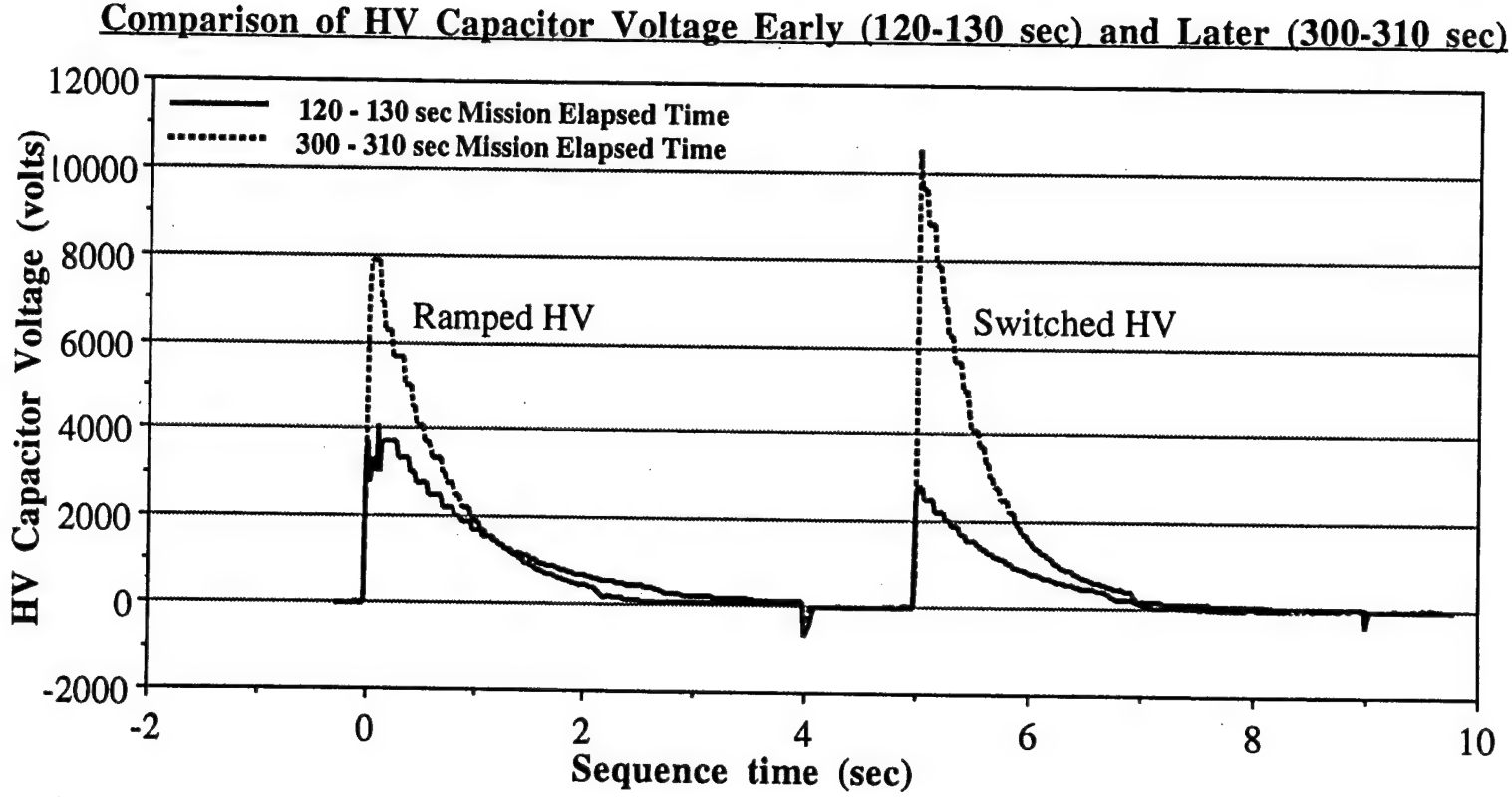


Figure 8-2. Variation of HV capacitor voltage for early (solid line) and later (broken line) periods in the flight.

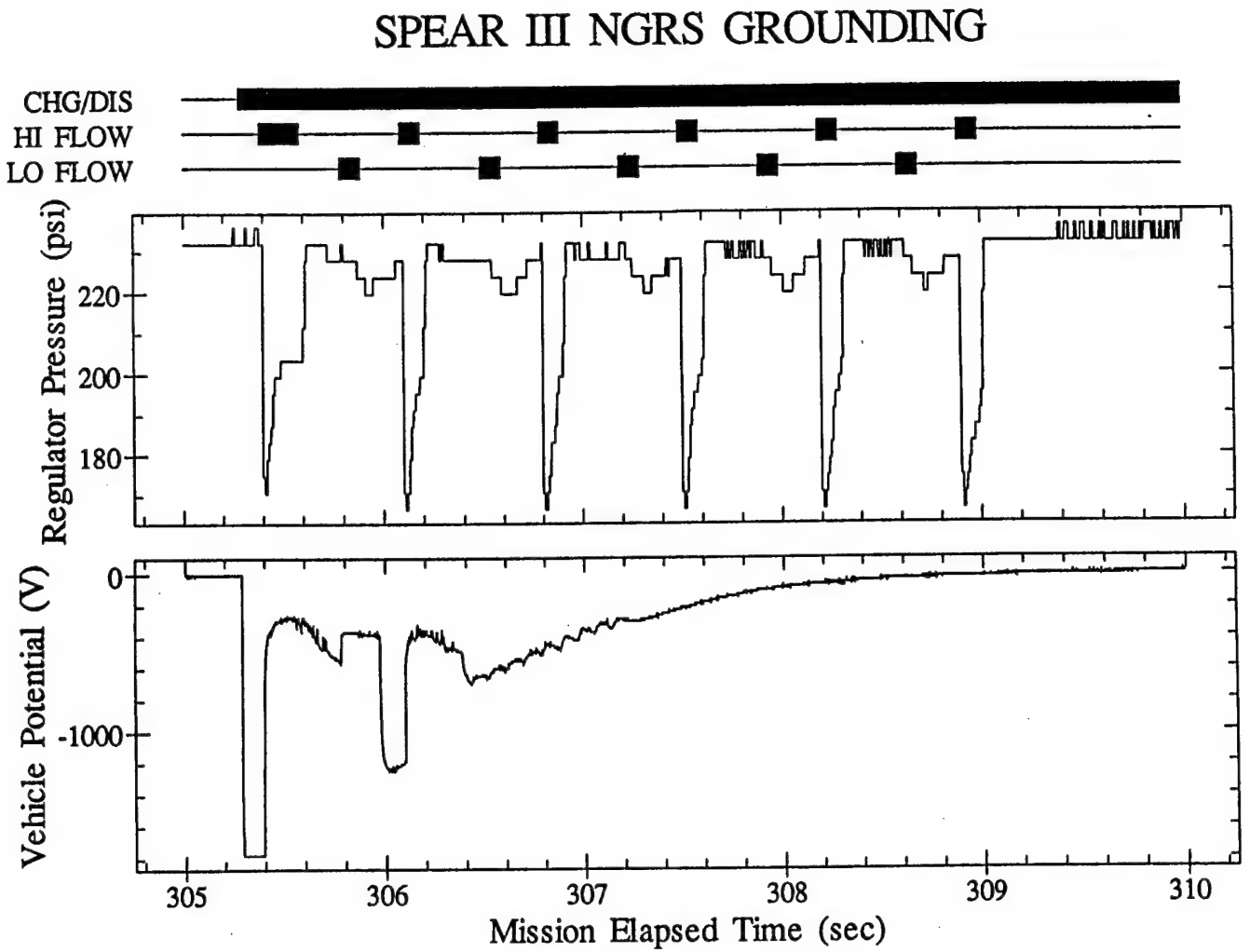


Figure 8-3. Variation of vehicle potential as a function of time when the neutral gas release system was active.

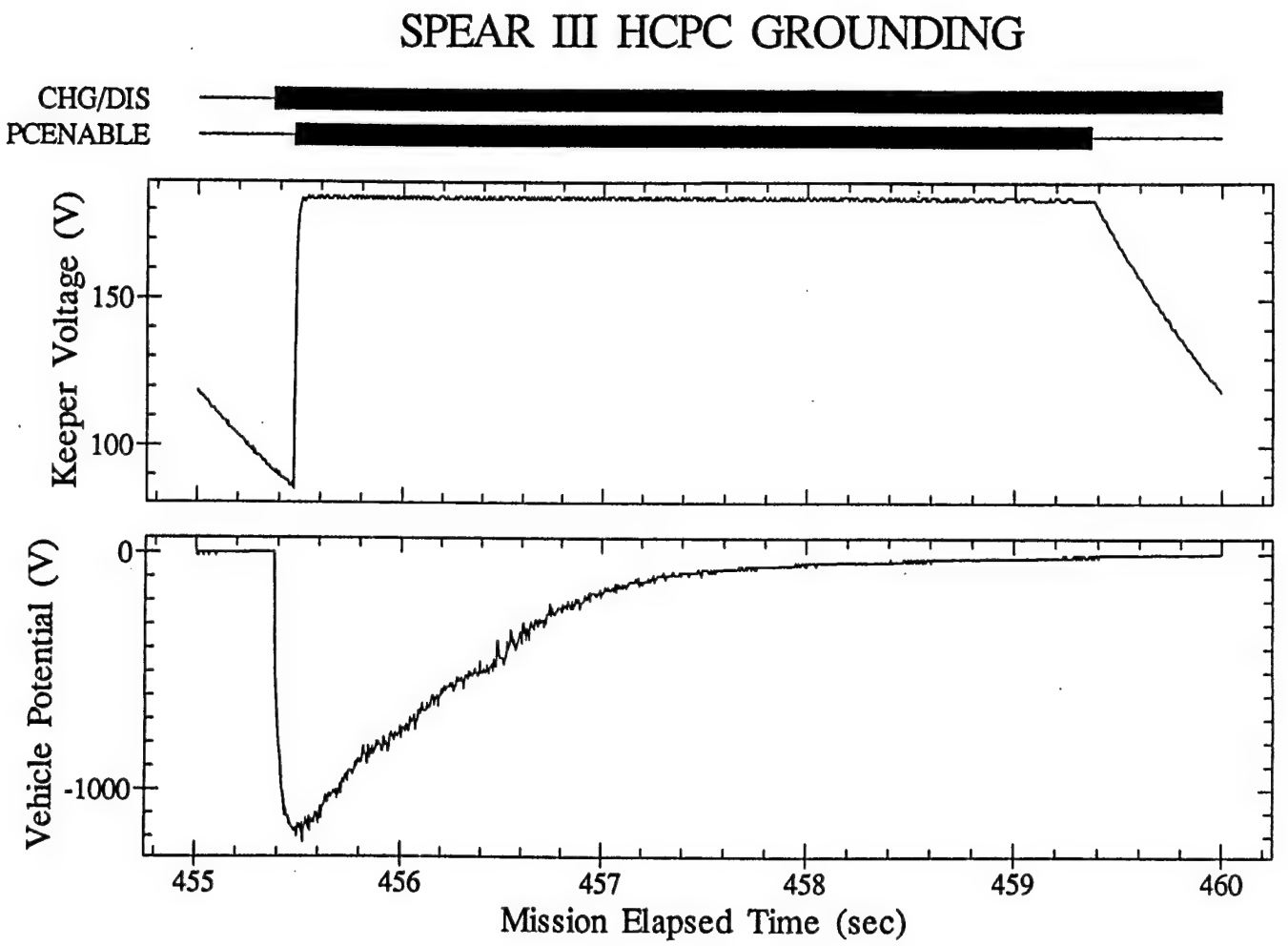


Figure 8-4. Variation of vehicle potential as a function of time when the hollow cathode plasma contactor was active.

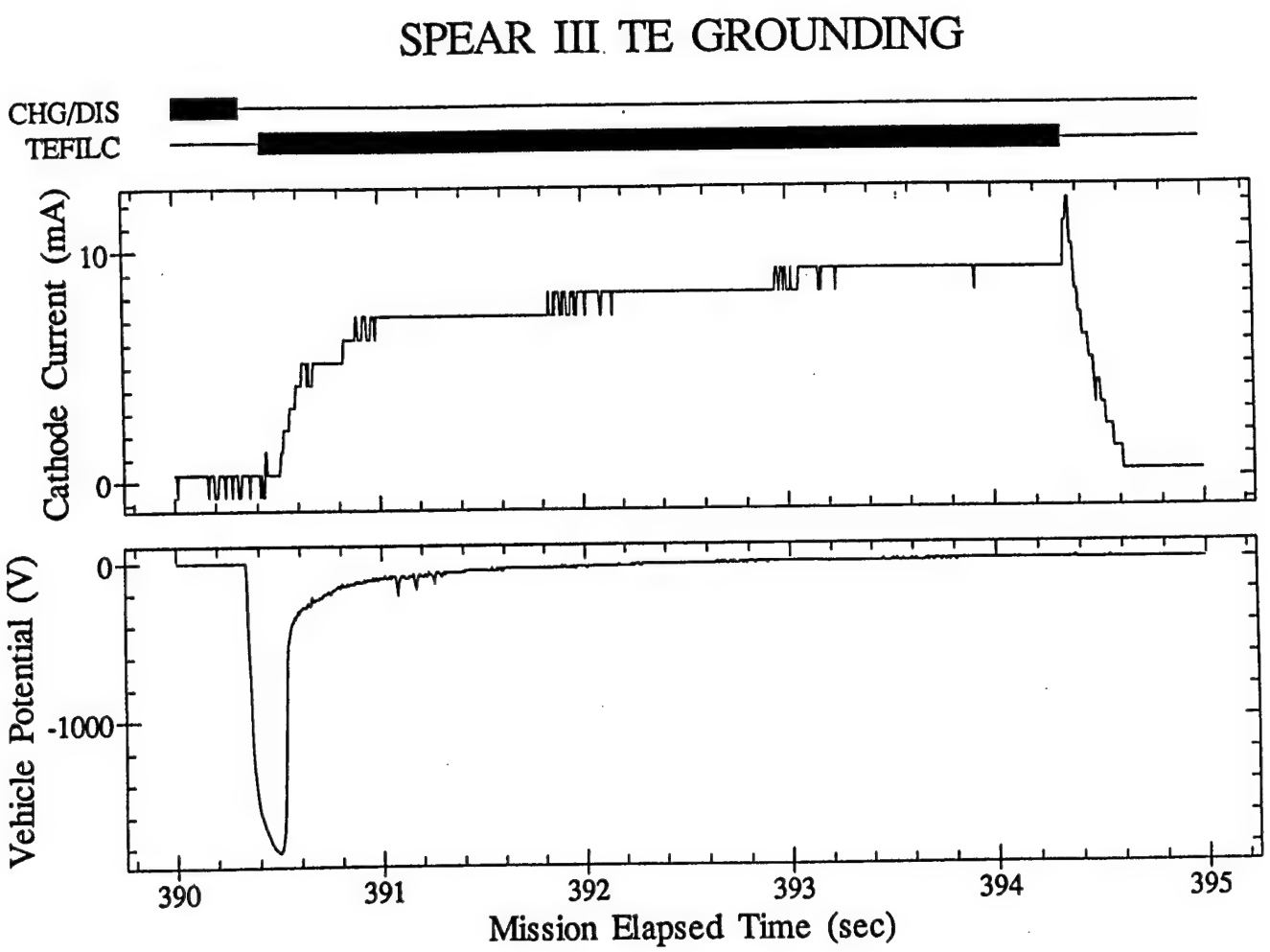


Figure 8-5. Variation of vehicle potential as a function of time when the thermionic emitter was active.

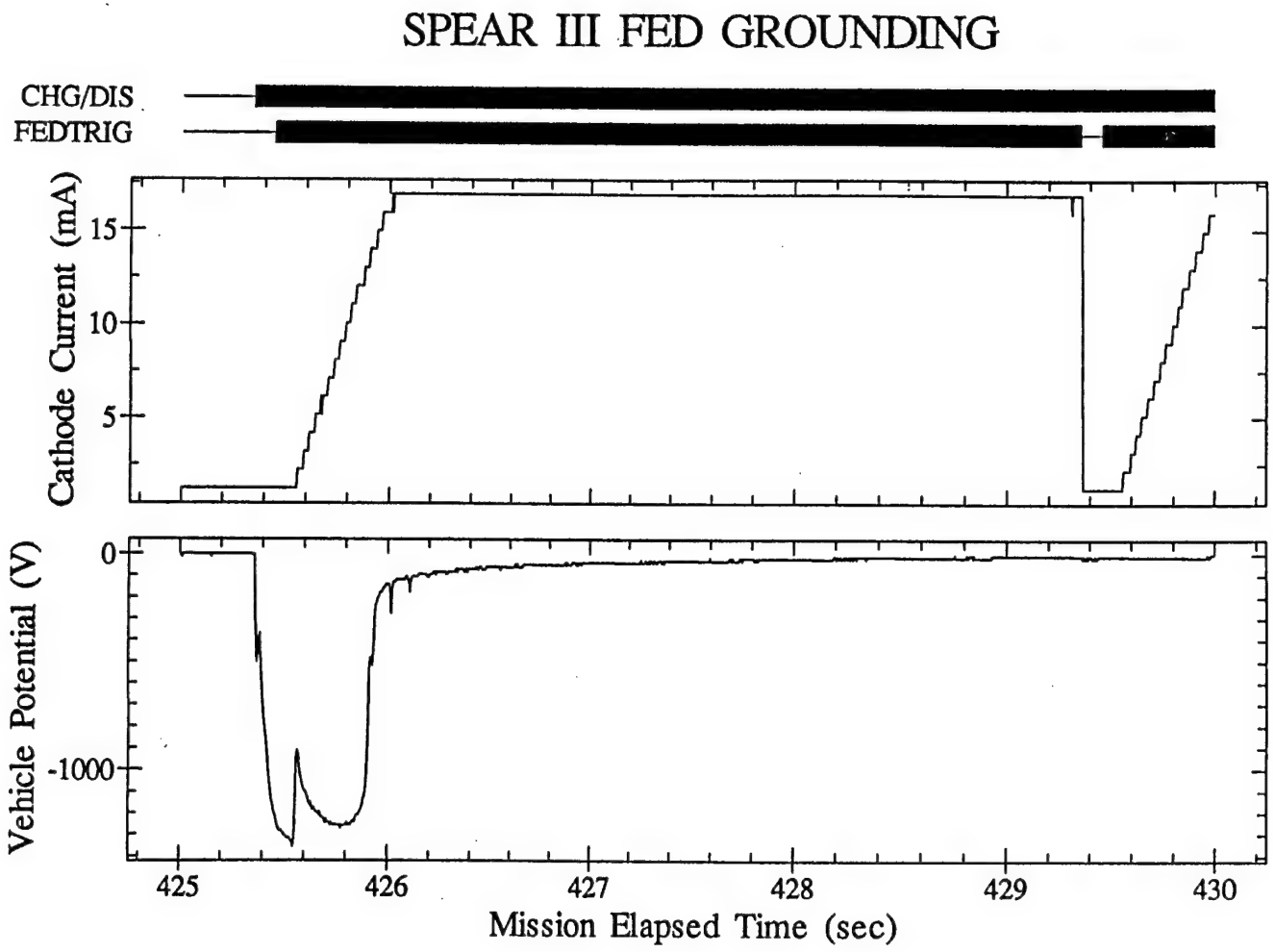


Figure 8-6. Variation of vehicle potential as a function of time when the field effect device was active.

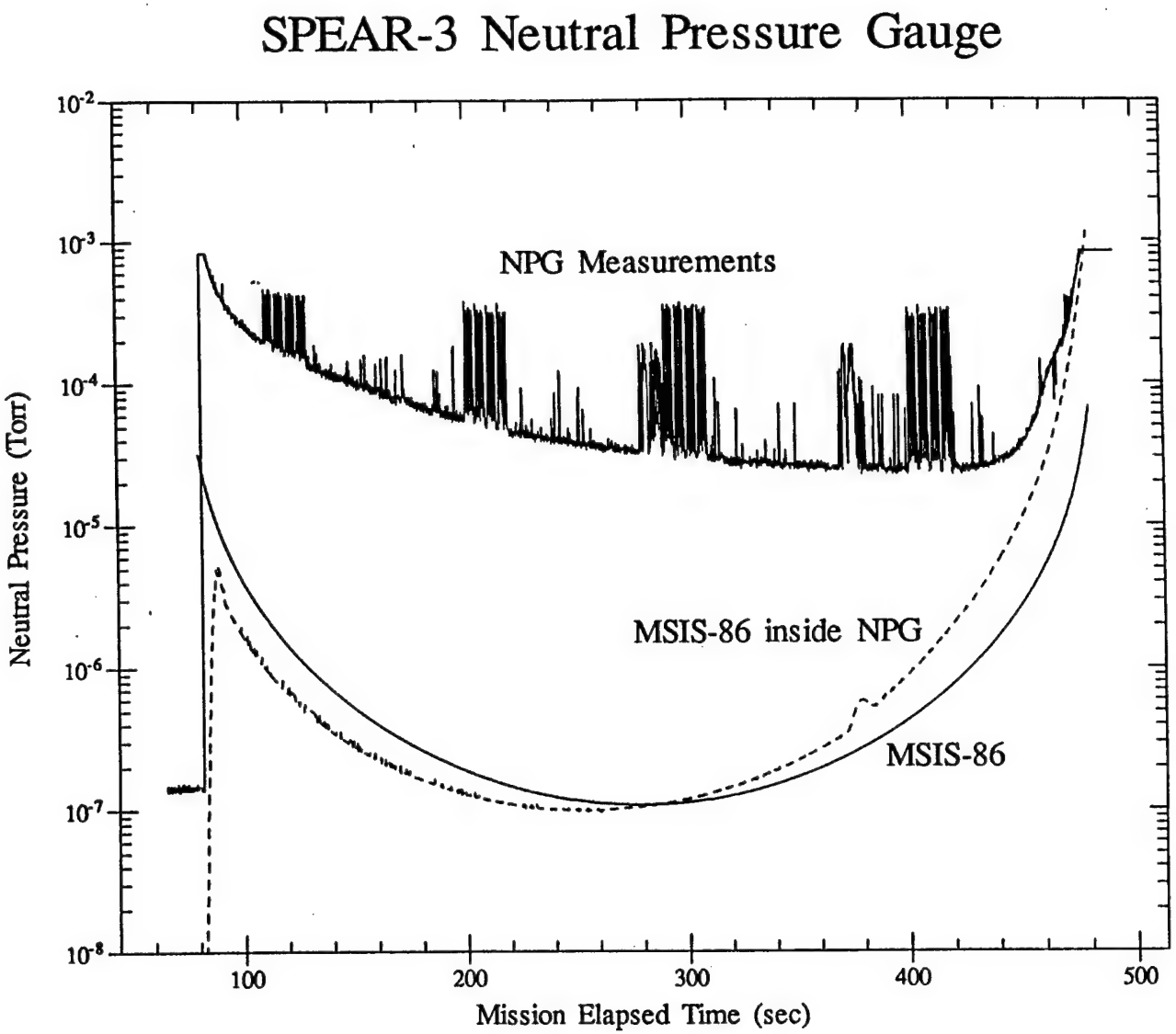


Figure 8-7. Comparison of neutral pressure gauge meausrements with the MSIS-86 model atmosphere outside the gauge and inside the gauge.

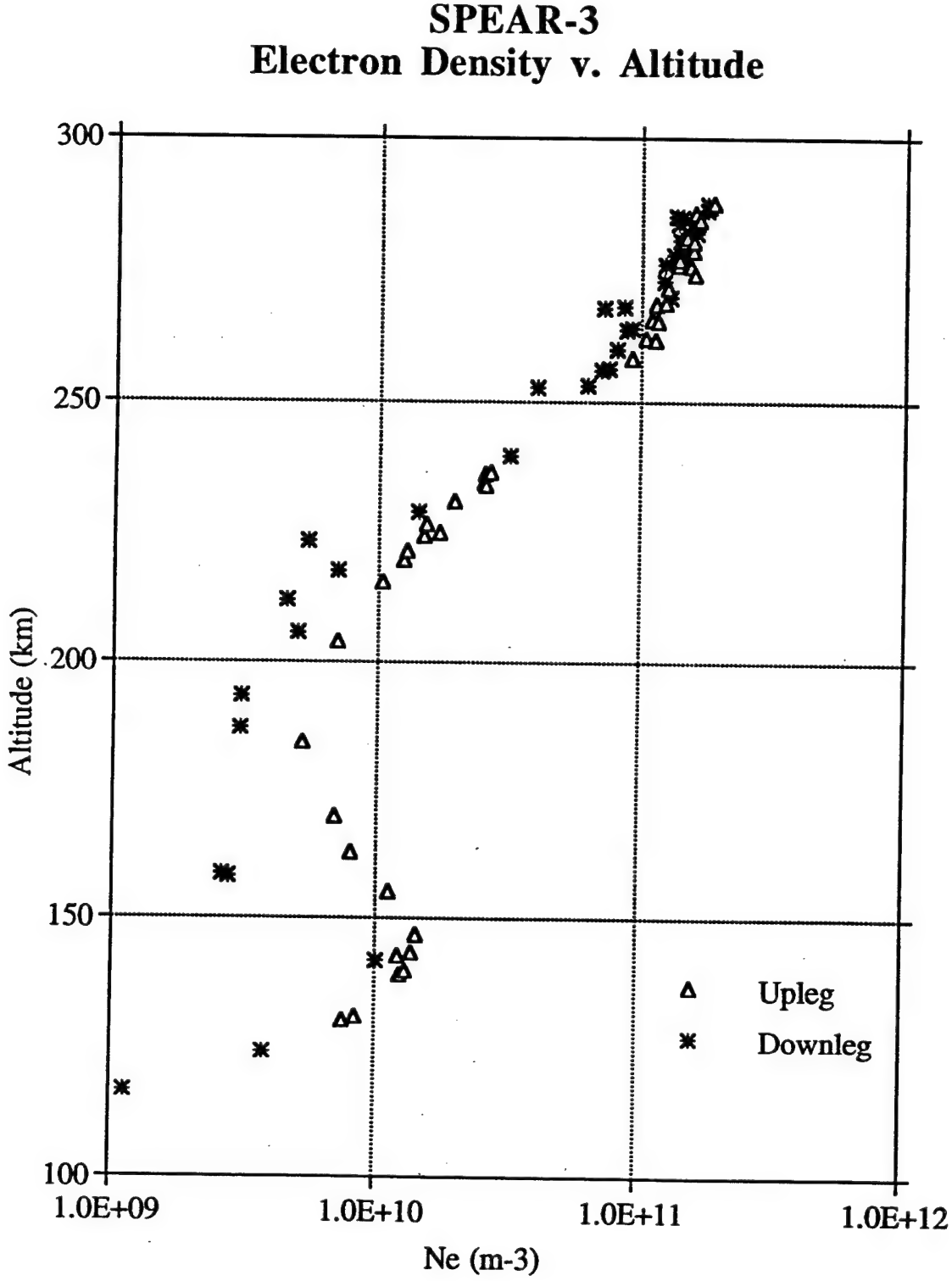


Figure 8-8. Electron density profiles deduced from Langmuir probe data.

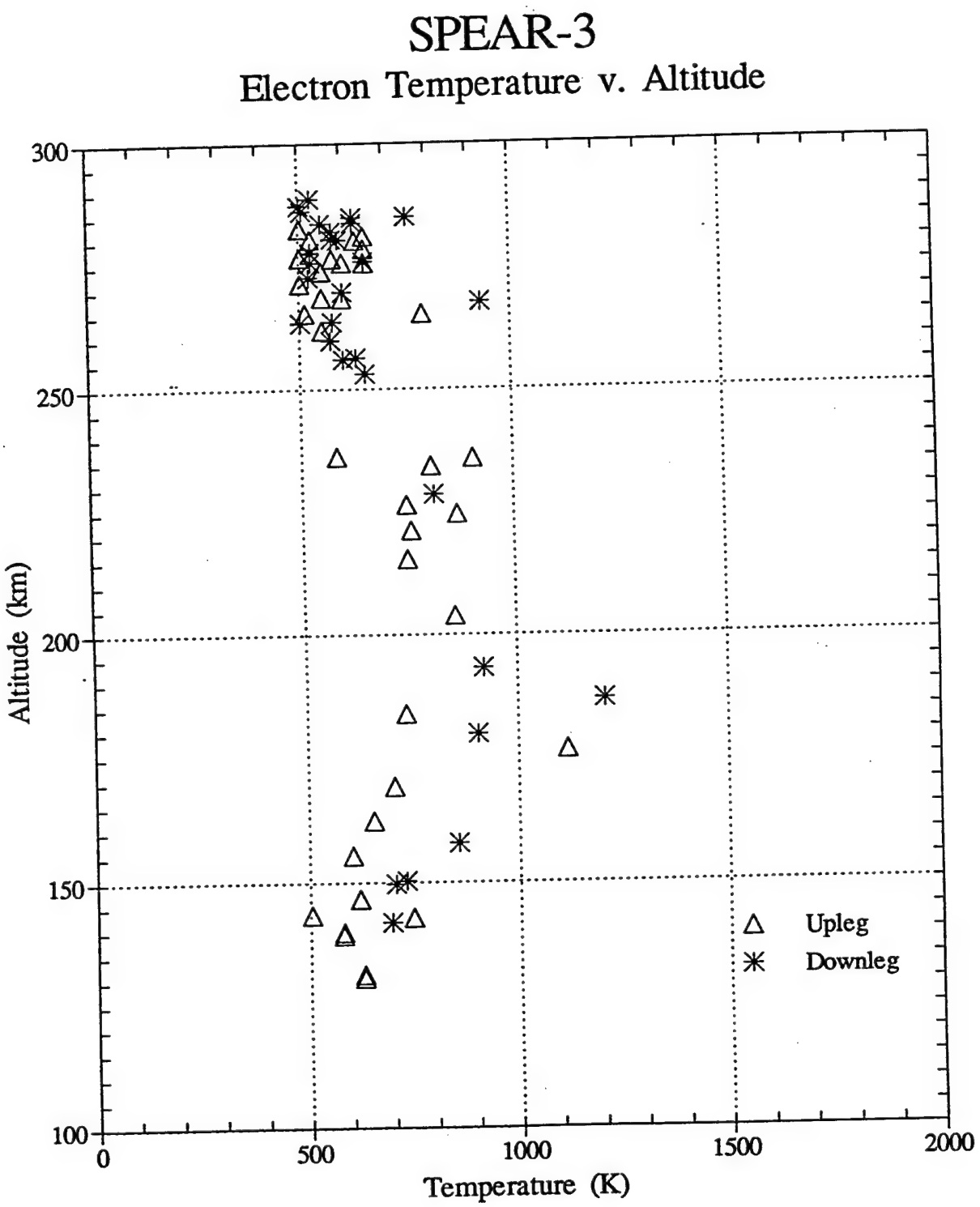


Figure 8-9. Electron temperatures deduced from Langmuir probe data.

# APPENDIX A

# LIST OF ABBREVIATIONS and ACRONYMS

| | |
|---|---|
| angstrom | Å |
| attitude control system | ACS |
| charged coupled device | CCD |
| differential charge device | DCD |
| electron temperature | $T_e$ |
| electrostatic analyzer | ESA |
| field effect device | FED |
| grams per second | g/sec |
| high voltage | HV |
| hollow cathode plasma contactor | HCPC |
| Kelvin | K |
| kilohertz | kHz |
| kilometers | km |
| kilohms | kΩ |
| kilovolt | kV |
| low-earth-orbit | LEO |
| low light level television | LLLTV |
| megahertz | MHz |
| megaohm | MΩ |
| meter | m |
| microamperes per square meter | $\mu A/m^2$ |
| microfarads | μF |
| milliamp | mA |
| millimeters | mm |
| millisecond | msec |
| neutral gas release system | NGRS |
| neutral pressure gauge | NPG |
| pounds per square inch | psi |
| resistor capacitor | RC |
| skin current probe | SCP |
| space power experiments aboard rockets | SPEAR |
| thermionic emitter | TE |

# APPENDIX B

# SPEAR-3 DATA ACCESS

The SPEAR-3 data archive at Utah State University.

The SPEAR-3 dataset is available on-line at Utah State University. It can be accessed via the internet. Telnet to "demise.cass.usu.edu" and log in with the username "spear" (if demise acts bogged down, you can also telnet to "malice.cass.usu.edu"). You will be prompted for the account password. Send e-mail to Don Thompson, "thompson@demise.cass.usu.edu", if you do not know the password. It will be changed periodically and e-mailed to those on the spear3 electronic mailing list. If you would like to be on this list, send a request to "thompson@demise.cass.usu.edu".

After logging in, you will be prompted for your terminal type. If your terminal type does vt100 emulation, just hit return. Otherwise enter your terminal type and hit return.

Next, you should change directories to your personal working directory, using the command "cd name", where 'name' is the name of your directory. If you do not have a personal directory, make one with the command "mkdir name" and then "cd name". When you are finished working on demise, issue "logout" to exit.

There are three data files available: "spear3_horiz.data", "spear3_vert.data", and "spear3_flight.data". The first two contain data taken during the horizontal and vertical tests at Phillips Lab. The third file contains the actual flight data.

These data files are binary. The files are formated similarly to the SPEAR-3 telemetry page, except that the time is appended to each minor frame. That is, the files are composed of fixed length records; 20 minor frames of 88 bytes. Bytes 1 through 77 are as defined in the telemetry page. Bytes 78, 79 and 80 are spares and reserved for future use. For the Phillips Lab data, bytes 80 and 81 are the SPEAR-3 sync word; for the flight data they are spares. Bytes 83 through 88 are the minor frame time, in BCD (binary coded decimal) as encoded by the tape digitizer (either Phillips lab or Wallops).

There is an extraction program available for use at Utah State University.

```
-------------------------------------------
Using the USU/CASS PCM data reduction utility
-------------------------------------------

Questions regarding the use of the data reduction utility
should be addressed via email to Don Thompson "thompson@usu.edu".

The following is a brief listing of usage:

spear3 {switches} {variables {variable_switches}}       ; for flight data
spear3_vert {switches} {variables {variable_switches}}  ; for vertical test
spear3_horiz {switches} {variables {variable_switches}} ; for horizontal test

variables:

Allowed variable names can be seen by issuing the command:
"more ~/spear3/spear3.setup".  Use the short name, the first column.

variable_switches:

        -include lo hi                  == Output only those values of the
                                           the variable that occur between
                                           lo and hi, must immediately follow
                                           the affected variable on the
                                           command line.

        -exclude lo hi                  == Output only those values of the
                                           the variable that occur outside
                                           lo and hi, must immediately follow
                                           the affected variable on the
                                           command line.

switches:

        -input filename                 == The name of a datafile to be used
                                           as input, defaults to the
                                           appropriate data file.

        -from time                      == The time to begin extraction,
                                           defaults to the beginning of the
                                           input file.  Times are in seconds.
                                           If you are using gmt as the time
                                           then both from and to times can
                                           be entered in "ddd/hh:mm:ss.sss"
                                           format.

        -to time                        == The time to stop extraction,
                                           defaults to the end of input file.

        -calibrate                      == Forces simple calibrations to
                                           be applied to the telemetered data,
                                           this is the default.

        -nocalibrate                    == Extract raw, uncalibrated data.

        -met                            == Extract using MET as time, this
                                           is the default.

        -gmt                            == Extract using GMT as time.

        -header                         == Output data with simple header
                                           naming each column of numbers,
                                           this is the default.

        -noheader                       == No column name header output.
```

| | |
|---|---|
| -oversample | == Oversample low speed data. |
| -nooversample | == Do not oversample low speed data, rather, subsample higher speed channels. This is the default. |
| -rate (rate) | == The rate at which to sample the data, in Hertz. Valid rates are; 1, 2, 4, 5, 10, 20, 40, 50, 100, 200, 400, 500, 1000, and 2000. Other values may work but will not result in evenly spaced sample intervals. |
| -binary | == Produces binary output with met milliseconds as a big-endian four-byte integer followed by one byte for each of the specified channels. This forces -nocalibrate, -met, -noplotl, and -noheader. |
| -nobinary | == Produces ascii output. This is the default. |
| -plot | == Output plotl graphics commands instead of columns of numbers. The first variable on the command will be used as the x-axis, additional variables will be used as the y-axes in one or more panels. |
| -noplotl | == Do not output graphics commands, this is the default. |
| -autoscale | == Autoscale plots generated using plotl. This is only valid when the -plot switch has been used. This is the default |
| -fullscale | == Use the channels full scale when plotting with the -plot switch, only valid in conjunction with the -plotl switch. |
| -symbols | == Places a symbol at each data point when using plotl. This is only valid when the -plot switch has been used. |
| -nosymbols | == Does not place symbols on plotl plots. This is the default. |
| -xgrid | == Places gridlines at each x-axis tic mark when using plotl. This is only valid when the -plot switch has been used. |
| -ygrid | == Places gridlines at each y-axis tic mark when using plotl. This is only valid when the -plot switch has been used. |
| -grid | == Does both -xgrid and -ygrid. |
| -noxgrid | == Does not print x-axis gridlines. This is the default. |

```
        -noxgrid                        == Does not print y-axis gridlines.
                                           This is the default.

        -nogrid                         == Does both -noxgrid and -noygrid.
```

Examples:

```
spear3 -from 100 -to 105 logspher logscp1 > spear3.dat
```

Outputs time, log sphere voltage, and log skin current probe 1 current to the file "spear3.dat" from 100 to 105 seconds.

```
spear3 -from 100 -to 105 met logspher logscp1 -plot1 | plot1 -s > spear3.ps
```

as above except that output is in the form of plot1 graphics commands which are filtered by plot1, which generates PostScript code. The code is saved in the file "spear3.ps" and is suitable for downloading to any PostScript compatible printer. Note the inclusion of "met" on the command line. This will plot logspher and logscp1 versus time. Excluding the "met" would plot logscp1 versus logspher.

Note: plot1 is a plotting package available for use on demise.

---

Porting the USU/CASS extraction tool.

The extraction tool is written in FORTRAN. It should compile an run on most unix computers, but it might not. The code is in spear3.f. The files "spear3.include" and "spear3.defaults" are also required.

There are several possible problems.

First, the parameter nrecl in spear3.include may have to be changed, depending on how the local computer treats the recordlength of random acces files.

Second, the function millisec, which converts BCD to integer milliseconds, is written assuming that integers are big-endian. That is, Digital Equipment Corp., in its own way, swaps the bytes of integer*2 numbers relative to how it's done on most computers. This may need to be altered to be compatible with your computer.

Third, the startup line parameters are read with the routines "iargc()" and "getarg()" which are provided as part of the f77 library on DECstations and most Unix implementations of FORTRAN. They may not be available on your local machine. If they are not you will need to change all the startup line parameter reading code to more standard FORTRAN read/write.

| ShortName | Long Name | Cl | Rw | Int | Slope | Const. | Note |
|---|---|---|---|---|---|---|---|
| GMT | GMT | 0 | 1 | 1 | 1 | 0 | |
| MET | Mission Elapsed Time (sec) | 0 | 1 | 1 | 1 | 0 | |
| ALT | Altitude (km) | 1 | 1 | -1 | CAL={-60.71112 2.55693 met mul add -4.88392e-03 met 2 exp mul add 1.03883e-06 met 3 exp mul add -9.27493e-10 met 4 exp mul add} TWOBYTES 1 1 | | |
| LAT | Latitude (deg) | 1 | 1 | -1 | CAL={37.86084 -8.73104e-04 met mul add -1.61157e-08 met 2 exp mul add -1.13083e-10 met 3 exp mul add -2.81644e-13 met 4 exp mul add} TWOBYTES 1 1 | | |
| LON | East Longitude (deg) | 1 | 1 | -1 | CAL={-75.61688 5.35922e-03 met mul add -3.46924e-06 met 2 exp mul add 4.12015e-09 met 3 exp mul add -1.49243e-13 met 4 exp mul add} TWOBYTES 1 1 | | |
| ACSNZ | ASC Nozzle Discretes | 11 | 1 | 1 | 1.0 | 0.0 | |
| ACSNZ1 | ACS 0 Deg Nozzle | 11 | 1 | 1 | 1.0 | 0.0 | BIT 0 INV ERT |
| ACSNZ2 | ACS 180 Deg Nozzle | 11 | 1 | 1 | 1.0 | 0.0 | BIT 1 INV ERT |
| ACSNZ3 | ACS 90 Deg Nozzle | 11 | 1 | 1 | 1.0 | 0.0 | BIT 2 INV ERT |
| ACSNZ4 | ACS 270 Deg Nozzle | 11 | 1 | 1 | 1.0 | 0.0 | BIT 3 INV ERT |
| ACSNZ5 | ACS CCWa Nozzle | 11 | 1 | 1 | 1.0 | 0.0 | BIT 4 INV ERT |
| ACSNZ6 | ACS CWa Nozzle | 11 | 1 | 1 | 1.0 | 0.0 | BIT 5 INV ERT |
| ACSNZ7 | ACS CWb Nozzle | 11 | 1 | 1 | 1.0 | 0.0 | BIT 6 INV ERT |
| ACSNZ8 | ACS CCWb Nozzle | 11 | 1 | 1 | 1.0 | 0.0 | BIT 7 INV ERT |
| ACSPP | Pitch Position (Degrees) | 12 | 1 | 20 | 1.412 | -180.0 | |
| ACSYP | Yaw Position (Degrees) | 12 | 2 | 20 | 0.7059 | -90.0 | |
| ACSRP | Roll Position (Degrees) | 12 | 3 | 20 | 1.412 | -180.0 | |
| ACSPR | Pitch Rate (Degrees/sec) | 12 | 4 | 20 | 0.08824 | -11.25 | |
| ACSYR | Yaw Rate (Degrees/sec) | 12 | 5 | 20 | 0.08824 | -11.25 | |
| ACSRR | Roll Rate (Degrees/sec) | 12 | 6 | 20 | 0.08824 | -11.25 | |
| ACSPN | Pitch Error (Degrees) | 12 | 7 | 20 | 0.04412 | -5.625 | |
| ACSYN | Yaw Error (Degrees) | 12 | 8 | 20 | 0.04412 | -5.625 | |
| ACSRN | Roll Error (Degrees) | 12 | 9 | 20 | 0.04412 | -5.625 | |
| ACSD | ACS Discretes (V) | 36 | 10 | 20 | 0.01961 | 0.0 | |
| ACSTPRES | Tank Pressure (psi) | 36 | 11 | 20 | 19.61 | 0.0 | |
| ACSIMP | Impulse (V) | 36 | 13 | 20 | 0.01961 | 0.0 | |
| ACSBM | ACS Battery Monitor (V) | 36 | 14 | 20 | 0.03922 | 24.0 | |
| SCSSER1 | SCS Cell #1 Counter | 24 | 1 | 20 | 1.0 | 0.0 | TWOBYTES 24 2 |
| SCSSER2 | SCS Cell #2 Counter | 24 | 6 | 20 | 1.0 | 0.0 | TWOBYTES 24 7 |
| SCSSER3 | SCS Cell #3 Counter | 24 | 11 | 20 | 1.0 | 0.0 | TWOBYTES 24 12 |
| SCSSER4 | SCS Cell #4 Counter | 24 | 16 | 20 | 1.0 | 0.0 | TWOBYTES 24 17 |
| SCSCUR1 | SCS Cell #1 Current (uA) | 32 | 2 | 2 | 0.07859 | -11.03 | |
| SCSCUR2 | SCS Cell #2 Current (uA) | 28 | 1 | 2 | 0.07929 | -11.22 | |
| SCSCUR3 | SCS Cell #3 Current (uA) | 28 | 2 | 2 | 0.07780 | -10.88 | |
| SCSCUR4 | SCS Cell #4 Current (uA) | 13 | 2 | 2 | 0.07722 | -10.83 | |
| SCS+15MB | SCS +15V B Monitor (V) | 12 | 10 | 20 | -0.3922 | 50.0 | ? |
| SCS-15MB | SCS -15V B Monitor (V) | 12 | 11 | 20 | -0.3922 | 50.0 | |
| SCSHVMN | SCS 600V Monitor (V) | 12 | 14 | 20 | -7.843 | 1000. | |
| SCS+5MD | SCS +5V D Monitor (V) | 12 | 17 | 20 | 0.03922 | -5.0 | ? |
| SCSPRESS | SCS Pressure | 50 | 17 | 20 | -0.1421 | 16.30 | |
| SCSDREJM | SCS Door Eject Monitor | 59 | 3 | 20 | 1.0 | 0.0 | BIT 0 |
| ESADATA1 | ESA Serial Data Out 1 | 18 | 1 | 1 | 1.0 | 0.0 | |
| ESADATA2 | ESA Serial Data Out 2 | 22 | 1 | 1 | 1.0 | 0.0 | |
| ESADATA3 | ESA Serial Data Out 3 | 26 | 1 | 1 | 1.0 | 0.0 | |
| ESADATA4 | ESA Serial Data Out 4 | 30 | 1 | 1 | 1.0 | 0.0 | |
| ESADATA5 | ESA Serial Data Out 5 | 34 | 1 | 1 | 1.0 | 0.0 | |
| ESADATA6 | ESA Serial Data Out 6 | 38 | 1 | 1 | 1.0 | 0.0 | |
| ESADATA7 | ESA Serial Data Out 7 | 42 | 1 | 1 | 1.0 | 0.0 | |

```
ESADATA8        ESA Serial Data Out 8           46 1  1   1.0       0.0
ESASTEP         ESA Energy Step                 18 1  1   CAL={ 0 esacal }
ESACOUNTS1      ESA Channel 1 Counts            26 1  1   CAL={ 1 esacal }
ESACOUNTS2      ESA Channel 2 Counts            30 1  1   CAL={ 2 esacal }
ESACOUNTS3      ESA Channel 3 Counts            38 1  1   CAL={ 3 esacal }
ESACOUNTS4      ESA Channel 4 Counts            42 1  1   CAL={ 4 esacal }
ESAENERGY1      ESA Channel 1 Energy            18 1  1   CAL={ 5 esacal }
ESAENERGY2      ESA Channel 2 Energy            18 1  1   CAL={ 6 esacal }
ESAENERGY3      ESA Channel 3 Energy            18 1  1   CAL={ 7 esacal }
ESAENERGY4      ESA Channel 4 Energy            18 1  1   CAL={ 8 esacal }
ESAFLUX1        ESA Channel 1 FLUX              18 1  1   CAL={ 9 esacal }
ESAFLUX2        ESA Channel 2 FLUX              18 1  1   CAL={10 esacal }
ESAFLUX3        ESA Channel 3 FLUX              18 1  1   CAL={11 esacal }
ESAFLUX4        ESA Channel 4 FLUX              18 1  1   CAL={12 esacal }
#ESASTEP        ESA Energy Step                 18 1  1   CAL={ v 127 iand dup 63 gt
 if 127 flip sub }
#ESACOUNTS1     ESA Channel 1 Counts            26 1  1   CAL={ 34 row page 15 iand
256 mul v add }
#ESACOUNTS2     ESA Channel 2 Counts            30 1  1   CAL={ 34 row page 240 iand
 16 mul v add }
#ESACOUNTS3     ESA Channel 3 Counts            38 1  1   CAL={ 46 row page 15 iand
256 mul v add }
#ESACOUNTS4     ESA Channel 4 Counts            42 1  1   CAL={ 46 row page 240 iand
 16 mul v add }
ESAP15M         ESA +15V Monitor (V)            50 1  20  0.02020  12.03
ESAM15M         ESA -15V Monitor (V)            50 2  20  0.01980 -18.09
ESAP5M          ESA +5V Monitor (V)             50 3  20  0.01961  1.23
ESABHVM         ESA HV Monitor (V)              50 4  20 -19.61    0.0
ESAPSWHM        +High Sweep Monitor (V)         2  1  1   19.319    0.0
ESAMSWHM        -High Sweep Monitor (V)         6  1  1  -19.679    0.0
ESAPSWLM        +Low Sweep Monitor (V)          10 1  1   0.59843  0.0
ESAMSWLM        -Low Sweep Monitor (V)          14 1  1  -0.61000  0.0
ESASWPM         ESA Sweep Program Monitor (V)   50 5  20  0.1980    0.0
ESATPWR         ESA LV Power Conv. Temp (DegC)  50 6  20  0.3765  -11.30
ESATBHV         ESA Bias Pwr Conv. Temp (DegC)  50 7  20  0.3765  -11.30
ESATSWP         ESA Sweep Conv Temp (DegC)      50 8  20  0.3765  -11.30
ESATDIG         ESA Digital System Temp (DegC)  50 9  20  0.3765  -11.30
ESATSAH         ESA Sensor 1 Temp (DegC)        50 10 20  0.3765  -11.30
ESATSAL         ESA Sensor 2 Temp (DegC)        50 11 20  0.3765  -11.30
ESATSBH         ESA Sensor 3 Temp (DegC)        50 12 20  0.3765  -11.30
ESATSBL         ESA Sensor 4 Temp (DegC)        50 13 20  0.3765  -11.30
ESATREG         ESA Sweep Regulator Temp (DegC) 50 14 20  0.3765  -11.30
ESAD15M         ESA Delayed 15 Monitor          50 15 20  0.02039  12.34
ESAD30M         ESA Delayed 30 Monitor          50 16 20  0.02039  26.40
DCD+15MN        DCD +15V Monitor (V)            36 7  20 -0.3922   50.0
DCD-15MN        DCD -15V Monitor (V)            36 8  20 -0.3922   50.0
DCDHVMON        DCD High Voltage Monitor (V)    36 9  20 -0.3922   50.0
DCDCUR          DCD Current (uA)                13 1  2  -0.7843   110.2
DCDLIN/VSM      DCD Linear Voltage (V)          52 1  2  -19.61    2499.
DCDLOG          DCD Log Voltage (V)             52 2  2   (c<108 ? -10.**(-0.03322*c
+3.642) : c<148 ? 0.09373*c-11.47 : 10.**(0.03322*c-4.404)) FILE=/users/data4/spear/
spear3/DCDLOG.cal
DCDPRESS        DCD Pressure                    69 2  2   0.1421  -19.93
DCDDREJM        DCD Door Eject Monitor          59 3  20  1.0       0.0     BIT 1
TEACTHIM        TE Cathode Current (mA)         29 1  2   0.9804  -22.22
TEACBUSVM       TE AC Bus Voltage (Vrms)        12 18 20  0.1581  -3.839
TEBIASVM        TE Bias Voltage (V)             12 19 20  0.1210  -2.741
TEFILVM         TE Filament Voltage (V)         12 20 20  0.1544  -3.748
TEFILIM         TE Filament Current (Arms)      36 1  20  0.06557 -1.582
TEDREJM         TE Door Eject Monitor           59 3  20  1.0       0.0     BIT 2
FEDGATEI        FED Gate Current (uA)           31 1  2   15.81   -1816.
FEDCATHI        FED Cathode Current (mA)        31 2  2   0.9804  -112.5
FED+15MA        FED +15V A Monitor (V)          36 2  20 -0.3922   50.0
FED-15MA        FED -15V A Monitor (V)          36 3  20 -0.3922   50.0
FED+15MB        FED +15V B Monitor (V)          36 4  20 -0.3922   50.0
FED-15MB        FED -15V B Monitor (V)          36 5  20 -0.3922   50.0
FEDPRESS        FED Pressure                    36 6  20 -0.1421   16.30
FEDCATHV        FED Cathode Voltage (V)         32 1  2  -0.9839   112.8
```

```
FEDDREJM        FED Door Eject Monitor              59 3  20  1.0       0.0      BIT 3
GRTPM           NGRS Tank Pressure (psi)            72 15 20  12.217    -98.064
GRTTM           NGRS Tank Temperature (DegC)        72 16 20  0.3247    -24.88   FILE=/use
rs/data4/spear/spear3/GRTTM.cal
GRREGPR         NGRS Regulator Pressure (psi)       59 9  20  4.0849    -41.667
GRLOVM          NGRS Lo-Pressure Valve Mon          37 1  2   1.0       0.0      BIT 0
GRHIVM          NGRS Hi-Pressure Valve Mon          37 1  2   1.0       0.0      BIT 1
RNGIM           Ring (Boom) Current (mA)            39 1  2   0.4195    -7.002
RNGVM           Ring (Boom) Voltage (V)             39 1  2   436.28    -7155.
HVS1DM          Relay 1 Coil Voltage (V)            43 1  20  0.1673    -4.275
HVS2DM          Relay 2 Coil Voltage (V)            43 2  20  0.1671    -4.269
HVS3DM          Relay 3 Coil Voltage (V)            43 3  20  0.1674    -4.303
HVS4DM          Relay 4 Coil Voltage (V)            43 4  20  0.1677    -4.276
HVENDM          HV Enbl Relay Coil Voltage (V)      43 5  20  0.1664    -4.655
LEDDM           LED Voltage (V)                     43 6  20  0.1664    -4.662
DISIM           Discharge Current (mA)              54 1  2   (c<153 ? 1.606*c-42.26 : 8
.864*c-1151.) FILE=/users/data4/spear/spear3/DISIM.cal
CHGIM           Charge Current (mA)                 43 8  20  0.08923   -2.389
P28VM           +28V Monitor (V)                    43 9  20  0.1847    -4.842
P28IM           +28I Monitor (A)                    43 10 20  0.07843   0.0
P28VIM          Isolated +28V Monitor (V)           43 11 20  0.1850    -4.859
P5VM            +5V Monitor (V)                     43 12 20  0.02779   -0.7299
P15VM           +15V Monitor (V)                    43 13 20  0.08271   -2.172
N15VM           -15V Monitor (V)                    43 14 20  -0.08288  2.177
PRES1M          Pressure 1 Monitor (psi)            43 15 20  0.07354   -1.875
PRES2M          Pressure 2 Monitor (psi)            43 16 20  0.07354   -1.875
HVPSVM          HV Power Supply Voltage (V)         43 17 20  47.58     -1211.
HVPSIM          HV Power Supply Current (mA)        43 18 20  0.04726   -1.208
ACVM            400 Hz AC Voltage (Vrms)            43 19 20  0.4669    6.429
DCVM            +28V Int/Ext Monitor (V)            43 20 20  0.13495   0.0
TV2ICCDM        LLLTV #2 ICCD AGC Monitor (V)       36 17 20  -0.01966  5.004
TV2P12M         LLLTV #2 +12V Monitor (V)           36 18 20  (c<14 ? 0.5164*log((c+1.e-
6)/6.543e-9) : 0.007025*c+10.99) FILE=/users/data4/spear/spear3/TV2P12M.cal
TV2PRESM        LLLTV #2 Pressure Monitor (psi)     36 19 20  0.06949   -1.634
TV3ICCDM        LLLTV #3 ICCD AGC Monitor (V)       36 20 20  -0.01958  4.999
TV3P12M         LLLTV #3 +12V Monitor (V)           59 1  20  (c<20 ? 0.4061*log((c+1.e-
6)/2.605e-11) : 0.007131*c+10.96) FILE=/users/data4/spear/spear3/TV3P12M.cal
TV3PRESM        LLLTV #3 Pressure Monitor (psi)     59 2  20  0.06933   -1.674
TV3SM           LLLTV #3 Shutter Mech.              37 1  2   1.0       0.0      BIT 2
TV3LVM          Illum. Lamp 12VDC Monitor (V)       59 4  20  (c<24 ? 0.3656*log((c+1.e-
6)/1.562e-12) : 0.007106*c+10.93) FILE=/users/data4/spear/spear3/TV3LVM.cal
TV3LCM          Illum. Lamp Control Monitor         37 1  2   1.0       0.0      BIT 3
TV3DREJM        LLLTV #3 Door Eject Monitor         59 3  20  1.0       0.0      BIT 4
LPELEC          LP Electron Current (A)             15 1  1   (c<51 ? -2.982e-9*10**(-c/
34.85) : 3.686e-12*10**(c/38.09)) FILE=/users/data4/spear/spear3/LPELEC.cal
LPION           LP Positive Ion Current (A)         21 1  1   0.02737   -9.5016  10**
LPSWEEP         LP Sweep Monitor (V)                20 1  1   0.01961   0.0
LPVOLTS         LP Voltage (V)                      20 1  1   0.02353   -1.0
LPDEJM          LP Door Eject Monitor               59 3  20  1.0       0.0      BIT 5
LPDPLYM         LP Deploy Monitor                   59 3  20  1.0       0.0      BIT 6
NPNPM           NPG Neutral Pressure (torr)         29 2  2   0.01494   -6.889   10**
NPTM            NPG Temperature (DegC)              23 2  2   0.3922    -40.0
NPVPM           NPG Valve Position Monitor (%)      59 19 20  -1.4967   335.1
NPDEJM          NPG Door Eject Monitor              59 3  20  1.0       0.0      BIT 7
NPDPLYM         NPG Deploy Monitor                  59 7  20  1.0       0.0      BIT 0
TV1PRESM        OS Pressure Gauge (psi)             59 8  20  0.07206   -1.838
TV1ICCDM        OS Gain (V)                         37 2  2   0.03922   0.0
PCPVMON         HCPC Power Supply Monitor           37 1  2   1.0       0.0      BIT 4
PCSYSI          HCPC System Current (mA)            59 11 20  1.683     0.0
PCHEATV         HCPC Heater Voltage (V)             59 12 20  0.03020   0.0
PCKEEPV         HCPC Keeper Voltage (V)             54 2  2   0.8549    0.0
PCSYSTEMP       HCPC System Temperature             59 13 20  (40.82*(6.086-log(c))) FIL
E=/users/data4/spear/spear3/PCSYSTEMP.cal
PCHEATI         HCPC Heater Current (A)             59 14 20  0.06953   0.0
PCKEEPI         HCPC Keeper Current (mA)            55 1  2   7.003     0.0
PCRETNI         HCPC Neutralize Current (mA)        3  1  -16 2.196     0.0
PCINTPRES       HCPC Internal Pressure (torr)       55 2  2   0.6525    -46.95
PCSUPPRES       HCPC Gas Supply Pressure (psi)      59 16 20  1.417     -59.99
```

```
PCENCLPRES      HCPC Enclosure Pressure (psi)   59 17 20  0.1043    0.0
PCDOOR          HCPC Door Eject Monitor         59 7  20  1.0       0.0     BIT 1
PCDPLYM         HCPC Deploy Monitor             59 7  20  1.0       0.0     BIT 2
SCP1+15M        SCP #1 +15V Monitor (V)         72 17 20 -0.3922    50.0
SCP1-15M        SCP #1 -15V Monitor (V)         72 18 20 -0.3922    50.0
SCP1CUR         SCP #1 Current (mA)             23 1  2  -7.412e-3 0.9562
LOGSCP2         SCP #2 Log Current (mA)         27 1  2   (c<113 ? -10.**(-0.03224*c
+1.105) : c<147 ? 1.875e-4*c-0.02435 : 10.**(0.03224*c-7.193)) FILE=/users/data4/spe
ar/spear3/LOGSCP2.cal
SCP2+15M        SCP #2 +15V Monitor (V)         72 19 20 -0.3922    50.0
SCP2-15M        SCP #2 -15V Monitor (V)         72 20 20 -0.3922    50.0
SCP2CUR         SCP #2 Current (mA)             27 2  2   (c<128 ? -0.08471*c+10.857
3 : -0.07647*c+9.8073) FILE=/users/data4/spear/spear3/SCP2CUR.cal
TPMPAMP1        Efield Pos. Amplitude (V/m)     60 1  2   1.0       0.0     10** FILE
=/users/data4/spear/spear3/TPMPAMP1.cal
TPMNAMP1        Efield Neg. Amplitude (V/m)     60 2  2   1.0       0.0     10** FILE
=/users/data4/spear/spear3/TPMNAMP1.cal
TPMPDER1        Efield Pos. Derivative (V/m-s)  61 1  2   1.0       0.0     10** FILE
=/users/data4/spear/spear3/TPMPDER1.cal
TPMNDER1        Efield Neg. Derivative (V/m-s)  61 2  2   1.0       0.0     10** FILE
=/users/data4/spear/spear3/TPMNDER1.cal
TPMINT1         Efield Integral (V-s/m)         62 1  2   1.0       0.0     10** FILE
=/users/data4/spear/spear3/TPMINT1.cal
TPMPAMP2        B-dot Pos. Amplitude (A/m)      62 2  2   1.0       0.0     10** FILE
=/users/data4/spear/spear3/TPMPAMP2.cal
TPMNAMP2        B-dot Neg. Amplitude (A/m)      63 1  2   1.0       0.0     10** FILE
=/users/data4/spear/spear3/TPMNAMP2.cal
TPMPDER2        B-dot Pos. Deriv. (A/m-s)       63 2  2   1.0       0.0     10** FILE
=/users/data4/spear/spear3/TPMPDER2.cal
TPMNDER2        B-dot Neg. Deriv. (A/m-s)       64 1  2   1.0       0.0     10** FILE
=/users/data4/spear/spear3/TPMNDER2.cal
TPMINT2         B-dot Integral (A-s/m)          64 2  2   1.0       0.0     10** FILE
=/users/data4/spear/spear3/TPMINT2.cal
TPMPAMP3        SCS Current Pos. Amplitude (A)  66 1  2   1.0       0.0     10** FILE
=/users/data4/spear/spear3/TPMPAMP3.cal
TPMNAMP3        SCS Current Neg. Amplitude (A)  66 2  2   1.0       0.0     10** FILE
=/users/data4/spear/spear3/TPMNAMP3.cal
TPMPDER3        SCS Current Pos. Deriv. (A/s)   68 1  2   1.0       0.0     10** FILE
=/users/data4/spear/spear3/TPMPDER3.cal
TPMNDER3        SCS Current Neg. Deriv. (A/s)   68 2  2   1.0       0.0     10** FILE
=/users/data4/spear/spear3/TPMNDER3.cal
TPMINT3         SCS Current Integral (A-s)      69 1  2   1.0       0.0     10** FILE
=/users/data4/spear/spear3/TPMINT3.cal
TPMHKP1         TPM Power Supply Temp. (deg C)  74 1  20  2.180    -295.8
TPMHKP2         TPM Processor Temp. (deg C)     74 2  20  2.180    -295.8
TPMHKP3         TPM Negative Supply Voltage (V) 74 3  20  0.1169   -14.9
TPMHKP4         TPM Positive Supply Voltage (V) 74 4  20  0.1153   -14.7
TPMHKP5         TPM E-Sensor Potential (V)      74 5  20  0.4588   -58.5
LOGSPHER        Sphere Voltage (V)              40 1  2   1.0       0.0     FILE=/use
rs/data4/spear/spear3/LOGSPHER.cal
LOGROG          Rogowski Current (mA)           40 2  2   1.0       0.0     FILE=/use
rs/data4/spear/spear3/LOGROG.cal
LOGSCP1         SCP #1 Log Current (mA)         70 1  2   (c<72 ? 10.**(-0.03922*c+0
.92) : c<186 ? -2.051e-4*c+0.02840 : -10.**(0.03922*c-9.30)) FILE=/users/data4/spear
/spear3/LOGSCP1.cal
DSPHSER         HSDS Sphere Voltage (V)         4  1 -40  1.0       0.0     FILE=/use
rs/data4/spear/spear3/DSPHSER.cal
DROGSER         HSDS Rogowski Current (mA)      7  1 -40  1.0       0.0     FILE=/use
rs/data4/spear/spear3/DROGSER.cal
DSCPSER         HSDS SCP #1 Current (mA)        16 1 -40  1.0       0.0     FILE=/use
rs/data4/spear/spear3/LOGSCP1.cal
VSMMFS1         Minor Frame Sync #1             78 1  1   1.0       0.0
VSMMFS2         Minor Frame Sync #2             79 1  1   1.0       0.0
VSMMFS3         Minor Frame Sync #3             80 1  1   1.0       0.0
VSMSFID         Sub Frame ID                    58 1  1   1.0       0.0
VSMRFI          VSM RF Power Inc                74 6  20  1.0       0.0
VSMRFR          VSM RF Power Ref                74 7  20  1.0       0.0
VSM+5VM         VSM +5V Monitor                 74 8  20  1.0       0.0
```

| | | | | | | |
|---|---|---|---|---|---|---|
| VSM+12VM | VSM +12V Monitor | 74 9 | 20 | 1.0 | 0.0 | |
| VSM-12VM | VSM -12V Monitor | 74 10 | 20 | 1.0 | 0.0 | |
| VSMTPB | VSM Temp PCM Box | 74 11 | 20 | 1.0 | 0.0 | |
| VSMTEB | VSM Temp Electronics Box | 74 12 | 20 | 1.0 | 0.0 | |
| VSMHSR | VSM Half Scale Ref | 74 14 | 20 | 1.0 | 0.0 | |
| VSMHLP | VSM Hard Line Power | 74 16 | 20 | 1.0 | 0.0 | |
| VSMDDCT | VSM DC/DC Conv Temp | 74 17 | 20 | 1.0 | 0.0 | |
| VSMBV1 | VSM Batt Voltage 1 | 74 18 | 20 | 1.0 | 0.0 | |
| VSMBV2 | VSM Batt Voltage 2 | 74 19 | 20 | 1.0 | 0.0 | |
| VSMBV3 | VSM Batt Voltage 3 | 74 20 | 20 | 1.0 | 0.0 | |
| VSMBV4 | VSM Batt Voltage 4 | 77 1 | 20 | 1.0 | 0.0 | |
| VSMBV5 | VSM Batt Voltage 5 | 77 2 | 20 | 1.0 | 0.0 | |
| VSMBV6 | VSM Batt Voltage 6 | 77 3 | 20 | 1.0 | 0.0 | |
| VSMBV7 | VSM Batt Voltage 7 | 77 4 | 20 | 1.0 | 0.0 | |
| VSMBV8 | VSM Batt Voltage 8 | 77 5 | 20 | 1.0 | 0.0 | |
| VSMBV9 | VSM Batt Voltage 9 | 77 6 | 20 | 1.0 | 0.0 | |
| VSMMPRES | VSM Motor Pressure | 77 7 | 20 | 1.0 | 0.0 | |
| VSMMSCM1 | VSM Squib Current #1 | 77 8 | 20 | 1.0 | 0.0 | |
| VSMMSCM2 | VSM Squib Current #2 | 77 9 | 20 | 1.0 | 0.0 | |
| VSMXT1 | VSM Link1 Xmtr Temp | 77 16 | 20 | 1.0 | 0.0 | |
| VSMXT2 | VSM Link2 Xmtr Temp | 77 17 | 20 | 1.0 | 0.0 | |
| VSMXT3 | VSM Link3 Xmtr Temp | 77 18 | 20 | 1.0 | 0.0 | |
| VSMC5VM | VSM Controller 5V Monitor | 77 19 | 20 | 1.0 | 0.0 | |
| VSMACC | VSM Accelerometer | 77 20 | 20 | 1.0 | 0.0 | |
| VSMCC1 | VSM Controller Clock 1 | 72 1 | 20 | 1.0 | 0.0 | |
| VSMCC2 | VSM Controller Clock 2 | 72 2 | 20 | 1.0 | 0.0 | |
| VSMPT1 | VSM Plate Temp 1 | 72 3 | 20 | 1.0 | 0.0 | |
| V44B | Bus 7 Int/Ext | 72 5 | 20 | 1.0 | 0.0 | BIT 1 |
| V44C | Bus 6 Int/Ext | 72 5 | 20 | 1.0 | 0.0 | BIT 2 |
| V44D | Bus 5 Int/Ext | 72 5 | 20 | 1.0 | 0.0 | BIT 3 |
| V44E | Bus 4 Int/Ext | 72 5 | 20 | 1.0 | 0.0 | BIT 4 |
| V44F | Bus 3 Int/Ext | 72 5 | 20 | 1.0 | 0.0 | BIT 5 |
| V44G | Bus 2 Int/Ext | 72 5 | 20 | 1.0 | 0.0 | BIT 6 |
| V44H | Bus 1 Int/Ext | 72 5 | 20 | 1.0 | 0.0 | BIT 7 |
| V45A | OS Deploy Prim | 72 6 | 20 | 1.0 | 0.0 | BIT 0 |
| V45B | HV Boom Release Sec | 72 6 | 20 | 1.0 | 0.0 | BIT 1 |
| V45C | HV Boom Release Prim | 72 6 | 20 | 1.0 | 0.0 | BIT 2 |
| V45D | Nose Cone Eject Sec | 72 6 | 20 | 1.0 | 0.0 | BIT 3 |
| V45E | Nose Cone Eject Prim | 72 6 | 20 | 1.0 | 0.0 | BIT 4 |
| V45F | Arm/Safe Sec | 72 6 | 20 | 1.0 | 0.0 | BIT 5 |
| V45G | Arm/Safe Prim | 72 6 | 20 | 1.0 | 0.0 | BIT 6 |
| V46A | TV3 Door Eject Prim | 72 7 | 20 | 1.0 | 0.0 | BIT 0 |
| V46B | ESA Door Eject Sec | 72 7 | 20 | 1.0 | 0.0 | BIT 1 |
| V46C | ESA Door Eject Prim | 72 7 | 20 | 1.0 | 0.0 | BIT 2 |
| V46D | DCD/TE Door Eject Sec | 72 7 | 20 | 1.0 | 0.0 | BIT 3 |
| V46E | DCD/TE Door Eject Prim | 72 7 | 20 | 1.0 | 0.0 | BIT 4 |
| V46F | SCS Door Eject Sec | 72 7 | 20 | 1.0 | 0.0 | BIT 5 |
| V46G | SCS Door Eject Prim | 72 7 | 20 | 1.0 | 0.0 | BIT 6 |
| V46H | OS Deploy Sec | 72 7 | 20 | 1.0 | 0.0 | BIT 7 |
| V47A | LP Door Eject Prim | 72 8 | 20 | 1.0 | 0.0 | BIT 0 |
| V47B | FP Boom Deploy Sec | 72 8 | 20 | 1.0 | 0.0 | BIT 1 |
| V47C | FP Boom Deploy Prim | 72 8 | 20 | 1.0 | 0.0 | BIT 2 |
| V47D | FP Door Eject Sec | 72 8 | 20 | 1.0 | 0.0 | BIT 3 |
| V47E | FP Door Eject Prim | 72 8 | 20 | 1.0 | 0.0 | BIT 4 |
| V47F | FED Door Eject Sec | 72 8 | 20 | 1.0 | 0.0 | BIT 5 |
| V47G | FED Door Eject Prim | 72 8 | 20 | 1.0 | 0.0 | BIT 6 |
| V47H | TV3 Door Eject Sec | 72 8 | 20 | 1.0 | 0.0 | BIT 7 |
| V48A | HV Control Arm/Safe Prim | 72 9 | 20 | 1.0 | 0.0 | BIT 0 |
| V48B | NPG Door Eject Sec | 72 9 | 20 | 1.0 | 0.0 | BIT 1 |
| V48C | NPG Door Eject Prim | 72 9 | 20 | 1.0 | 0.0 | BIT 2 |
| V48D | HCPC Deploy Sec | 72 9 | 20 | 1.0 | 0.0 | BIT 3 |
| V48E | HCPC Deploy Prim | 72 9 | 20 | 1.0 | 0.0 | BIT 4 |
| V48F | HCPC Door Eject Sec | 72 9 | 20 | 1.0 | 0.0 | BIT 5 |
| V48G | HCPC Door Eject Prim | 72 9 | 20 | 1.0 | 0.0 | BIT 6 |
| V48H | LP Door Eject Sec | 72 9 | 20 | 1.0 | 0.0 | BIT 7 |
| V49A | TE Filament | 72 10 | 20 | 1.0 | 0.0 | BIT 0 |
| V49B | FED Simulator | 72 10 | 20 | 1.0 | 0.0 | BIT 1 |
| V49C | FED Trigger | 72 10 | 20 | 1.0 | 0.0 | BIT 2 |

| | | | | | |
|---|---|---|---|---|---|
| V49D | TV2 LED | 72 10 20 | 1.0 | 0.0 | BIT 3 |
| V49E | HV Enable | 72 10 20 | 1.0 | 0.0 | BIT 4 |
| V49F | HV Connect/Disconnect | 72 10 20 | 1.0 | 0.0 | BIT 5 |
| V49G | HV Network | 72 10 20 | 1.0 | 0.0 | BIT 6 |
| V49H | HV Event Trigger | 72 10 20 | 1.0 | 0.0 | BIT 7 |
| V50B | LLLTV3 Shutter | 72 11 20 | 1.0 | 0.0 | BIT 1 |
| V50C | SCS HV Mode | 72 11 20 | 1.0 | 0.0 | BIT 2 |
| V50D | SCS Test Mode | 72 11 20 | 1.0 | 0.0 | BIT 3 |
| V50E | SCS Lamp | 72 11 20 | 1.0 | 0.0 | BIT 4 |
| V50F | NGRS Hi Flow | 72 11 20 | 1.0 | 0.0 | BIT 5 |
| V50G | NGRS Low Flow | 72 11 20 | 1.0 | 0.0 | BIT 6 |
| V50H | DCD HV | 72 11 20 | 1.0 | 0.0 | BIT 7 |
| V51B | NPG Motor Power | 72 12 20 | 1.0 | 0.0 | BIT 1 |
| V51C | NPG Valve | 72 12 20 | 1.0 | 0.0 | BIT 2 |
| V51D | NPG HV | 72 12 20 | 1.0 | 0.0 | BIT 3 |
| V51E | HCPC Gas Valve | 72 12 20 | 1.0 | 0.0 | BIT 4 |
| V51F | HCPC Enable/Disable | 72 12 20 | 1.0 | 0.0 | BIT 5 |
| V51G | HCPC Preheater | 72 12 20 | 1.0 | 0.0 | BIT 6 |
| V51H | HCPC Heater | 72 12 20 | 1.0 | 0.0 | BIT 7 |
| V52A | ESA Inst Power | 72 13 20 | 1.0 | 0.0 | BIT 0 |
| V52B | SCP Inst Power | 72 13 20 | 1.0 | 0.0 | BIT 1 |
| V52C | TE Inst Power | 72 13 20 | 1.0 | 0.0 | BIT 2 |
| V52D | HSDS Inst Power | 72 13 20 | 1.0 | 0.0 | BIT 3 |
| V52E | OS Inst Power | 72 13 20 | 1.0 | 0.0 | BIT 4 |
| V52F | TV3 Inst Power | 72 13 20 | 1.0 | 0.0 | BIT 5 |
| V52G | TV2 Inst Power | 72 13 20 | 1.0 | 0.0 | BIT 6 |
| V52H | HV Inst Power | 72 13 20 | 1.0 | 0.0 | BIT 7 |
| V53A | LP Inst Power | 72 14 20 | 1.0 | 0.0 | BIT 0 |
| V53B | DCD Service Power | 72 14 20 | 1.0 | 0.0 | BIT 1 |
| V53C | DCD Inst Power | 72 14 20 | 1.0 | 0.0 | BIT 2 |
| V53D | FED Service Power | 72 14 20 | 1.0 | 0.0 | BIT 3 |
| V53E | FED Inst Power | 72 14 20 | 1.0 | 0.0 | BIT 4 |
| V53F | SCS Service Power | 72 14 20 | 1.0 | 0.0 | BIT 5 |
| V53G | SCS Inst Power | 72 14 20 | 1.0 | 0.0 | BIT 6 |
| V53H | ESA Delayed Power | 72 14 20 | 1.0 | 0.0 | BIT 7 |
| V54A | Xmit #1 Power | 77 10 20 | 1.0 | 0.0 | BIT 0 |
| V54B | VSM Inst Power | 77 10 20 | 1.0 | 0.0 | BIT 1 |
| V54C | NGRS Inst Power | 77 10 20 | 1.0 | 0.0 | BIT 2 |
| V54D | HCPC Service Power | 77 10 20 | 1.0 | 0.0 | BIT 3 |
| V54E | HCPC Inst Power | 77 10 20 | 1.0 | 0.0 | BIT 4 |
| V54F | FP Inst Power | 77 10 20 | 1.0 | 0.0 | BIT 5 |
| V54G | TPM Inst Power | 77 10 20 | 1.0 | 0.0 | BIT 6 |
| V54H | NPG Inst Power | 77 10 20 | 1.0 | 0.0 | BIT 7 |
| V55A | SCS Test Mode | 77 11 20 | 1.0 | 0.0 | BIT 0 |
| V55B | SCP Cal Mode | 77 11 20 | 1.0 | 0.0 | BIT 1 |
| V55C | Event Trigger | 77 11 20 | 1.0 | 0.0 | BIT 2 |
| V55D | Event Trigger | 77 11 20 | 1.0 | 0.0 | BIT 3 |
| V55E | Event Trigger | 77 11 20 | 1.0 | 0.0 | BIT 4 |
| V55F | Radar Beacon Power | 77 11 20 | 1.0 | 0.0 | BIT 5 |
| V55G | Xmit #3 Power | 77 11 20 | 1.0 | 0.0 | BIT 6 |
| V55H | Xmit #2 Power | 77 11 20 | 1.0 | 0.0 | BIT 7 |
| V56A | HV Control Arm/Safe Sec | 77 12 20 | 1.0 | 0.0 | BIT 0 |
| V56A | HV Control Arm/Safe Sec | 77 12 20 | 1.0 | 0.0 | BIT 0 |
| OSDPLYP | OS Deploy Prim | 72 6 20 | 1.0 | 0.0 | BIT 0 |
| HVBRS | HV Boom Release Sec | 72 6 20 | 1.0 | 0.0 | BIT 1 |
| HVBRP | HV Boom Release Prim | 72 6 20 | 1.0 | 0.0 | BIT 2 |
| NTES | Nose Cone Eject Sec | 72 6 20 | 1.0 | 0.0 | BIT 3 |
| NTEP | Nose Cone Eject Prim | 72 6 20 | 1.0 | 0.0 | BIT 4 |
| PARMS | Arm/Safe Sec | 72 6 20 | 1.0 | 0.0 | BIT 5 |
| PARMP | Arm/Safe Prim | 72 6 20 | 1.0 | 0.0 | BIT 6 |
| TV3DEJP | TV3 Door Eject Prim | 72 7 20 | 1.0 | 0.0 | BIT 0 |
| ESADEJS | ESA Door Eject Sec | 72 7 20 | 1.0 | 0.0 | BIT 1 |
| ESADEJP | ESA Door Eject Prim | 72 7 20 | 1.0 | 0.0 | BIT 2 |
| DCDTEDEJS | DCD/TE Door Eject Sec | 72 7 20 | 1.0 | 0.0 | BIT 3 |
| DCDTEDEJP | DCD/TE Door Eject Prim | 72 7 20 | 1.0 | 0.0 | BIT 4 |
| SCSDEJS | SCS Door Eject Sec | 72 7 20 | 1.0 | 0.0 | BIT 5 |
| SCSDEJP | SCS Door Eject Prim | 72 7 20 | 1.0 | 0.0 | BIT 6 |
| OSDPLYS | OS Deploy Sec | 72 7 20 | 1.0 | 0.0 | BIT 7 |

```
LPDEJP          LP Door Eject Prim          72 8  20  1.0      0.0     BIT 0
FPDPLYS         FP Boom Deploy Sec          72 8  20  1.0      0.0     BIT 1
FPDPLYP         FP Boom Deploy Prim         72 8  20  1.0      0.0     BIT 2
FPDEJS          FP Door Eject Sec           72 8  20  1.0      0.0     BIT 3
FPDEJP          FP Door Eject Prim          72 8  20  1.0      0.0     BIT 4
FEDDEJS         FED Door Eject Sec          72 8  20  1.0      0.0     BIT 5
FEDDEJP         FED Door Eject Prim         72 8  20  1.0      0.0     BIT 6
TVEDEJS         TV3 Door Eject Sec          72 8  20  1.0      0.0     BIT 7
HVARMP          HV Control Arm/Safe Prim    72 9  20  1.0      0.0     BIT 0
NPGDEJS         NPG Door Eject Sec          72 9  20  1.0      0.0     BIT 1
NPGDEJP         NPG Door Eject Prim         72 9  20  1.0      0.0     BIT 2
PCDPLYS         HCPC Deploy Sec             72 9  20  1.0      0.0     BIT 3
PCDPLYP         HCPC Deploy Prim            72 9  20  1.0      0.0     BIT 4
PCDEJS          HCPC Door Eject Sec         72 9  20  1.0      0.0     BIT 5
PCDEJP          HCPC Door Eject Prim        72 9  20  1.0      0.0     BIT 6
LPDEJS          LP Door Eject Sec           72 9  20  1.0      0.0     BIT 7
TEFILC          TE Filament                 72 10 20  1.0      0.0     BIT 0
FEDSIM          FED Simulator               72 10 20  1.0      0.0     BIT 1
FEDTRIG         FED Trigger                 72 10 20  1.0      0.0     BIT 2
ILULED          TV2 LED                     72 10 20  1.0      0.0     BIT 3
HVENABL         HV Enable                   72 10 20  1.0      0.0     BIT 4
SPHCON          HV Connect/Disconnect       72 10 20  1.0      0.0     BIT 5
DCHGNET         HV Network                  72 10 20  1.0      0.0     BIT 6
CHGDIS          HV Event Trigger            72 10 20  1.0      0.0     BIT 7
TV3SC           LLLTV3 Shutter              72 11 20  1.0      0.0     BIT 1
SCS600RL        SCS HV Mode                 72 11 20  1.0      0.0     BIT 2
SCSRELAY        SCS Test Mode               72 11 20  1.0      0.0     BIT 3
TV3LC           SCS Lamp                    72 11 20  1.0      0.0     BIT 4
GRHPVC          NGRS Hi Flow                72 11 20  1.0      0.0     BIT 5
GRLPVC          NGRS Low Flow               72 11 20  1.0      0.0     BIT 6
DCDHVREL        DCD HV                      72 11 20  1.0      0.0     BIT 7
NPVPWR          NPG Motor Power             72 12 20  1.0      0.0     BIT 1
NPVC            NPG Valve                   72 12 20  1.0      0.0     BIT 2
NPHVCNTRL       NPG HV                      72 12 20  1.0      0.0     BIT 3
PCGASONOFF      HCPC Gas Valve              72 12 20  1.0      0.0     BIT 4
PCENABLE        HCPC Enable/Disable         72 12 20  1.0      0.0     BIT 5
PCPHTR          HCPC Preheater              72 12 20  1.0      0.0     BIT 6
PCHTRON         HCPC Heater                 72 12 20  1.0      0.0     BIT 7
XMIT1P          Xmit #1 Power               77 10 20  1.0      0.0     BIT 0
XMIT2P          Xmit #2 Power               77 11 20  1.0      0.0     BIT 7
XMIT3P          Xmit #3 Power               77 11 20  1.0      0.0     BIT 6
ESAVSMFS        ESA Full-Scale Reference    50 19 20  1.0      0.0
ESAVSMHS        ESA Half-Scale Reference    50 20 20  1.0      0.0
FPHF21          FP High Frequency V21 (V)   1  1  -8   0.7608  -97.0
FPV12M          FP V12 Medium Gain (V)      8  1  -40 -1.5196   194.0
FPV21H          FP V21 High Gain (V)        70 2  2    0.1900  -24.2
FPV21L          FP V21 Low Gain (V)         71 1  2    12.157  -1550.0
FPV12L          FP V12 Low Gain (V)         71 1  2   -12.157   1550.0
FPV1S           FP V1S Medium Gain (V)      71 2  2   -3.2353   115.0
FPDEJM          FP Door Eject Monitor       59 7  20  1.0      0.0     BIT 3
FPDPLYMC        FP Limit Switch Common      59 7  20  1.0      0.0     BIT 4
BYTE3           TM Page byte 3              3  1  1    1.0      0.0
BYTE19          TM Page byte 19             19 1  1    1.0      0.0
BYTE35          TM Page byte 35             35 1  1    1.0      0.0
BYTE51          TM Page byte 51             51 1  1    1.0      0.0
BYTE67          TM Page byte 67             67 1  1    1.0      0.0
BYTE83          TM Page byte 83             83 1  1    1.0      0.0
BYTE84          TM Page byte 84             84 1  1    1.0      0.0
BYTE85          TM Page byte 85             85 1  1    1.0      0.0
BYTE86          TM Page byte 86             86 1  1    1.0      0.0
BYTE87          TM Page byte 87             87 1  1    1.0      0.0
BYTE88          TM Page byte 88             88 1  1    1.0      0.0
FPV21L_FIX      FP V21 Low Gain Fixed (V)   71 1  2    CAL={ -1550 12.157 v mul a
dd 79 2 rowoffset 20 div int 20 mul add page 256 mul 80 2 rowoffset 20 div int 20 mu
l add page add 10000 sub sub }
FPV12L_FIX      FP V12 Low Gain Fixed (V)   71 1  2    CAL={ -1550 12.157 v mul a
dd 79 2 rowoffset 20 div int 20 mul add page 256 mul 80 2 rowoffset 20 div int 20 mu
l add page add 10000 sub sub -1 mul}
```

```
ESA_PEAK        ESA Derived Vehicle Potential   79 3  20  0.2 0.0 TWOBYTES 80 3
ESA_FLUX        ESA Integrated Ion Flux         79 14 20  CAL={ v 10 80 14 mpage 1 s
ub exp mul }
MSIS_HE         MSIS He Density (m^-3)          79 4  20  0.001 0.0 10** TWOBYTES 80
 4
MSIS_O          MSIS O Density (m^-3)           79 5  20  0.001 0.0 10** TWOBYTES 80
 5
MSIS_N2         MSIS N2 Density (m^-3)          79 6  20  0.001 0.0 10** TWOBYTES 80
 6
MSIS_O2         MSIS O2 Density (m^-3)          79 7  20  0.001 0.0 10** TWOBYTES 80
 7
MSIS_AR         MSIS Ar Density (m^-3)          79 8  20  0.001 0.0 10** TWOBYTES 80
 8
MSIS_N          MSIS N Density (m^-3)           79 9  20  0.001 0.0 10** TWOBYTES 80
 9
MSIS_H          MSIS H Density (m^-3)           79 10  20  0.001 0.0 10** TWOBYTES 8
0 10
MSIS_DENS       MSIS Neutral Density (m^-3)     79 11  20  0.001 0.0 10** TWOBYTES 8
0 11
MSIS_TEMP       MSIS Neutral Temperature (K)    79 12  20  0.1 0.0 TWOBYTES 80 12
MSIS_PRESS      MSIS Neutral Pressure (Torr)    79 13  20 -0.0005 0.0 10** TWOBYTES
80 13
LP_DENS         LP Derived Density (cm^-3)      79 15  20 10.0 0.0 TWOBYTES 80 15
SPHERE_FIX      Sphere Voltage Fixed (V)        78 1   2  0.5  -2000. TWOBYTES 78 2
PLASMAI         Plasma Current (mA)             76 1   2  0.1  -200. TWOBYTES 76 2
```

**DISTRIBUTION LIST**
**DNA-TR-95-68**

**DEPARTMENT OF DEFENSE**

DEFENSE SPECIAL WEAPONS AGENCY
ATTN: ESA, W SUMMA
ATTN: EST, K WARE
2 CY ATTN: TRC

DEFENSE TECHNICAL INFORMATION CTR
2 CY ATTN: DTIC/OCP

FC DEFENSE SPECIAL WEAPONS AGENCY
ATTN: FCTT, DR BALADI

**DEPARTMENT OF THE ARMY**

ELECTRONICS TECH & DEVICES LAB
ATTN: PULSE POWER CTR
ATTN: SLCET-D, C THORNTON

**DEPARTMENT OF THE NAVY**

NAVAL POSTGRADUATE SCHOOL
ATTN: CODE 61SW, F SCHWIRZKE

NAVAL RESEARCH LABORATORY
ATTN: CODE 6700, S OSSAKOW
ATTN: CODE 6750, R MEGER
ATTN: CODE 6770, G COOPERSTEIN
ATTN: CODE 6770, R COMMIISSO

NAVAL SURFACE WARFARE CENTER
ATTN: CODE B-20

**DEPARTMENT OF THE AIR FORCE**

AIR FORCE OFFICE OF SCIENTIFIC RSCH
ATTN: DR R BARKER

AIR WEATHER SERVICE, MAC
ATTN: AWS TECH LIBRARY

**DEPARTMENT OF ENERGY**

LOS ALAMOS NATIONAL LABORATORY
ATTN: R REINOVSKY
ATTN: J BROWNELL

SANDIA NATIONAL LABORATORIES
ATTN: J HARRIS
ATTN: J MARTIN
ATTN: M BUTTRAM
ATTN: W BEEZHOLD

**OTHER GOVERNMENT**

CENTRAL INTELLIGENCE AGENCY
ATTN: OSWR, J PINA

NASA LANGLEY RESEARCH CENTER
ATTN: J LEE

NATIONAL INSTITUTES OF STANDARDS AND TECHNOLOGY
ATTN: R HEBNER

**DEPARTMENT OF DEFENSE CONTRACTORS**

APPLIED PHYSICAL ELECTRONICS RESEARCH CTR
ATTN: DR W NUNNALLY

BERKELEY RSCH ASSOCIATES, INC.
ATTN: R KARES
ATTN: S BRECHT

ENERGY COMPRESSION RESEARCH CORP
ATTN: D S WEIN

FORD MOTOR COMPANY CORPORATION
ATTN: M MOSBROOKER

FORD MOTOR COMPANY CORPORATION
ATTN: C NAKAYAMA

GA TECHNOLOGIES, INC.
ATTN: DOCUMENT CONTROL

JAYCOR
ATTN: CYRUS P KNOWLES

KAMAN SCIENCES CORP.
ATTN: D MOFFETT

KAMAN SCIENCES CORPORATION
ATTN: DASIAC
ATTN: DASIAC/DARE

LOCKHEED MARTIN VOUGHT SYSTEMS
ATTN: LIBRARY EM-08

MINNESOTA MINING AND MANUFACTURING CO.
ATTN: D REDMOND
ATTN: E HAMPL

MISSION RESEARCH CORP.
ATTN: B GOPLEN

PRIMEX PHYSICS INTERNATIONAL
ATTN: C STALLINGS
ATTN: P SINCERNY

PULSE SCIENCES, INC.
ATTN: P W SPENCE

TETRA CORP
ATTN: W MOENY

TEXAS TECH UNIVERSITY
ATTN: DR M KRISTIANSEN

UNIVERSAL VOLTRONICS CORP
ATTN: W CREWSON

UTAH STATE UNIVERSITY
2 CY ATTN: W JOHN RAITT

W J SCHAFER ASSOCIATES, INC.
ATTN: E ALCARAZ

WESTINGHOUSE STC
ATTN: DR A H COOKSON

AUBURN UNIVERSITY
ATTN: M ROSE

UNIVERSITY OF NEW YORK-BUFFALO
ATTN: R DOLLINGER

UNIVERSITY OF CALIFORNIA-DAVIS
ATTN: J S DEGROOT